UNIVERSITÀ DEGLI STUDI DI SALERNO

UNIVERSITÀ DEGLI STUDI DI SALERNO

Dipartimento di Farmacia

PhD Program

in **Drug Discovery and Development**

XXXIII Cycle — Academic Year 2020/2021

PhD Thesis

Effects of the isoprenoid derivative N6-benzyladenosine in cancer progression

Candidate

Chiara Piscopo

Supervisor

Prof. *Patrizia Gazzerro*

PhD Program Coordinator: Prof. *Gianluca Sbardella*

SCIENTIFIC PRODUCTION DURING THE PHD PROGRAM

Publications

Proto, M.C.; Fiore, D.; **Piscopo, C.**; Pagano, C.; Galgani, M.; Bruzzaniti, S.; Laezza, C.; Gazzerro, P.; Bifulco, M. Lipid homeostasis and mevalonate pathway in COVID-19: basic concepts and potential therapeutic targets. *Prog Lipid Res*. **2021**; *82*, 101099.

Bifulco, M.; Fiore, D.; **Piscopo, C.**; Gazzerro, P.; Proto, M.C. Commentary: Use of Cannabinoids to Treat Acute Respiratory Distress Syndrome and Cytokine Storm Associated with Coronavirus Disease-2019. *Front. Pharmacol*. **2021**, *12*, 631646.

Di Zazzo, E.; Rienzo, M.; Marino, M.M.; Fiore, D.; **Piscopo, C.;** Casamassimi, A.; Moncharmont, B.; Abbondanza, C. Accepted for publication in: Obesity and cancer: linked molecular mechanisms. *Springer Nature*. Obesity and Diabetes (Chapter 28). **2020**.

Laezza, C.; Pagano, C.; Navarra, G.; Pastorino, O.; Proto, M.C.; Fiore, D.; **Piscopo, C.;** Gazzerro, P.; Bifulco, M. The Endocannabinoid System: A Target for Cancer Treatment. *Int. J. Mol. Sci.* **2020**, *21*, 747.

Fiore, D.; **Piscopo, C.;*** Proto, M.C.; Vasaturo, M.; Dal Piaz, F.; Fusco, B.M.; Pagano, C.; Laezza, C.; Bifulco, M.; Gazzerro P. N6-isopentenyladenosine inhibits colorectal cancer and improve sensitivity to 5-Fluorouracil targeting FBXW7 tumor suppressor. *Cancers.* **2019**, *11*, 1456. *Co-first author

Fiore, D.; Ramesh, P.; Proto, M.C.; **Piscopo, C.;** Franceschelli, S.; Anzelmo, S.; Stassi, G.; Medema, J.P.; Bifulco, M.; Gazzerro, P. Rimonabant kills Colon Cancer Stem Cells without inducing toxicity in normal colon organoids. *Front. Pharmacol.* **2018**, *8*, 949.

Conference proceedings

Proto, M.C.; Fiore, D.; **Piscopo, C.;*** Laezza, C.; Fusco, B.M.; Bifulco, M.; Gazzerro, P. N6-isopentenyladenosine as tool to overcome chemoresistance in glioblastoma and colorectal cancer. Presented as poster at the *61st Annual Meeting of The Italian Cancer Society.* Napoli, November 6-8, **2019.** *Presenting author

Piscopo, C.;* Proto, M.C.; Cascone, A.M.; Zeppa, P.; Fiore, D.; Fusco, B.M.; Bifulco, M.; Gazzerro, P. Interplay between cannabinoids and inflammatory cytokines in human breast cancer. Presented as poster at the *4th Joint Meeting of Pathology and Laboratory Medicine – SIPMeT*, Catania, October 23-25, **2018.** *Presenting author

Piscopo, C.;* Fiore, D.; Proto, M.C.; Fusco, B.M.; Bifulco, M.; Gazzerro, P. N6-isopentenyladenosine inhibits proliferation of colorectal cancer cells through up-regulation of tumor suppressor FBXW7. Presented as poster at the *60th Annual Meeting of The Italian Cancer Society*. Milan, September 19-22, **2018**. *Presenting author

Fiore, D.; Ramesh, P.; Proto, M.C.; **Piscopo, C.;** Medema, J.P.; Bifulco, M.; Gazzerro, P. Rimonabant kills Colon Cancer Stem Cells without inducing toxicity in normal colon organoids. Presented at the *38th National Meeting of Pharmacology Italian Society*, Rimini, October 25-28, **2017**.

TABLE OF CONTENTS

ABSTRACT

N6-isopentenyladenosine (IPA) and its analogue N6-benzyladenosine (N6-BA) are modified nucleosides endowed with potent *in vitro* antitumor activity on different types of human cancers, including colorectal cancer (CRC) and glioblastoma multiforme (GBM). Although the molecules seem to exert their anti-proliferative effects partially through the inhibition of Farnesyl Diphosphate Synthase (FDPS), their precise mechanisms of action remain to be uncovered. The main aim of my PhD project was to investigate the effects of the isoprenoid derivative N6-BA, by comparing them to those of the lead compound IPA, on the modulation of cancer-related pathways. I found that both IPA and N6-BA affect CRC and GBM cell lines proliferation by modulating the expression of the F-box WD repeat domain-containing 7 (FBXW7), widely considered a tumor suppressor since its crucial role in the turnover of many proteins (i.e. c-Myc, SREBPs and Mcl1) contributing to malignant progression.

In CRC, FBXW7/SREBP/FDPS axis was identified as a target of the compounds. IPA was found to induce the ubiquitination of c-Myc, inhibiting its transcriptional activity through the increase of FBXW7/c-Myc binding and N6-BA acts almost in a similar way. Moreover, IPA involvement in chemoresistance was also investigated. IPA synergized with 5-Fluorouracil in FBXW7- and TP53-wild type CRC cells and sensitized GBM cells to the toxic effect of Temozolomide.

Overall, results here showed provide novel insights into the molecular mechanism of the modified adenosines and suggested the existence of an epigenetic regulation underlying their pleiotropic effects in cancer. Restoring of FBXW7 tumor-suppressor represents a valid therapeutic tool, enabling modified adenosines as optimizable compound for patient-personalized therapies in both CRC and GBM.

INTRODUCTION

Naturally occurring cytokinins in plants and mammals.

Cytokinins (CKs) are a group of phytohormones first detected in tobacco tissue cultures as DNA degradation products able to induce cell division in roots meristem. The term "kinin", initially used to describe these compounds promoting growth, were soon replaced by "cytokinin" which literally means stimulus of cell movement (from the Greek word *cytokinesis*), but it is also referred to cell division [Skoog et al, 1965]. Together with auxins, CKs were found to be involved in almost all aspects of plant physiology, including several developmental and differentiation events [Kieber and Schaller, 2018]. More recently, CKs role in plant immune response against pathogens and parasites has also been recognised [Spallek et al, 2017; Akhtar et al, 2020]. Naturally occurring CKs are adenine derivatives, existing as free bases, ribosides, or nucleotides, with an isoprenoid or aromatic sidechain at the N6 position of the adenine which determine their biological functions. The most common isoprenoid compounds are N6-isopentenyladenine (iP), *trans*-zeatin (tZ), *cis*-zeatin (cZ) and dihydrozeatin (DZ), while less has been documented about the aromatic CKs, such as N6-benzyladenine [Kieber and Schaller, 2018]. The accepted isoprenoid biosynthetic pathway starts with an isopentenyltransferase (IPT) using adenosine-phosphates (ATP, ADP or AMP) as substrates and dimethylallyl diphosphate (DMAPP) or hydroxymethylbutenyl diphosphate (HMBDP) as isoprenyl donors. HMBDP derives from the methylerythritol phosphate (MEP) pathway which occurs in bacteria and plastids, DMAPP is a metabolite of mevalonate (MVA) pathway, which is commonly found in eukaryotes cytosol [Sakakibara, 2006]. The iP ribotides prevalently derive from *de novo* biosynthesis and can be converted into tZ- or DZ-type via hydroxylation of the isoprenoid chain by cytochrome P450 enzymes and/or subsequent saturation. In contrast, the biosynthesis of the *cis* isomer cZ likely involves IPTs catalyzing the N6-prenylation of adenine on tRNA, so that tRNA degradation is suggested to be cZ major source in plants. Free-bases, representing the CKs active forms, are synthesized from ribotides in a single enzymatic step driven by a cytokinin nucleoside 5′-monophosphate phosphoribohydrolases belonging to the LOnely Guy (LOG) family. CKs active levels can be modulated by reversible or irreversibile glucosylation (at O and N7/N9 positions, respectively): *O*-glucosides are proposed to be the inactive storage forms to rely on when needed [Kieber and Schaller, 2018]. It was originally thought that CKs were synthesized in the roots and then transported to the shoot, but it is now clear that their metabolism takes place locally in various plant tissues and their transport occurs at long distance through the xilematic and

phloematic flux. In the shoots, CKs promote cell proliferation, including the activity of apical and axillary meristems, and favour cell differentiation of the apical meristem in the roots.

Several studies examined the CKs content in young and old leaves and evidenced that they are negative regulators of senescence. Transcriptomic analysis of Arabidopsis revealed the existence of genes regulated by CKs and involved in senescence response signalling, such as a CK receptor (AHK3), a type-B response regulator (ARR2) and the CK response factor 6 (CRF6) [Zwack and Rashotte, 2013]. Less is known about the endogenous metabolism of aromatic CKs. It has been hypothesized that the benzylic side chain probably derives from the metabolism of phenolics [Strnad, 1997].

Once thought to be exclusively present in plants, CKs have been discovered so far in all kingdoms of life, except for Archaea. The modified nucleoside N6-isopentenyladenosine (referred as i6A) is the only known CK occurring endogenously in mammals either as free base or bounded at position 37 of the anticodon loop in a subset of cytosolic and mitochondrial tRNAs that bind codons starting with uracil. This modification stabilizes the weak adjacent codon-anticodon base pairs and increases the ribosome binding thus increasing the fidelity and the efficiency of translation [Bifulco et al, 2008]. Like plants, it was believed that tRNA degradation was the main source of free CKs, including i6A. However, sequence homology revealed that IPTs genes are highly conserved through evolution. In fact, tRNA i6A37 modification can be functionally complemented in *S. cerevisiae* lacking its IPT by cDNAs encoding IPTs from human (TRIT1), silkworm (GRO-1), *S. pombe* (Tit1), plants or even prokaryote-type IPTs [Khalique et al, 2020]. In mammals, the isoprenylation on N6 residue of A37 is required for full expression of proteins carrying the rare aminoacid selenocysteine (Sec). The ability to decode UGA as a Sec codon is affected when the $tRNA^{Sec}$ lacks i6A at position 37 as demonstrated in *Xenopus* [Spinola et al, 2005]. Most mitochondrial-tRNAs carrying i6A are further modified into 2-methylthio-N6-isopentenyladenosine (ms2i6A) by the radical S-andenosylmethionine (SAM) enzyme cyclin-dependent kinase 5 regulatory subunit associated-protein 1 (CDK5RAP1) [Schweizer et al, 2017]. Although the role of hypermodified adenosine ms2i6A is not fully elucidated, CDK5RAP1 is known to ensure the precise translation of mitochondrial DNA-encoded genes, contributing to the maintenance of cellular respiration and metabolism in skeletal and cardiac muscles. CDK5RAP1 deficiency and subsequent ms2i6A conversion loss was recently associated to the intracellular accumulation of i6A, which triggers excessive autophagy in Glioma Initiating Cells (GICs) [Yamamoto et al, 2019].

N6-isopentenyladenosine and its analogue N6-benzyladenosine in tumor biology.

Knowledge about CKs functions in plants led to hypothesis that they could also affect growth and differentiation in animals and have potential utility for treating human diseases that involve dysfunctional cell proliferation and/or differentiation, just like human cancer. So far, early studies revealed that exogenous administration of i6A (referred as IPA from here on) could exert either pro- and anti-proliferative effects on human cell growth, respectively at submicromolar (< 1 μM) or higher concentrations, depending on the cell cycle phase. Moreover, it was also demonstrated that IPA affected DNA, RNA and protein synthesis and the mechanism of RNA inhibition, preceding the others, might have occurred as result of the competition with substrates like adenosine-3-phosphate, adenosine or 2'-deoxyadenosine 5'-triphosphate [Gallo et al, 1969]. IPA was also found to induce apoptosis in human peripheral blood lymphocytes, but the effect was even stronger in the cancer cell lines Caco-2 and HL-60 [Meisel et al, 1998]. Searching for plausible mechanisms of action, IPA anti-tumor potential was further investigated in other malignant systems. In K-ras transformed thyroid cells (KiMol) the IPA-induced antiproliferative effect *in vitro* was related to the inhibition, in both expression and activity, of the farnesyl diphosphate synthase (FDPS), a key enzyme of the mevalonate pathway crucial for cholesterol biosynthesis and prenylation of oncogenic proteins, mainly belonging to the RAS super-family, often deregulated in tumors [Laezza et al, 2006; Abate et al, 2017]. In DLD1, a human colon adenocarcinoma cell line, IPA was found to induce cell cycle arrest through downregulation of cyclin E, cyclin A and cyclin D1, concomitant with an increase in the levels of cyclin-dependent kinase inhibitor and p27kip1. As already reported for KiMol cells, FDPS activity and its transcript significantly decreased in DLD1 cells [Laezza et al, 2009]. The IPA-immunomodulating ability to selectively expand and activate natural killer (NK) cells was also related to FDPS modulation [Ciaglia et al, 2014]. As consequence, IPA-induced NK cells activation allowed recognition of glioma cells, achieved by the upregulation of ULBP2, NKG2D ligand, in TP53 wild type cells or MICA/B in p53 mutant gliomas [Ciaglia et al, 2018]. It was reported that IPA, phosphorylated by adenosine kinase (ADK) into 5′-iPA-monophosphate (iPAMP), activated AMP-Kinase (AMPK), thus inhibiting the angiogenic process *in vitro* and in a model of angiogenesis *in vivo* [Pisanti et al, 2014]. The AMPK-activation in melanoma allows mTOR inhibition, autophagosome accumulation and late-stage autophagy inhibition. Here too, the IPA effect seems to comply with the downstream inhibition of Rab7 prenylation, because of FDPS negative modulation [Ranieri et al, 2018]. Finally, a structural interaction between IPA and FPPS

has been shown *in silico*, supporting previous observations overall suggesting FDPS as possible biochemical target of the molecule [Scrima et al, 2014].

To better understand the relation between IPA structure and biological activity, as well to obtain new compounds endowed of antiproliferative effect, Ottria and collegues synthesized and tested for their anticancer activity several analogues with N6-modifications to the IPA scaffold. The insertion of a benzyl group at the N6 position led to a molecule, the N6-benzyladenosine (N6-BA), whose activity was comparable to IPA in suppressing clonogenicity and growth of bladder carcinoma T24, colon carcinoma CaCo2 and breast carcinoma MDA-MB231 cells [Ottria et al, 2010]. N6-BA, as well as IPA, was found to inhibit the growth of MCF7 human breast adenocarcinoma cells, to modulate their transcription profiles by altering the expression of genes involved in the response to oxidative stress, to inhibit *in vivo* TPA-induced inflammation in Car-S mice [Dassano et al, 2014]. More recently, N6-BA showed a marked cytostatic effect and selective cytotoxic activity, greater than IPA, in glioma patient-derived cells compared to normal astrocyte cells. Similar to IPA, also N6-BA action was related, at least in part, to the inhibition of FDPS, that counteracts EGF receptor (EGFR) functions and activity providing critical lipid moieties for post-translational modification of downstream signalling molecules (small GTP-ase that undergo prenylation) [Ciaglia et al, 2017b]. However, the chemical structure of modified nucleosides allows IPA and N6-BA to potentially influence multiple cell processes, in addition to the direct FDPS modulation. Several observations indicated that IPA could have roles in ubiquitin proteasome system (UPS) regulation. A computational docking study revealed that IPA could bind a domain of the ubiquitin ligase tumor necrosis factor receptor–associated factor 6 (TRAF6) and mediate apoptosis in HeLa cells inhibiting both AKT and transforming growth factor β-activated kinase 1 signaling pathways [Li et al, 2017]. Our research group showed that IPA induces EGFR proteasomal degradation through the specific c-Cbl E3 ligase, suppressing the tyrosine-kinase receptor signalling cascade [Ciaglia et al, 2017a]. Gene expression profile in IPA-treated breast and lung cancer cells highlighted a transcriptional regulation of genes classified into the functional gene ontology (GO) categories “cell cycle arrest” and “protein modification response”, many of which encode for UPS proteins (or domains of them). Among these, the upregulation of WD Repeat and SOCS box-containing 1 (WSB1), F-box and leucine-rich repeat protein 12 (FBXL12) and Ras-like without CAAX 1 (RIT1, also known as RBX1) genes [Colombo et al, 2009] seems to be a remarkable evidence, since F-box proteins and SCF ligases, received gaining attention as molecular targets in several human malignancies [Skaar

et al, 2014; Humphreys et al, 2021]. The chemical structure of IPA and N6-BA is represented in Figure 1.

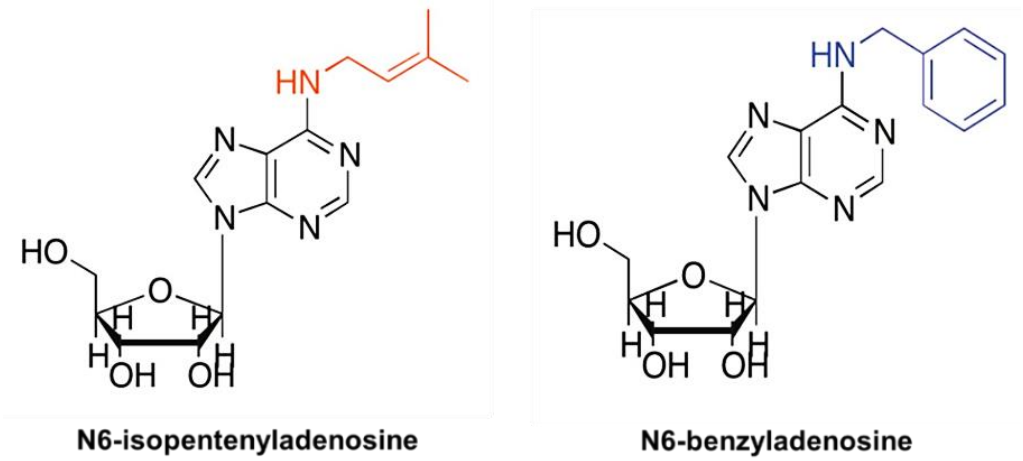

Figure 1. Chemical structure of the modified adenosines. N6-isopentenyladenosine, generally referred as i6A or IPA, is a naturally occurring modified nucleoside structurally formed by an adenosine, deriving from the purine metabolism, with an isopentenyl moiety originating from the mevalonate pathway at the N6 position. N6-benzyladenosine is an isoprenoid aromatic derivative with a benzyl group as N6-substituent.

FBXW7 ubiquitin ligase: a tumour suppressor at the crossroads of cell growth and survival.

Proteasomal degradation through UPS ensures proper protein spatial and temporal availability, contributing to all aspects of cell life cycle. Aberrant turnover of oncogenic products, because of degradation machinery dysfunctions, often promotes tumor progression [Yumimoto and Nakayama, 2020]. Ubiquitination is the covalent attachment of the small protein ubiquitin to the lysine residues of target proteins. The process involves an enzymatic reaction starting with ubiquitin activation by linkage to an E1 ubiquitin-activating enzyme and proceeding with its transfer to an E2 ubiquitin-conjugating enzyme, and finally to a free amine group of a substrate by an E3 ubiquitin ligase. Substrates can either be mono-ubiquitylated (on one or more sites) or poly-ubiquitinated after repeated iterations of the enzymatic cascade resulting in long chains of ubiquitin (polyubiquitin). While poly-ubiquitination at Lys-48 generally represents a tag for degradation via the 26S proteasome and regulates protein stability, mono-ubiquitination tends to control processes ranging from membrane transport to transcription. Ubiquitination process is reversible and de-ubiquitylating (DUB) enzymes, functionally opposed to E3 ubiquitin ligases, are responsible for removal of ubiquitin tag to prevent proteolysis [Skaar et al, 2014].

Although there are only few E1 and E2 known ligases, there are over 700 human E3 ligases characterized for their different catalytic domains into three main subgroups: Really Interesting

New Gene (RING), Homologous to E6-AP Carboxyl Terminus (HECT), or Ring-Between-Ring (RBR). The SCF complex belongs to the cullin-RING family consisting of a RING-domain protein (RBX1, also known as ROC1), an adaptor subunit (SKP1), a scaffold protein (CUL1), and an F-box protein that specifically recognizes substrates. In turn, F-box proteins are categorized into three subclasses differing for their COOH-terminal regions: FBXW (containing a WD40-repeat domain), FBXL (containing a leucine-rich–repeat domain), and FBXO (containing another type of protein-interaction domain or no recognizable domain) [Yumimoto and Nakayama, 2020]. Among them, F-box with 7 tandem WD40 repeats (FBXW7; also known as Fbw7, Sel-10, hCdc4, hAgoF) is considered as a strong p53-dependent tumor suppressor regulating stability of a great number of oncogenic substrates with essential roles in cell cycle progression, cell growth, and tumor development [Sailo et al, 2019] summarized in Table 1. In mammals, FBXW7α, FBXW7β, and FBXW7γ isoforms, differing in their 5'-UTR and N-terminal coding regions, originate from the same gene locus and have a conserved CDC4 phosphodegron (CPD) motif, which requires substrate phosphorylation at specific residues in order to be recognized and targeted with ubiquitin. The phosphorylation of substrates undergoing FBXW7-dependent degradation is mainly operated by the glycogen synthase kinase 3 beta (GSK3β) [Yeh et al, 2018].

A schematic representation of the FBXW7 mediated degradation is reported in Figure 2.

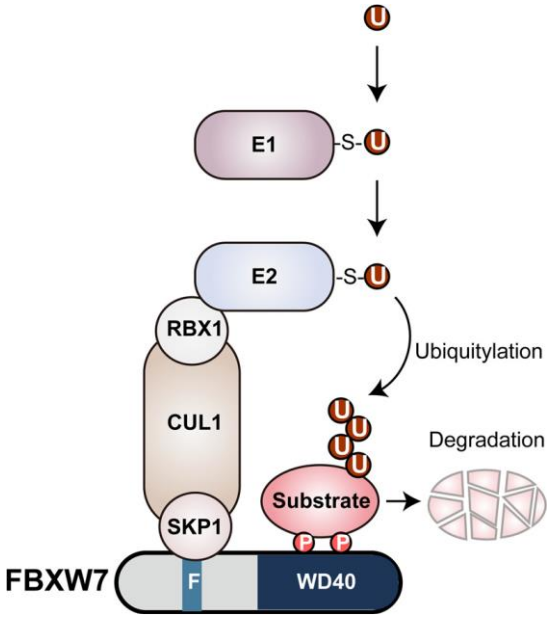

Yumimoto K. and. Nakayama K.I. *Seminars in Cancer Biology*, **2020**, *67*, 1–15.

Figure 2. Schematic representation of SCF^{FBXW7} mediated degradation. Ubiquitin (U) activation and transfer is mediated by E1 and E2 enzymes, respectively. FBXW7 binds to SKP1 via its F-box domain (F) and to a phosphorylated substrate via its WD40-repeat domain mediating the covalent attachment of ubiquitin to the substrate for degradation.

Mutation, deletion, and promoter hypermethylation are the main events causing FBXW7 inactivation and consequent unbalance of its oncogenic substrates, thereby leading to tumor progression in many types of human cancers. FBXW7 transcription is directly induced by p53 and inhibited by C/EBP-δ, but other factors including Numb, non-coding RNAs, Pin 1, Hes-5, BMI1, Ebp2 seem to play a role in FBXW7-transcriptional regulation. Mutations in p53, previously reported to be associated with DNA methyltransferase 1 (DNMT1) protein overexpression, are also associated with hypermethylation of the FBXW7 promoter, resulting in decreased FBXW7 transcript levels. In addition to DNA modifications, histone modifications are reported to control FBXW7 expression. Enhancer of zeste homolog 2 polycomb repressive complex 2 (EZH2), a histone methyltransferase that specifically catalyzes the addition of three methyl groups onto the histone H3 residue and this modification (H3K27me3) is frequently associated to epigenetically silencing genes, including FBXW7 [Yeh et al, 2018]. Recently, it has been shown that the histone lysine demethylase LSD1 (also known as KDM1) destabilizes FBXW7 acting as its pseudosubstrate, not being ubiquitinated but promoting FBXW7 self-ubiquitination and inactivation due to proteasomal or lysosomal degradation [Lan et al, 2019].

Table 1. FBXW7 substrates and their role in cellular processes.

FBXW7 substrate	Role
Aurora kinase A (AURKA)	Regulation of the mitotic checkpoint
Cyclin E	G1 to S phase cell cycle transition
c-Jun	Developmental processes and differentiation
c-Myc	Proliferation, metabolism, survival, self-renewal ability
Hypoxia inducible factor-1α (HIF-1α)	Regulation of adaptive responses to oxygen changes in cells
Kruppel-like factors (KLF)	Proliferation, development, differentiation, apoptosis
Mechanistic target of rapamycin (mTOR)	Proliferation, metabolism, survival, autophagy
Myeloid cell leukemia-1 (Mcl1)	Apoptosis
Mediator 13 (MED13)	Regulation of transcription factors association with RNA polymerase II
Neurofibromatosis type 1 (NF1)	Proliferation, differentiation
Notch	Developmental processes and differentiation
Nuclear factor E2-related factor 1 (NRF1)	Regulation of genes involved in oxidative stress and inflammation.
p53	Cell cycle progression and apoptosis
p100/NFκB	Regulation of genes involved in immune and inflammatory responses
Sterol regulatory element binding proteins (SREBP)	Transcriptional activation of lipid metabolism genes

General hints of colorectal cancer…

Colorectal cancer (CRC) is one of the most diagnosed cancers worldwide and encompass both hereditary and sporadic syndromes. The majority of cancers arise with aberrant crypt foci, evolving into a neoplastic precursor lesion (polyp), eventually progressing to *in situ* carcinoma and ultimately to invasive and metastatic tumor [Fearon, 2011]. Colorectal cancers are classified with TNM or Dukes systems as result of histopathological examination (differentiation grade, lymph node and serous surface involvement) and the demographic characteristics of patients. More than 90% of colorectal carcinomas are adenocarcinomas originating from epithelial cells of the colorectal mucosa [Fleming et al, 2012]. The malignant transformation is the result of a progressive accumulation of well characterized genetic and epigenetic alterations, arising from two distinct pathways: the traditional adenoma–carcinoma pathway, leading to 70–90% of colorectal cancers, and the serrated neoplasia pathway. The adenoma-carcinoma pathway is prevalently defined by chromosomal instability (CIN) and typically develop from an early mutation borne by Adenomatous Polyposis Coli (APC), tumor suppressor gene that negatively regulates Wnt/β-Catenin pathway, followed by RAS activation or TP53 loss of function. Conversely, serrated polyps are characterized by frequent BRAF (V600E) or less frequent KRAS mutations and by the so-called cytosine-phosphate-guanine (CpG) island methylator phenotype (CIMP), a condition of epigenetic instability leading to microsatellite stable and instable cancers. Microsatellite instability (MSI) is the hallmark of Lynch syndrome (Hereditary Non-Polyposis Colorectal Cancer), an autosomal dominant disorder caused by germline mutations in mismatch repair (MMR) genes, thus displaying increased cancer susceptibility. Global hypomethylation of the entire genome and local hypermethylation of specific CpG sites is an important feature of colon cancer (Figure 3). Aberrant methylation within promoter regions of tumor suppressor genes is very common in CRC and occurs, in the 80% of sporadic cancer, in the MLH1 repair gene [Dekker et al, 2019; De Palma et al, 2019]. The MMR system also corrects DNA damage induced by drugs generating a similar structural defect as mismatches, such as alkylating and intercalating agents. For instance, cells with MMR proteins deficiency are found to be 5-FU-resistant, as the case of Lynch syndrome patients, in retrospective and prospective studies [Sinicrope and Sargent, 2012]. FBXW7 has been identified as one of the most commonly mutated genes in CRC and its loss or missense mutations, mainly located in the substrate-binding domain, are associated to CRC severity and progression. FBXW7 and SMAD4 (Mothers Against DPP Homolog 4) mutations are prevalent in CRC patients resistant to anti-epidermal growth factor receptor (EGFR) immunotherapy treatment (Cetuximab or

Panitumumab), while FBXW7 loss is associated with drug resistance to Oxaliplatin and 5-FU in metastatic CRC [Yeh et al, 2018; Tong et al, 2017].

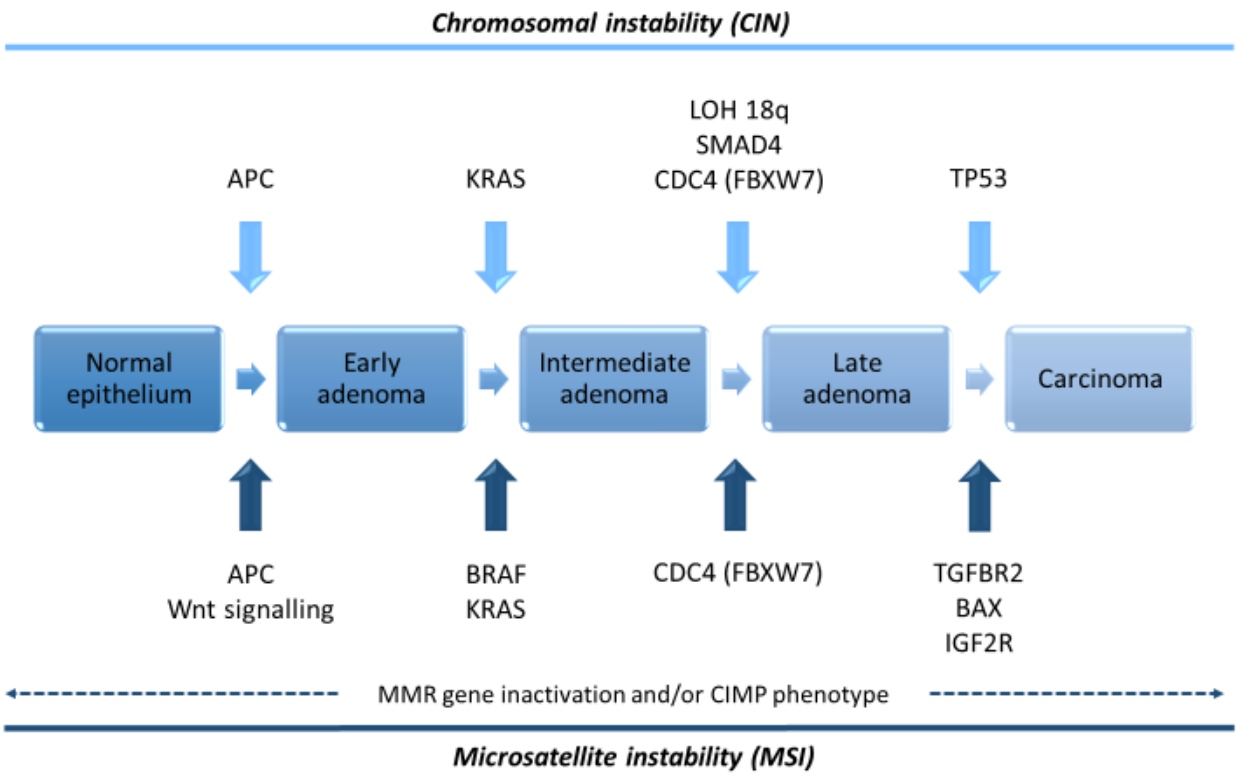

Figure 3. Malignant transformation features in colorectal carcinogenesis.

…and glioblastoma multiforme.

Gliomas comprise a disparate group of brain tumors with distinct biological and clinical properties, unfortunately sharing dismal prognosis due to an elevated tumor heterogeneity which limits therapeutic efficacy yet restricted because of the blood–brain barrier (BBB). Generally, the current international standard (World Health Organization, WHO) classified glioma subtypes into grade I to IV on the basis of malignancy, determined by histopathological criteria integrating molecular and phenotypic features [Louis et al, 2016]. Whereas grade I gliomas have low proliferative potential and can be managed with complete surgical resection, grade II to IV gliomas are highly malignant and invasive [Malta et al, 2018]. Glioblastoma multiforme (GBM) is the most aggressive grade IV subtype, with a median survival of about 15 months after surgery and subsequent treatment with radiations and temozolomide (TMZ) [Stupp et al, 2005]. GBM can be further divided according to clinical characteristics into primary and secondary GBM. Primary GBM arise *de novo* while,

conversely, secondary GBM slowly progress from pre-existing lower-grade lesions. Hallmark alterations of primary GBM include epidermal growth factor receptor (EGFR) activating mutation and amplification, overexpression of mouse double minute 2 (MDM2), deletion of p16 and loss of heterozygosity (LOH) of chromosome 10q, phosphatase tensin homolog (PTEN) and telomerase reverse transcriptase (TERT) promoter mutation. The characteristic features of secondary GBM include over expression of platelet-derived growth factor A and platelet-derived growth factor receptor alpha (PDGFA/PDGFRα), retinoblastoma (RB), LOH of 19q and mutations of isocitrate dehydrogenases (IDH1/2), TP53 and ATRX [Malta et al, 2018] (Figure 4). Several epigenomic markers also have shown prognostic and/or predictive values [Wenger et al, 2019]. DNA promoter methylation of the O6-methylguanine-DNA methyltransferase (MGMT) is related to an increased responsivity to cytotoxic effect of TMZ and to an increased overall survival after therapies [Oldrini et al, 2020]. Besides MGMT silencing, another important milestone highlighting the clinical importance of epigenetic signatures in gliomas was the discovery of the glioma CpG island methylator phenotype, identified as G-CIMP to differentiate it from the first discovered CIMP in CRC. Tumors carrying G-CIMP (G-CIMP+) are closely related to IDH mutation and generally had a more favorable prognosis than G-CIMP-. However, G-CIMP subsets (-low and -high) have shown distinct biological features and clinical implications associated with the establishment, recurrence, and progression of a malignant glioma phenotype, suggesting that DNA methylation changes could be determinant in this malignancy [Malta et al, 2018]. Dissecting molecular and epigenetic alterations in GBM is extremely important to expand the limited and ineffective therapeutic options or, at least, to identify new markers with prognostic value. As in other tumors, E3 ligases have central roles in pro-survival signalling and DNA damage response, thus affecting GBM recurrence and responsivity to the treatments [Humphreys et al, 2021]. In the brain, FBXW7 helps the neural stem cell differentiation and its abrogation may result in increased self-renewal ability because of the deregulation Notch, c-Jun and c-Myc [Takeishi and Nakayama, 2014]. Recently, clinical tissues and TCGA database analysis revealed that FBXW7 expression was correlated inversely with glioma histology and positively with patient survival time. Moreover, i*n vitro* FBXW7 overexpression significantly suppressed proliferation, invasion and migration and most importantly was found to increased temozolomide toxicity in a resistant clone [Lin et al, 2018]. Another recent study indicated that FBXW7 circular RNA potentially suppress in brain cancer and may serve as a prognostic marker for glioma [Yang et al, 2018].

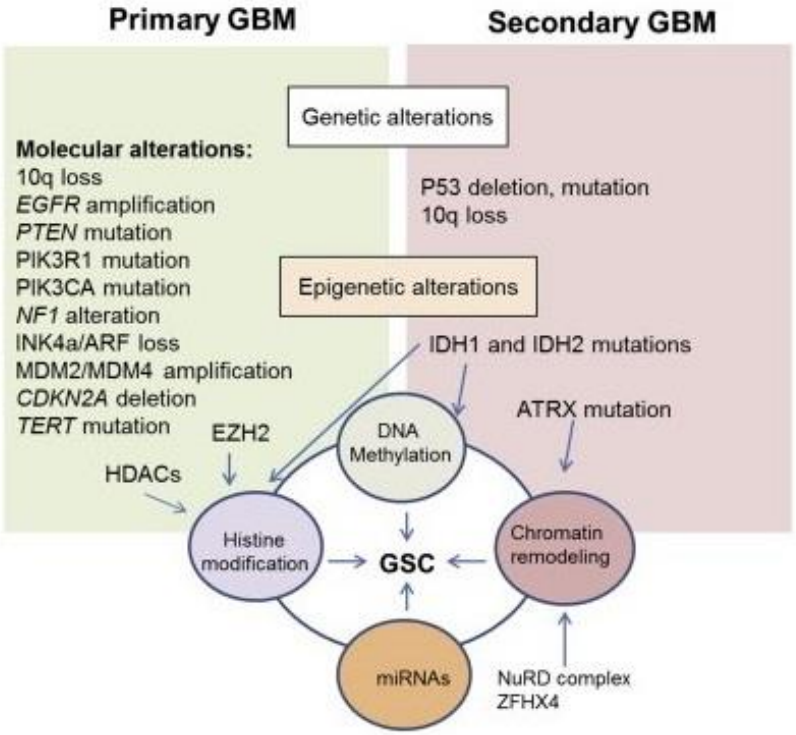

Adapted from Safa A.R. et al. *Genes Dis*. **2015**, *2*, 152-163

Figure 4. Frequent alterations in primary and secondary GBM.

MATERIALS AND METHODS

Reagents and antibodies

N6-isopentenyladenosine (IPA), N6-benzyladenosine (N6-BA), 5-fluorouracil (5-FU), Temozolomide (TMZ) and Decitabine (5-Aza-2'-deoxycytidine or 5-AZA-dC) were purchased from Sigma–Aldrich (St. Louis, MO, USA) and dissolved in sterile DMSO.

The following primary antibodies were purchased from Cell Signalling Technology (Beverly, MA, USA): anti-Caspase 3; anti-cleaved Caspase-3; anti-PARP; anti-GAPDH monoclonal; anti-Phospho-GSK-3β (Ser9); anti-GSK-3β; anti-Mcl-1; anti-Phospho-Histone H2Ax (Ser139);. Anti-c-Myc (monoclonal) and anti-SREBP-1 were purchased from Santa Cruz Biotechnology (Dallas, TX, USA). The following primary antibodies were purchased from Abcam (Cambridge, UK): anti-c-Myc (polyclonal); anti-FBXW7; anti-beta-Actin; anti-FDPS; anti-HDJ2; anti-MGMT; anti-DNMT1; anti-histone H3, H3K4me2; H3K27me3, H3K9me2; H3K9Ac (acetyl K9 + K14 + K18 + K23 + K27). Anti-phospho-c-Myc (Thr58) was purchased from Thermo Fisher Scientific (Waltham, MA, USA). The goat anti-rabbit secondary antibody and goat anti-mouse secondary antibody were purchased from Abcam.

Cell cultures

Human CRC cell lines DLD1, HCT116 and SW48 were obtained from the Interlab Cell Line Collection (IST, Genoa, Italy) and cultured in RPMI-1640, McCoy's 5A and DMEM-F12 medium, respectively, supplemented with 10% fetal serum bovine (FBS), 2 mM L-glutamine, 50 ng/mL streptomycin, 50 units/mL penicillin. Human GBM cell lines U87MG (U87), U251MG (U251) and T98G (T98) were purchased from Cell Lines Service GmbH (Eppelheim, Germany) and cultured in Eagle's Minimal Essential Medium (EMEM) with 10% FBS, 2 mM L-glutamine, 50 ng/mL streptomycin, 50 units/mL penicillin, 1% non-essential amino acids, 1 mM sodium pyruvate.

GBM primary cell lines were established as previously described [Ciaglia et al, 2017a]. Briefly, small pieces of surgical brain tissues containing tumor were collected at the time of craniotomy at the Neurosurgery Service of "G. Rummo" Medical Hospital (Benevento, Italy), divided into portions stored at −80°C for subsequent molecular characterization (RNA, DNA and protein extraction) or immediately processed to generate primary tumor cell lines. A second sample from each patient was also taken for clinical diagnosis performed by expert neuropathologists in accordance with the International Classification of CNS tumors drafted under the auspices of the

World Health Organization (WHO). The tumors were diagnosed as astrocytoma (WHO grade I-III), glioma (WHO grade II) or glioblastoma multiforme (WHO grade IV). All tissue samples were collected in accordance with the ethical standards of the Institutional Committee. The patients had been informed about the establishment of cellular models from their tumour and had given informed consent in written form. The preparation of adherent primary cultures of brain tumor cells was conducted through Miltenyi technology using Brain Tumor Dissociation Kit (Miltenyi Biotec, Calderara di Reno, Italy) and gentleMACS, combining enzymatic and mechanic dissociation. GBM primary cell lines (designated ad GBMn) were kept in culture in DMEM/F12 supplemented with 15% heat-inactivated fetal bovine serum (Euroclone), 2% L-glutamine, 1% antibiotic mixture, 1% sodium pyruvate, 1% non-essential aminoacids (Euroclone), routinely grown in monolayers and maintained at 37 °C in 5% CO2 humified atmosphere and regularly tested for mycoplasma presence. Experiments were performed using passages II-VI of these cells.

Cell proliferation and viability assay

Cell proliferation was evaluated through a colorimetric ELISA kit based on 5-Bromo-2′-deoxy-uridine (BrdU) labelling and detection (Roche Diagnostics GmbH, Mannheim, Germany). Briefly, CRC or GBM cells were seeded into 96-well plates at a density of 5-8×10^3 cells/well and treated in triplicate with IPA, N6-BA (ranging from 0.5 to 20 µM) or vehicle (DMSO) as control for 24 or 48 h. At the end of incubation time, medium was removed, and cells were fixed/denatured for 30 min. Then, cells were first incubated with an anti-BrdU peroxidase conjugated antibody solution (anti-BrdU-POD) for 90 min and then with a substrate solution for about 20 minutes. The colorimetric reaction was monitored and measured through a microplate reader (Multiskan™ GO Microplate Spectrophotometer, Thermo Scientific) at 370 nm. The blank was performed in each experimental setup. The absorbance value of the blank was subtracted from other experimental values and cell proliferation was expressed as the percentage of absorbance values ± SD of treated samples to untreated controls of three separate experiments in triplicate.

To evaluate the effect of IPA pre-treatment on TMZ toxicity, GBM cells were seeded into 96-well plates at a density of 5x10^3 cells/well and exposed to 10 µM IPA or vehicle alone for 24h. After the incubation, IPA-containing medium was removed and replaced with fresh medium added with 5, 50, 250, 500 µM TMZ or the relative vehicle alone for 72h. Cell viability was evaluated through colorimetric MTT metabolic activity assay. To this aim, MTT stock solution (5 mg/ml in PBS, Sigma) was added to each well and incubated for 4 h at 37°C in humidified CO2. At the end of the

incubation, the medium was removed, and the formazan crystals were solubilized with 100 µl of DMSO. MTT conversion to formazan by metabolically viable cells was monitored by spectrophotometer at an optical density of 540 nm. Each data point represents the average of at least three separate experiments in triplicate.

Cytofluorimetric analysis

For cell cycle analysis, HCT116 and DLD1 cells were plated and treated with vehicle or IPA 10 µM for 24 h. At the end of treatment, cells were collected, fixed in 70% ethanol and kept at -20°C overnight. Propidium iodide (PI; 50 µg/mL) was added to the cells for 15 min and for each sample at least 10,000 events were acquired. The analysis was performed using ModFit LT v3.2 software (Verity Software House, Inc., Topsham, ME, USA). For cytofluorimetric assessment of apoptosis, Annexin V/PI double staining was used. DLD1 cells treated with vehicle or IPA 10 µM for 24h, were harvested through trypsinization and stained with FITC-conjugated Annexin-V for 20 min at room temperature and then with PI for additional 15 min away from light. At least 10,000 events were acquired, and the analysis was performed with FlowJo v10.5 software (Becton, Dickinson and Company, Franklin Lakes, NJ, USA). Data are expressed as mean ± standard deviation (SD) of five independent experiments in triplicate.

Western blot analysis

Total protein extracts were obtained lysing cultured cells with ice-cold RIPA buffer (50 mM Tris–HCl pH 8.0, 150 mM NaCl, 1% Nonidet P-40) supplemented with protease and phosphatase inhibitors (Sigma). Cellular extracts optimized to preserve DNMTs enzymatic activity activity assay were obtained through the EpiQuik™ Nuclear Extraction kit (EpiGentek Group Inc., NY, USA) following manufacturer instructions. Purification of total histones was obtained according to the protocol provided by the Histone Extraction Kit (Abcam). Protein concentration was determined through Bradford method and samples were subjected to 10–12% SDS-PAGE. Gels were electroblotted into nitrocellulose membranes that were probed with the primary antibodies described above. Membranes were incubated with an enhanced chemiluminescence (ECL) reagent solution (GE Healthcare, Hilden, Germany) and exposed to X-ray film (Santa Cruz). Immunoreactive bands density was quantified with ImageLab v4.0 analysis software (Bio-Rad, Hercules, CA, USA).

Luciferase assay

Cells were transiently co-transfected with a firefly luciferase construct (100 ng) containing the Transcriptional Responsive Elements (TREs) of selected genes and the Renilla luciferase vector (10 ng) to normalize transfection efficiency (Cignal Finder Reporter assay kit, QIAGEN, Hilden, Germany). A non-inducible reporter construct encoding firefly luciferase under the control of a basal promoter element (TATA box), without any additional TREs was used as negative control. The efficiency of transfection was evaluated in cells transfected with a GFP construct as reporter. After 18h from transfection, a dual luciferase assay was performed according to manufacturer's instruction (Promega, Madison, WI, USA). Luciferase readings were measured using an EnSpire-2300 luminometer (Perkin Elmer, Waltham, MA, USA). Data were represented as relative luciferase activity, obtained by the ratio of firefly values (promoter reporter) to Renilla values (control reporter). Experiments in triplicate were repeated at least three times, and values were expressed as the mean ± SD.

Isolation and enrichment of ubiquitinated c-Myc

Isolation of ubiquitinylated proteins was performed using UBIQAPTURE-Q kit (Enzo Life Science, Lausen, Switzerland) following manufacturer's instructions. Briefly, total protein extracts were obtained using buffer A (20 mM TRIS, 100 mM NaCl, 5 mM EDTA) containing protease/phosphatase inhibitors. 25 µg of total lysate added to the affinity matrix and incubated at 4°C overnight. Samples were centrifuged to collect the supernatant representing the 'unbound fraction' (UF). The elution of ubiquitin-protein conjugates (EF) was carried out by adding SDS-PAGE gel loading buffer 1X (250 mM TRIS, pH 6.8, 15% SDS, 50% glycerol, 25% mercaptoethanol, 0.01% bromophenol blue), followed by mixing at room temperature for 5 min, heating to 95° C for 10 min and clarification. Equal volumes of the obtained 'eluted fractions', 'unbound fractions' and original lysates, prepared likewise, were subjected to western blotting analysis, using anti-c-Myc primary antibody. To assess the efficiency of ubiquitinated protein isolation, control lysate supplied in the kit was processed in parallel.

Immunoprecipitation assay

The IP experiments were performed using the Pierce Classic IP Kit (Thermo Scientific, Rockford, IL, USA). About 700 µg of whole lysates obtained in IP Lysis/Wash Buffer (25 mM TRIS, 150 mM NaCl, 1mM EDTA, 1% NP-40, 5% glycerol, pH 7.4) containing protease/phosphatase inhibitors,

were pre-cleared with the Control Agarose Resin for 1 h. The cleared lysates were combined with 7 µg of anti-FBXW7 primary antibody and incubated overnight at 4° C with gentle mixing to form the immune complexes. Subsequently, 20 µL of the Pierce Protein A/G Agarose resin suspension were placed into the spin columns provided, washed twice with ice-cold IP Lysis/Wash Buffer and then incubated with the antibody/lysate samples for two hours. Columns were spun by centrifuge at 1000g for 1 min to collect the flow-through and the resin was washed three times with IP Lysis/Wash Buffer and once with 1X Conditioning Buffer. Elution of immune complexes was carried out by adding 50 µL of 2X Non-reducing Lane Marker Sample Buffer with a final concentration of 20 mM DTT and incubated at 100° C for 10 min. Eluates were collected by spinning and applied to SDS-PAGE gel.

RNA extraction and PCR

Total RNA extraction, cDNA synthesis and reverse-transcription PCR were performed as previously described [Proto et al, 2012]. Primer pairs specific to human FDPS (50-CAGATCTGCTGGTATCAGAA-30 forward and 50-GTGCTCCTTCTCGCCATCAAT-30 reverse) or to human Actin B (50-ACTGGGACGACATGGAGAA-30 forward and 50-ATCTTCATGAGGTAGTCAGTCA-30 reverse) were used. All reactions were performed at least in triplicate in three independent experiments; the PCR products were quantified with ImageLab v4.0 analysis software (Bio-Rad) and results were normalized to those obtained from Actin B.

Genomic DNA extraction

U87, U251 and T98 cells were plated into 60mm dishes, treated with 10 µM IPA, 10 µM N6-BA, 500 µM 5-AZA-dC or IPA-5-AZA-dC and collected after 24h. Pellets of about $1x10^6$ cells were dissolved overnight in saline tris-EDTA (1X STE Buffer, 10 mM Tris-HCl pH 8, 1 mM EDTA, 100 mM NaCl) solution containing 0.5% sodium dodecyl sulfate and 0.2 mg/mL proteinase K (Sigma) at 55° C with shaking. After overnight incubation, phenol/chloroform extraction was performed to denature and remove the protein content. Briefly, the solution was mixed with Phenol:Chloroform:Isoamyl alcohol (25:24:1 in volume) solution (Sigma) for 10 minutes and centrifuged at 5000 rpm for 20 min at room temperature. The upper clear aqueous phase containing DNA was collected into a new tube, precipitated with 1/10 volume of 3M sodium acetate (pH 5.2) and 2,2 volume of cold absolute ethanol and then kept at −80° C for at least one hour. After

washing with cold 70% ethanol, the pelleted DNA was air-dried, then dissolved in 1X TE (1mM Tris-HCl pH 8, 0.1 mM EDTA) and quantified with NanoDrop 2000 (Thermo Fisher Scientific).
DNA extraction from frozen tissues of GBM patients resected tumors was conducted following the protocol described by Fan and Gulley (2001). Pure DNA with a ratio absorbance A260/ A280 > 1.7 was subjected to Next Generation Sequencing (Eurofins Scientific) for characterization of single nucleotide variants (SNVs), insertions and deletions (InDel), copy number variations (CNV) and fusion events.

Drug combination analysis

Drug combination analysis was performed as previously described [Fiore et al, 2018]. Briefly, HCT116, DLD1 and SW48 cells were exposed to various concentrations of IPA and/or 5-FU, to evaluate cells viability, colorimetric MTT assay was used. Pharmacological interaction between IPA and 5-FU, were calculated using CalcuSyn v2.0 software (BioSoft, Ferguson, MO, USA), a dedicated software based on the Chou-Talalay method. This allows to calculation of two parameters: Combination Index (CI)—to define synergism (CI < 1), additive effect (CI = 1) and antagonism (CI > 1) – and Dose Reduction Index (DRI) [Chou, 2010]. Assessment of drug interactions was performed calculating CI after treatment for 48 h with IPA and 5-FU in combination (constant molar ratio 1:2.5) and as single drugs, ranging from 0.08 µM to 10 µM of IPA and from 0.2 µM to 25 µM of 5-FU.

DNMT activity assay

In nuclear extracts obtained from GBM cells through the EpiQuik™ Nuclear Extraction kit (EpiGentek Group Inc., NY, USA), DNMTs enzymatic activity (*de novo*, maintenance) was measured using DNMT Activity Assay Kit (ab113467, Abcam), a colorimetric kit based on ELISA-like reaction following the manufacturer's instructions. In brief, optimized nuclear extracts (10 µg) containing purified DNMTs, positive and negative control were diluted with 1X AdoMet working buffer and incubated at 37°C for 120 min, in microplate wells coated with DNA substrate. Subsequently, the wells were washed three times with 1X Wash Buffer and then incubated with of the Diluted Capture Antibody for 60 min, at room temperature protected from the light. After washing, the plate was incubated with Diluted Detection Antibody and then with Diluted Enhancer Solution for 30 min. Finally, for signal detection Developer Solution were added and the colorimetric reaction was monitored for 10 min, away from direct light, until development of blue

colour was detected in positive control wells. The reaction was stopped by adding Stop Solution and the absorbance was immediately read at 450 nm and at 655nm for wavelength correction. The ratio which is proportional to enzyme activity was calculated with the formula:

$$\text{DNMT Activity (OD/h/mg)} = \frac{\text{Sample OD} - \text{Blank OD}}{\text{Protein Amount (μg) x Hour (h)}} \text{x1000}$$

Global DNA methylation assay

Global DNA methylation was evaluated through the MethylFlash™ Global DNA Methylation (5-mC) ELISA Easy Kit (EpiGentek Group Inc., NY, USA) measuring levels of 5-methylcytosine (5-mC). About 100 ng of input DNA from GBM cells, extracted with protocol described above, was added to a microplate well with high affinity for DNA binding. Negative control (NC) and different percentages of positive control (PC) were prepared according to the manufacturer's indications to set the standard curve and determine the slope. Plate was covered and incubated at 37°C for 60 minutes. Following washing, 5-mC Detection Complex Solution was added to the plate and removed after 50 minutes at room temperature. Colorimetric reaction was triggered by the addition of Developer Solution and stopped when the 5% PC turned into medium blue. Absorbance was immediately read at 450 nm. DNA methylation was calculated as:

$$\text{5mC\%} = \frac{\text{Sample OD} - \text{NC OD}}{\text{Slope x input DNA amount (ng)}} \text{x100}$$

Statistical analysis

Data obtained from multiple experiments were calculated as means ± SD, if not otherwise specified, and analysed for statistical significance by using the two tailed Student t-test. All data shown are representative of at least three independent experiments performed in triplicate. Values of $p < 0.05$ were considered statistically significant.

RESULTS

CRC RESULTS

IPA and N6-BA trigger cell death in CRC cells.

Previous findings evidenced the *in vitro* antiproliferative effect of IPA and N6-BA in human cancers [Laezza et al 2009; Rajabi et al, 2011; Ciaglia et al, 2017b]. We reported that IPA significantly inhibited HCT116 and DLD1 CRC cells proliferation, in a dose- and time-dependent manner, starting from 5 µM after 24h of treatment (Figure 1A and 1B). Cytofluorimetric analysis of PI stained DLD1 and HCT116 cells, revealed that the treatment with IPA arrested the cells in the S phase of cell cycle (Figure 1C). To understand if the inhibition of proliferation and S phase block matched with cell death induction, we performed apoptosis assay. Accordingly with previous results, IPA significantly increased PI/Annexin V-FITC double stained cells, suggesting the induction of apoptotic death (Figure 1D). Apoptosis was further confirmed by western blot analysis of activated Caspase 3 and PARP (Figure 1E), both cleaved after 24h of treatment.

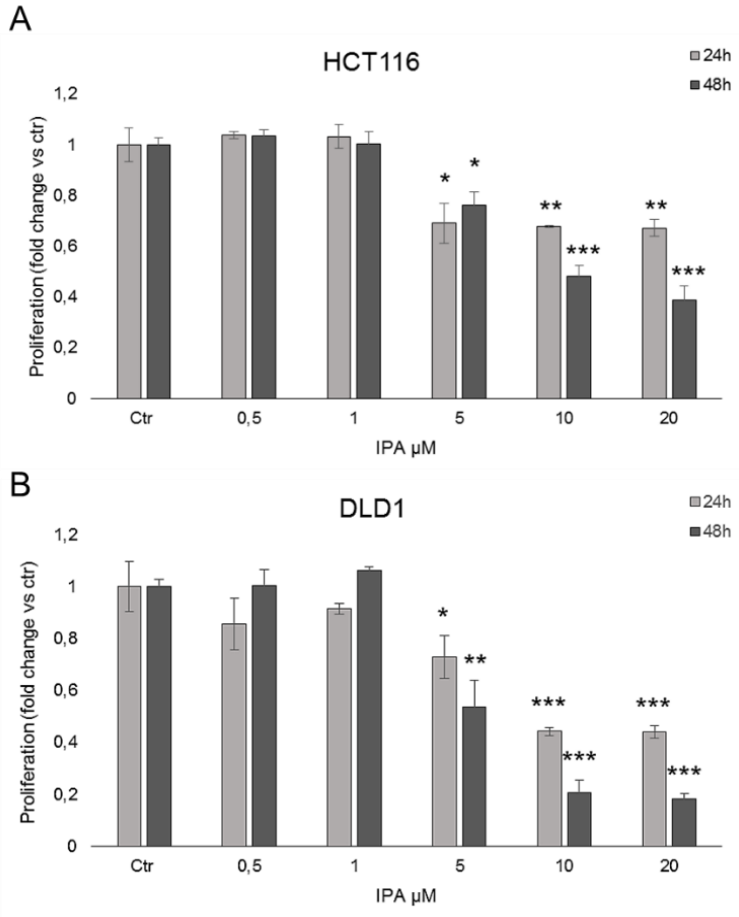

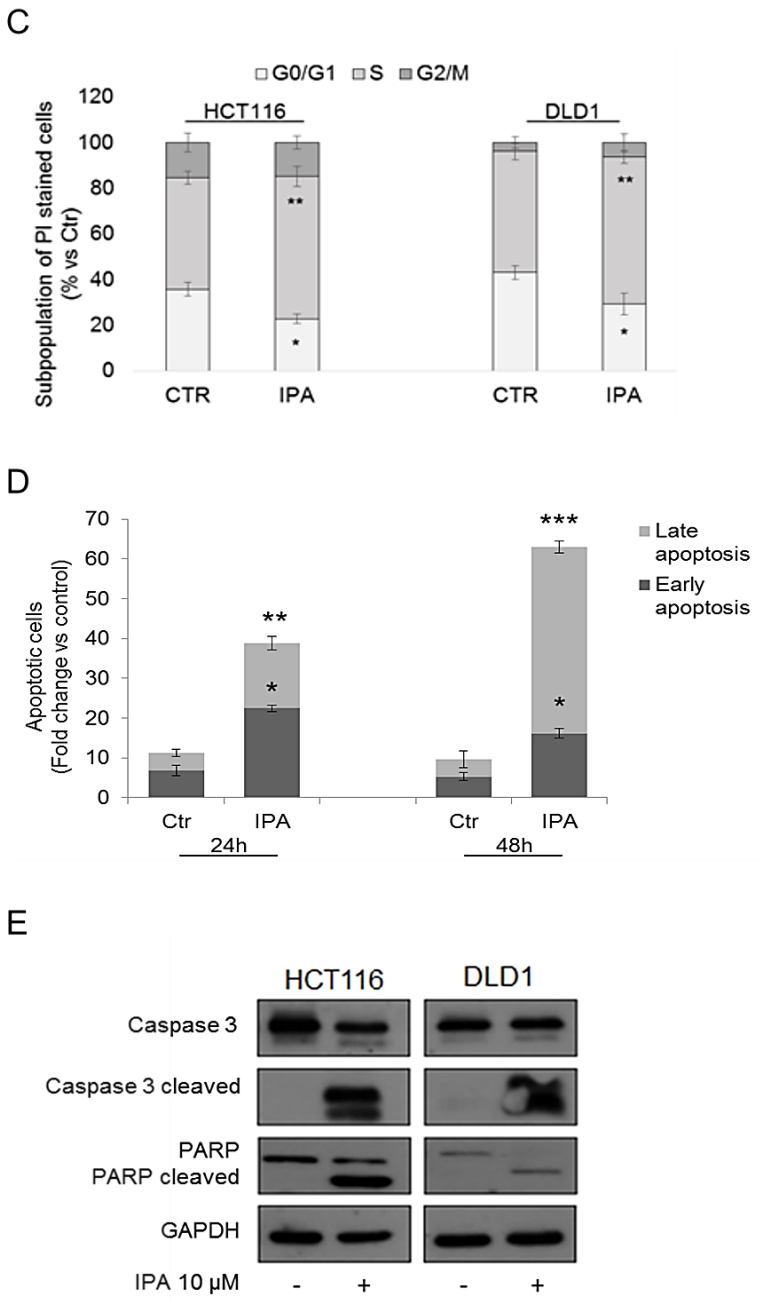

Figure 1. Effect of IPA on CRC cells *in vitro*. BrdU incorporation assay in HCT116 (**A**) and DLD1 (**B**) cells treated with indicated concentrations of IPA, for 24 h or 48 h. (**C**) Cell cycle analysis of HCT116 and DLD1 cells treated with IPA for 24 h and stained with PI. (**D**) Cytofluorimetric apoptosis analysis of Annexin V-FITC/PI double-stained DLD1 cells treated with 10 µM IPA, for 24 h and 48 h. Data are expressed as mean ± standard deviation (SD) of five independent experiments in triplicate. * $p < 0.05$, ** $p < 0.01$, *** $p < 0.005$ versus (vs.) control. (**E**) Representative western blot of apoptotic pathway activation in DLD1 and HCT116 cells. GAPDH was used as loading control.

Inhibition of cell proliferation and Caspase 3 cleavage were also verified in CRC cells treated with N6-BA, which produced an effect almost comparable to the parent compound IPA on equal terms.

Analogously to IPA, N6-BA significant inhibit proliferation with a dose-dependent effect starting from the intermediate 5 µM concentration after 24h of treatment and markedly after 48h in both HCT116 and DLD1 (Figure 2)

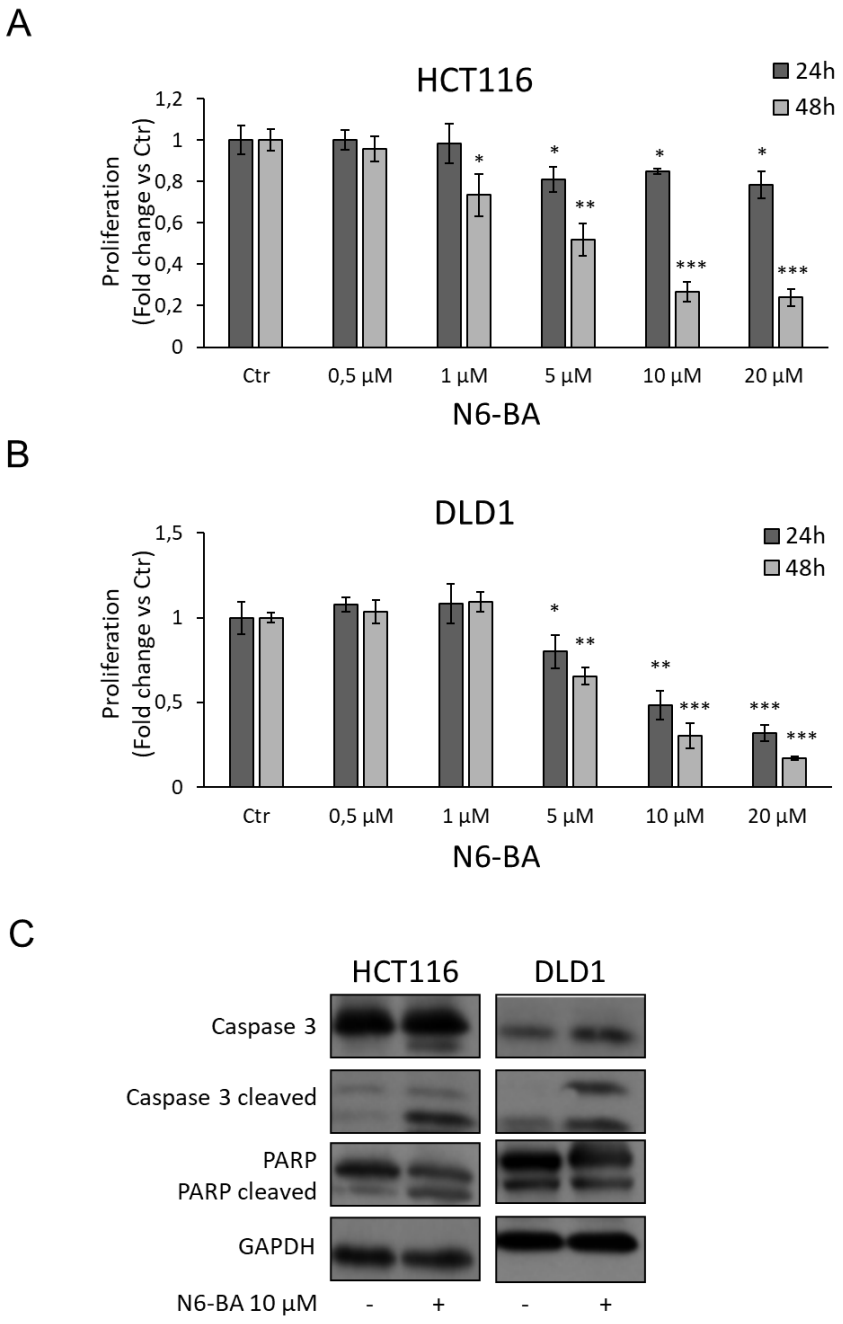

Figure 2. Effect of N6-BA on CRC cells *in vitro*. BrdU incorporation assay in HCT116 (**A**) and DLD1 (**B**) cells treated with indicated concentrations of N6-BA, for 24 h or 48 h. Data are expressed as mean ± SD of at least three independent experiments. * $p < 0.05$, ** $p < 0.01$, *** $p < 0.005$ vs. control. (**C**). Representative western blot of apoptotic pathway activation in HCT116 and DLD1 cells. GAPDH was used as loading control.

IPA and N6-BA up-regulate FBXW7 expression.

Our and others previous studies suggested that IPA seems to be involved in UPS regulation [Colombo et al, 2009; Ciaglia et al, 2017a]. We then focused our attention on FBXW7, tumor-suppressor strongly implicated in colorectal carcinogenesis [Yeh et al, 2018]. Since c-Myc is a well-known substrate of FBXW7 [Sailo et al, 2019], we analysed its protein expression in DLD1 and HCT116 cells harboring wild type FBXW7 gene [Tong et al, 2017], starting from 30 minutes of treatment with IPA. In HCT116 cells, IPA induced c-Myc expression after 2h and 6h of treatment. Coherently, FBXW7 expression was strongly induced by IPA after 6h of treatment, but after 24h of IPA exposure, compared to untreated cells, the levels of both c-Myc and FBXW7 tended to decrease (Figure 3A). In DLD1 cells - that have a high percentage of methylated CpG sites in FBXW7 promoter [Akhoondi et al, 2010] - expression trend after treatment with IPA was slightly different compared to HCT116. c-Myc expression showed a biphasic expression while FBXW7 expression increased after 2h of treatment, when c-Myc levels tended to decrease (Figure 3B). To gain further evidence about the involvement of FBXW7-c-Myc crosstalk in IPA molecular mechanism, we analysed IPA effect in SW48 cells, harboring FBXW7 heterozygous frame-shift deletion (c.2001delG), that affects substrate binding [Tong et al, 2017]. We observed that the treatment significantly inhibited SW48 proliferation and induced apoptosis, as well as in HCT116 and DLD1, but was not able to induce FBXW7 expression leading to a time-dependent accumulation of c-Myc (Figure 3C), most likely due to the loss of FBXW7-dependent degradation.

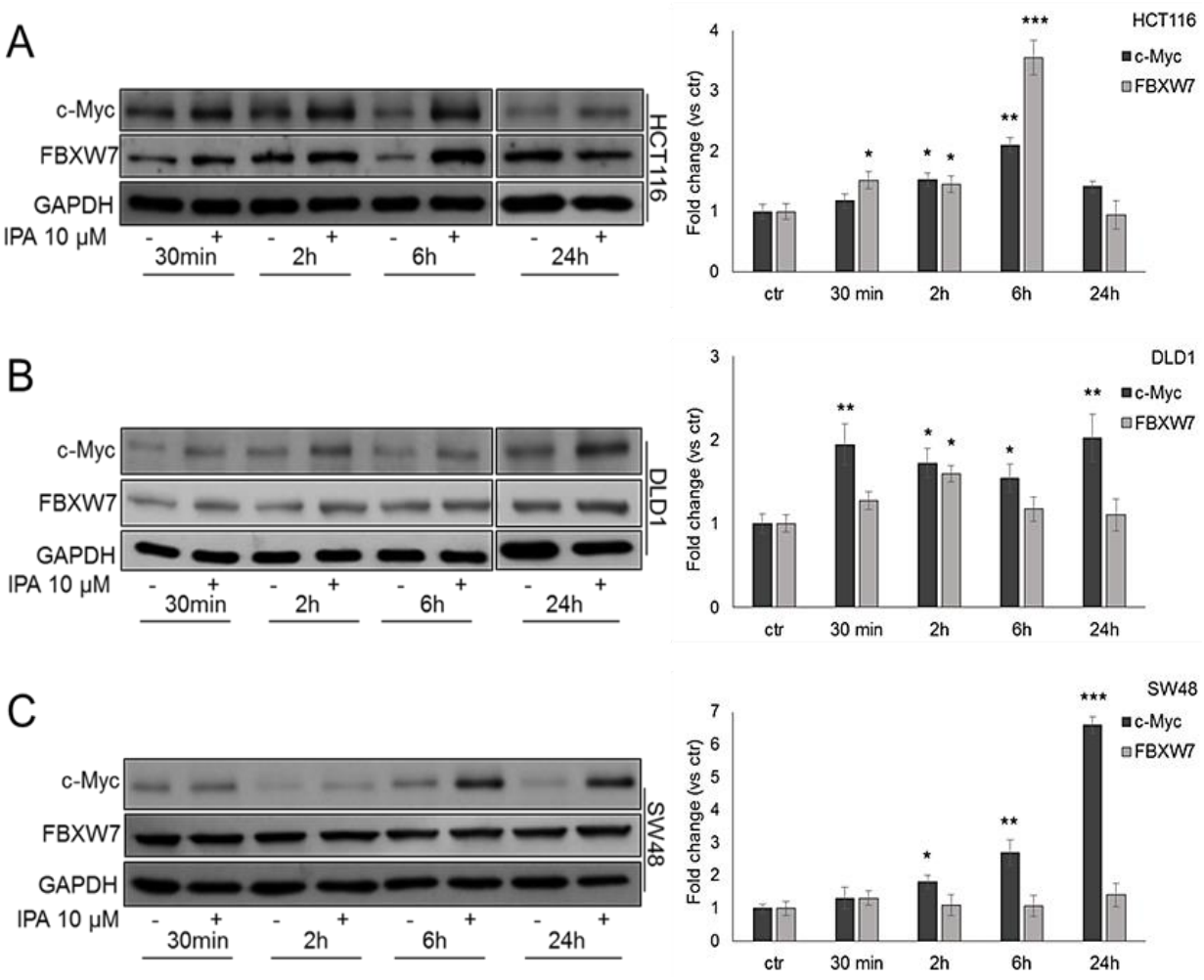

Figure 3. IPA modulates FBXW7 and c-Myc expression. Representative western blot and relative densitometry analysis (histograms on the right) of FBXW7 and c-Myc protein expression in HCT116 (**A**), DLD1 (**B**) and SW48 (**C**) cells, treated with IPA at the indicated time points. GAPDH was used as loading control. Data are expressed as mean ± SD of five independent experiments. * $p < 0.05$, ** $p < 0.01$, *** $p < 0.005$ vs. control.

To verify if the structural analogue N6-BA could yield a replicable effect on FBXW7 modulation, we first analysed FBXW7 expression in all CRC cell lines at chosen time points (2 and 24h). In HCT116, the F-box protein levels were significantly up-regulated at early time, with a marked and sustained effect at prolonged N6-BA exposure. In DLD1 cells, a significant increase of FBXW7 levels was only observed at 24h, while, analogously to IPA, FBXW7 was not altered by N6-BA treatment in SW48. These preliminary observations suggested that also the IPA benzyl-analogue, with a few differences, is able to modulate FBXW7 expression (Figure 4).

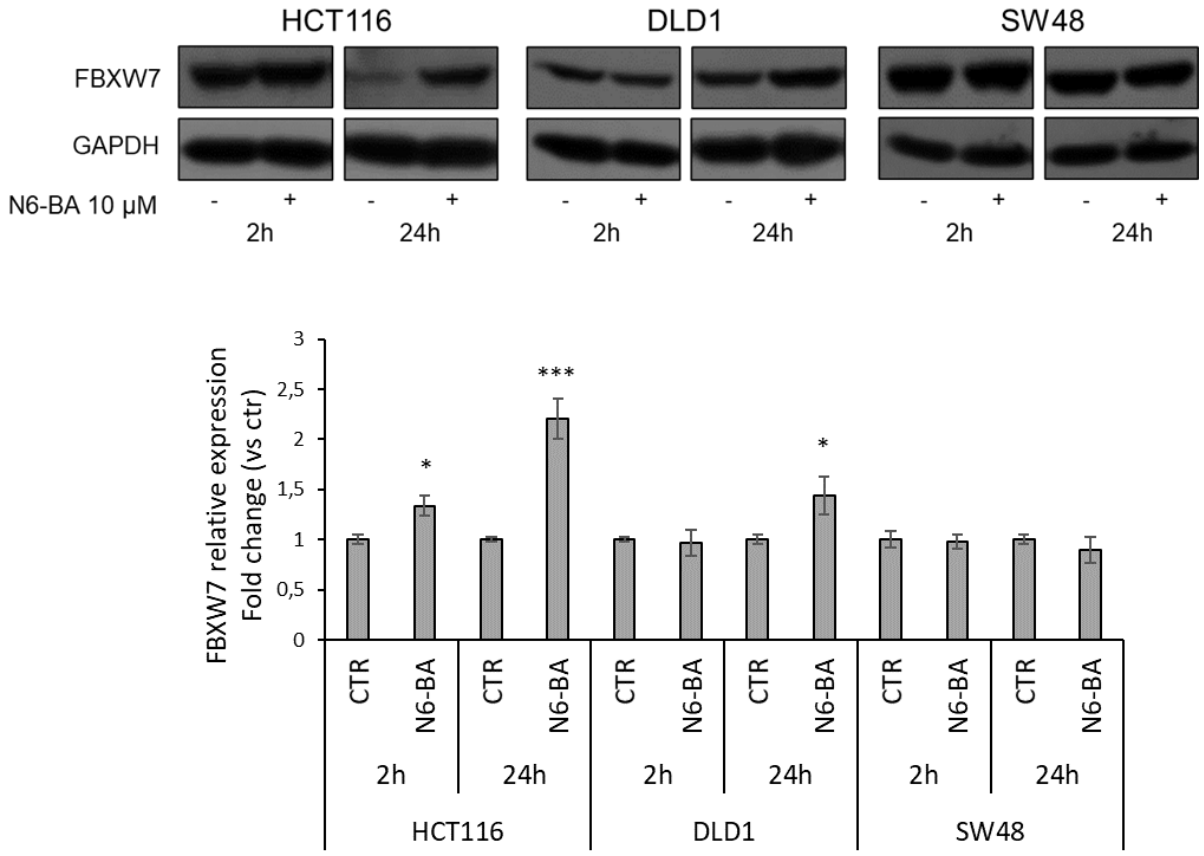

Figure 4. N6-BA modulates FBXW7 expression. Representative western blot and relative densitometric analysis of FBXW7 protein expression in HCT116, DLD1 and SW48 cells, treated with N6-BA for 2h or 24h. GAPDH was used as loading control. Data are expressed as mean ± SD of three independent experiments. * $p < 0.05$, *** $p < 0.005$ vs. control.

IPA inhibits c-Myc transcriptional activity.

To exclude that the observed c-Myc increase was accompanied by a gain of its oncogenic activity, we analysed the effect of IPA on c-Myc promoter activation through luciferase assay. In both HCT116 and DLD1 cells, transiently transfected with a reporter containing Transcriptional Responsive elements (TRE) for E-box binding element, after 24 h of treatment with IPA, luciferase activity was inhibited of about 50%, compared to untreated cells (Figure 5A). This result demonstrated that the increase of c-Myc protein levels produced by IPA did not coincide with an increase of c-Myc/Max transcriptional activity, rather suggesting it could be due to additional mechanisms such as Post Transcriptional Modifications (PTMs), and in particular, given the increase of FBXW7 expression, to its ubiquitination.

IPA induces FBXW7-dependent c-Myc ubiquitination.

c-Myc ubiquitination occurs after GSK3β-mediated phosphorylation on Thr-58 residue, in MYC Box I, that allows FBXW7 to physically recognize c-Myc for subsequent ubiquitination [Welcker et al, 2004]. We then analysed the amount of phosphorylated GSK3β on inhibitory residue Ser-9. Accordingly to c-Myc transcriptional inactivation, IPA strongly reduced Ser-9 phosphorylation after 24 h of treatment in our three CRC models, but in particular in HCT116 and DLD1 cells (Figure 5C). In line with this, c-Myc phosphorylation (Thr-58) significantly increased after 2 h of treatment with IPA in all cell lines analysed, but the induction persisted after 24h of treatment, in HCT116 and DLD1 cells only (Figure 5C). To verify the hypothesis of IPA-mediated c-Myc ubiquitination, we pulled-down mono- and poly-ubiquitinated proteins, using a high-binding affinity matrix. As shown in Figure 5B, the amount of c-Myc was significantly raised in eluted fraction (EF) containing ubiquitinated protein, from IPA-treated DLD1 and even more in HCT116 cells, compared to EF from untreated cells; this turning out that, in FBXW7 wild type cells, the increase of c-Myc protein expression was ascribable to its ubiquitination. In SW48, FBXW7$^{+/-}$ cell line, the amount of ubiquitinated c-Myc was very slight, compared to wild type cells (Figure 5B). Subsequently, we immunoprecipitated FBXW7 to assess its direct binding to c-Myc in CRC cell lines treated with the compound. Consistent with previous results, IPA strongly induced the binding of c-Myc and FBXW7 in both HCT116 and DLD1, but not in SW48 FBXW7+/− cells, thus confirming that in wild type cells, the IPA-mediated ubiquitination was FBXW7-dependent (Figure 5D).

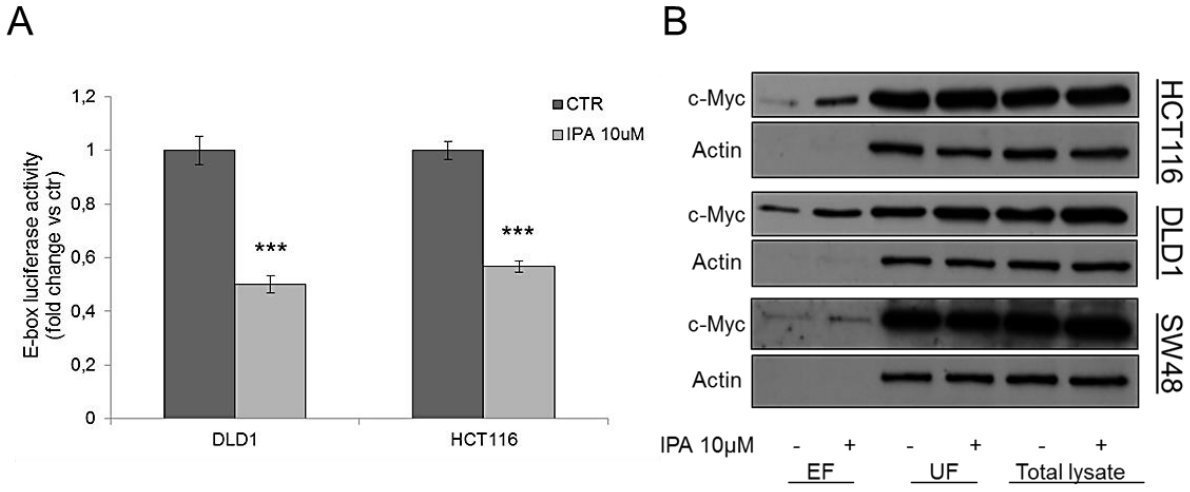

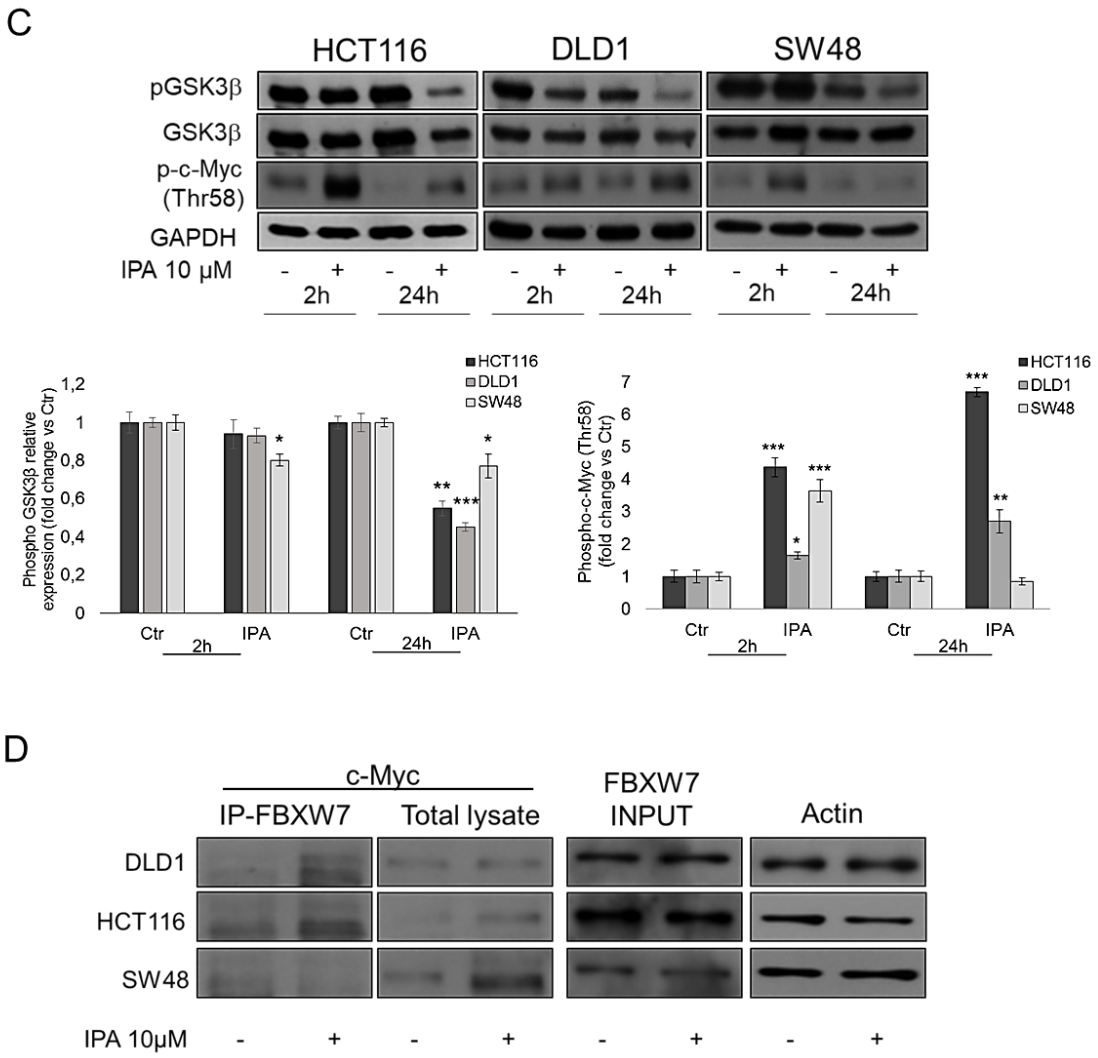

Figure 5. IPA affects c-Myc transcriptional activity through its ubiquitination. (**A**) Analysis of luciferase activity controlled by E-box elements in HCT116 and DLD1 cell lines. The histograms represent luciferase activity measured at 18 h from transfection of HCT116 and DLD1 cells transfected with reporter construct containing the E-box elements for c-Myc and treated with IPA 10 μM or vehicle. Firefly luciferase was normalized to *Renilla* luciferase reading and the data were plotted as fold change (mean ± SD of four independent experiments in triplicate; unpaired two tailed Student's *t*-test *** $p < 0.005$) compared to control cells. (**B**) Representative western blot analysis of c-Myc expression in eluted fraction (EF) containing ubiquitinated proteins, unbound fraction (UF) depleted of ubiquitinated protein and whole protein lysates from HCT116, DLD1 and SW48 cells, treated with IPA 10 μM for 2 h. Actin was used as loading control. (**C**) Representative western blot and densitometry analysis of phosphorylated (Thr-58) c-Myc, phosphorylated (Ser9) GSK3β and total GSK3β in HCT116, DLD1 and SW48 cells treated with IPA 10 μM at the indicated time points. The histogram represents densitometry analysis of phosphorylated (Thr-58) c-Myc (right) or phosphorylated GSK3β expressed as fold change vs. total GSK3β (left), normalized vs. GAPDH. Data are expressed as mean ± SD of five independent experiments. * $p < 0.05$, ** $p < 0.01$, *** $p < 0.005$ vs. control. (**D**) DLD1, HCT116 and SW48 cells were treated with IPA or vehicle for 2 h. FBXW7 was Immunoprecipitated using anti-FBXW7 antibody. c-Myc expression was analysed in FBXW7-IP fractions (to assess the reciprocal binding) and total cell lysates. FBXW7 protein levels before the IP was used as INPUT and Actin was used as loading control. Blots are representative of at least three independent experiments.

N6-BA induce GSK3β-dependent phosphorylation on c-Myc Thr58 residue

Since N6-BA produced effects comparable to IPA in inhibiting cell proliferation and modulating FBXW7 expression, we supposed it could act in a similar way on the same targets. Indeed, as expected, N6-BA reduced the inhibitory phosphorylation of GSK3β (Ser9) and increased the degradation tag of c-Myc (Thr58) in FBXW7wt cells (Figure 6). This suggest that the observed up-regulation of FBXW7 is downstream followed by a GSK-dependent degradation of its substrate c-Myc, and also that the modified adenosines could target the same axis.

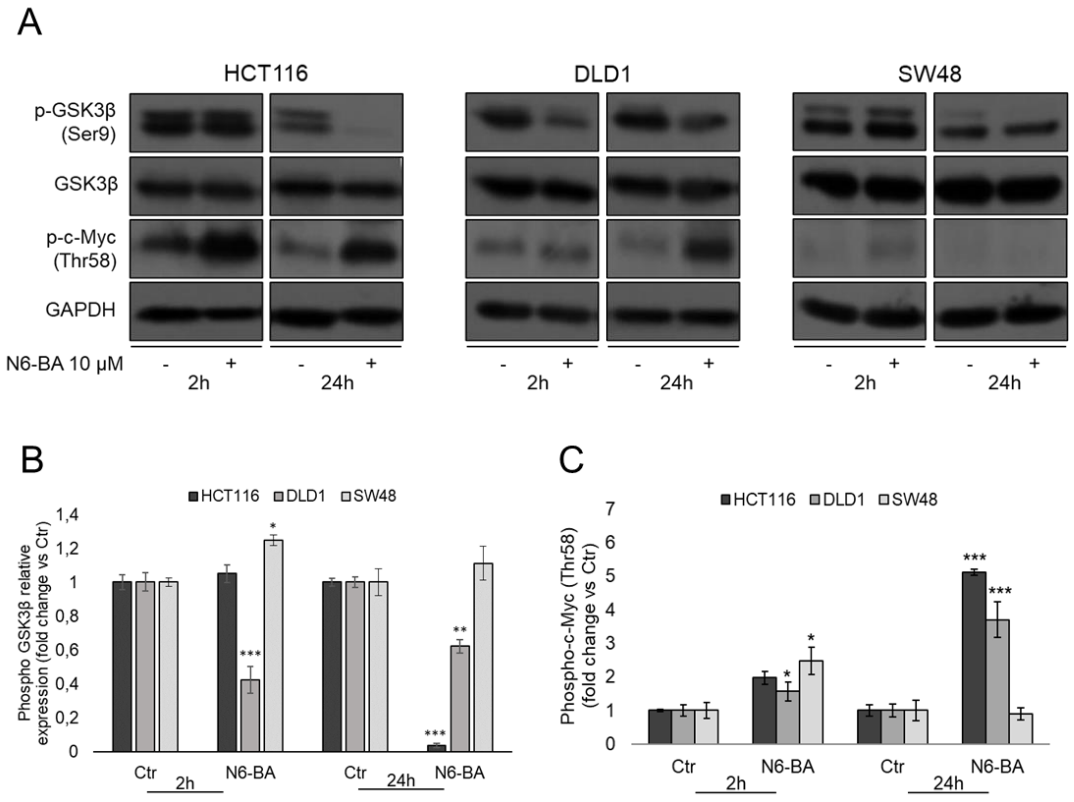

Figure 6. Representative western blot (**A**) and densitometric analysis of phosphorylated GSK3β (Ser9) (**B**) and total GSK3β and phosphorylated c-Myc (Thr-58) (**C**) in HCT116, DLD1 and SW48 cells treated with N6-BA 10 μM at the indicated time points. GAPDH was used as loading control. Data are expressed as mean ± SD of three independent experiments. * $p < 0.05$, ** $p < 0.01$, *** $p < 0.005$ vs. control.

IPA and N6-BA affect SREBP/FDPS axis in FBXW7-dependent manner.

Sterol regulatory element-binding proteins (SREBPs) are transcription factors regulating the expression of genes involved in cholesterol and lipid biosynthesis, including FDPS gene. In CRC, downregulation of SREBPs arrests tumor growth, altering cellular metabolism. SREBPs become transcriptional active after cleavage in mature forms that, upon DNA binding, are degraded via proteasome. In this step, GSK3β catalyzes the phosphorylation of mature SREBP1, mediating the

interaction with FBXW7 and thus its ubiquitination [Punga et al, 2006]. To evaluate the hypothesis that IPA and N6-BA probably regulate the FBXW7/SREBP/FDPS axis, we analysed protein levels of SREBP1 inactive precursor and mature form. In HCT116 and DLD1 cells, IPA significantly decreased protein expression of both precursor and active mature form of SREBP1, especially after 24h. In SW48 FBXW7$^{+/-}$ cells, IPA failed to reduce SREBP1 expression, leading to its accumulation, as expected (Figure 7A). These considerations were remarked when we treated CRC cells with N6-BA which modulated SREBP1 with a very replicable trend if compared to IPA (Figure 7C). In our previous study, IPA was found to inhibit both the activity and mRNA expression of FDPS, in DLD1 cells [Laezza et al, 2009]. Moreover, according to Saturation transfer difference-Nuclear Magnetic Resonance (STD-NMR) experiments and enzymatic cell-free assays, the cytostatic activity of N6-BA, just like IPA, was related at least in part to the structural interaction with FDPS [Ciaglia et al, 2017b]. Then, we confirmed that, coherently with FBXW7-mediated SREBP1 downregulation, FDPS mRNA expression clearly decreased after treatment with IPA, in HCT116 and DLD1 cells. In SW48 cells, the failed degradation and then the accumulation of SREBP1 translated into a slight increase of FDPS gene expression (Figure 7A and 7B).

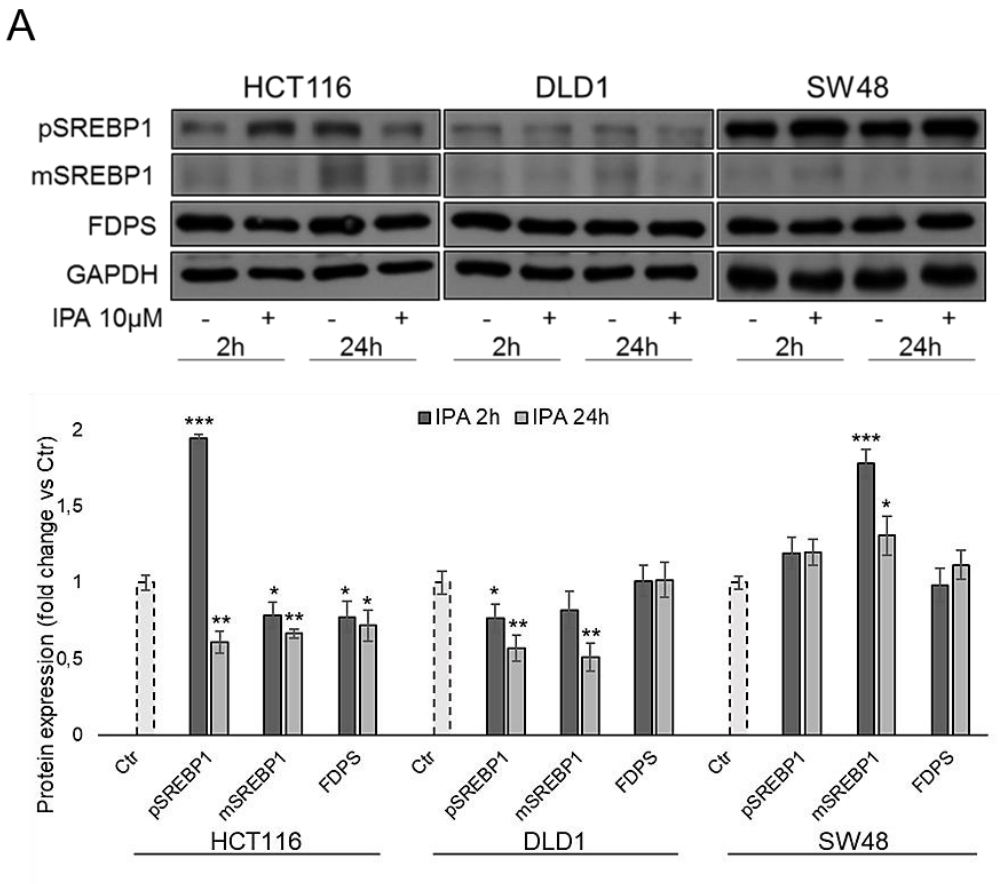

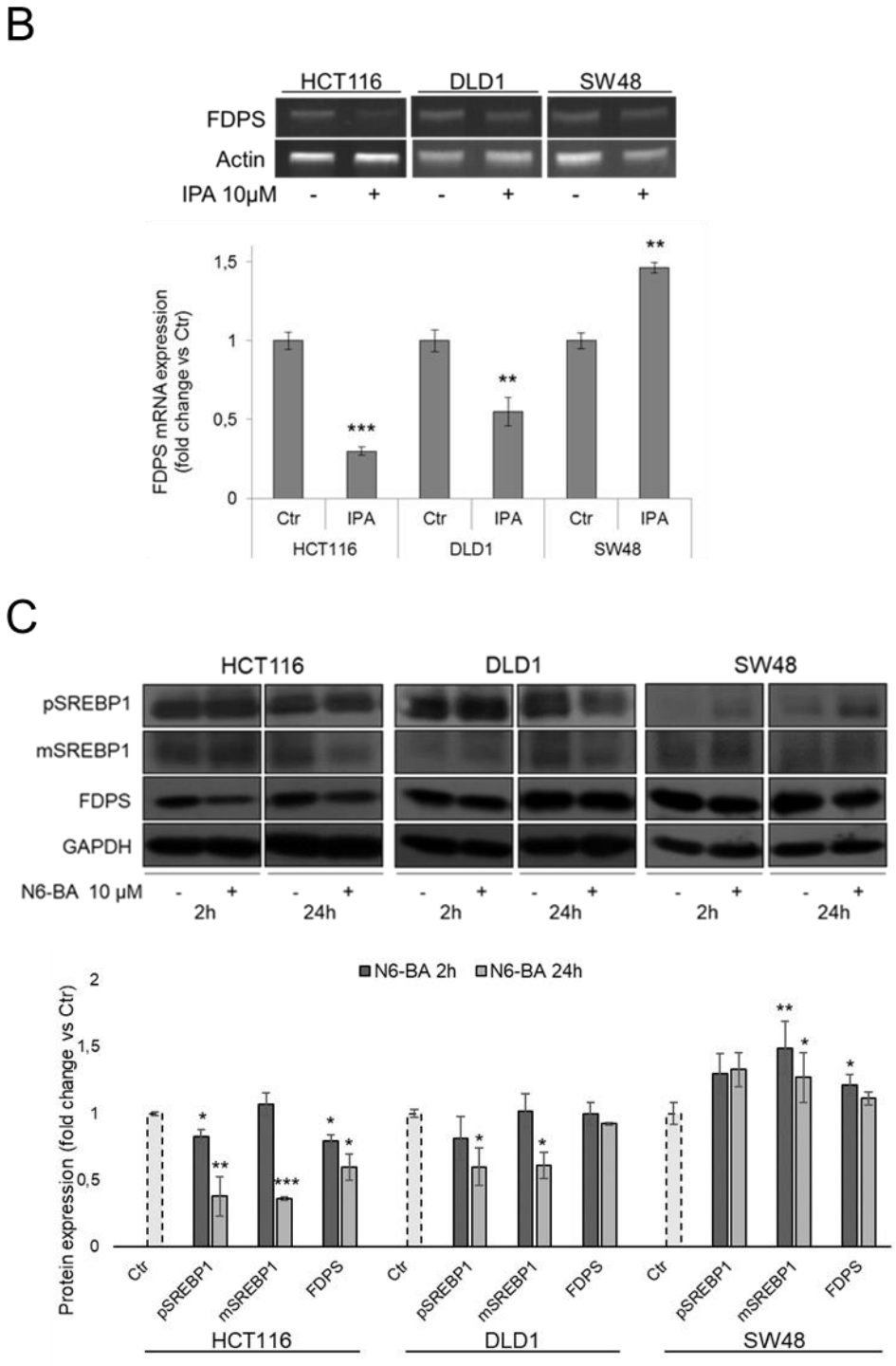

Figure 7. Modulation of SREBP/FDPS axis by IPA and N6-BA. Representative western blot and densitometric analysis of SREBP1 precursor (pSREBP1), mature form (mSREBP1) and FDPS expression in HCT116, DLD1 and SW48 cells treated with IPA (**A**) or N6-BA (**C**). GAPDH was used as loading control. Data are expressed as mean ± SD of six independent experiments. * $p < 0.05$, ** $p < 0.01$, *** $p < 0.005$ vs. control. (**B**) mRNA expression of FDPS gene determined by RT-PCR, in HCT116, DLD1 and SW48 cells after 24h of treatment with IPA 10 μM. Actin was used as loading control. The histograms report the quantification of the intensity bands expressed as mean ± SD of five independent experiments ** $p < 0.01$, *** $p < 0.005$ vs. control.

To verify if IPA and its analogue effectively inhibited FDPS activity in CRC cells, we analysed the levels of HDJ2, a chaperone protein that exclusively undergoes farnesylation. Unfarnesylated HDJ2, compared to farnesylated protein, runs with a higher molecular weight on SDS-PAGE gel, producing a mobility-shift identifiable by western blot analysis [Adjei et al, 2000]. The mobility shift of unfarnesylated HDJ2 observed in both FBXW7 wild type and mutant cells treated with IPA suggested the early inhibition of FDPS activity, persistent after 24h and even more significant in FBXW7wt cells treated with N6-BA (Figure 8), in agreement with previously obtained results [Laezza et al, 2009; Ciaglia et al, 2017b].

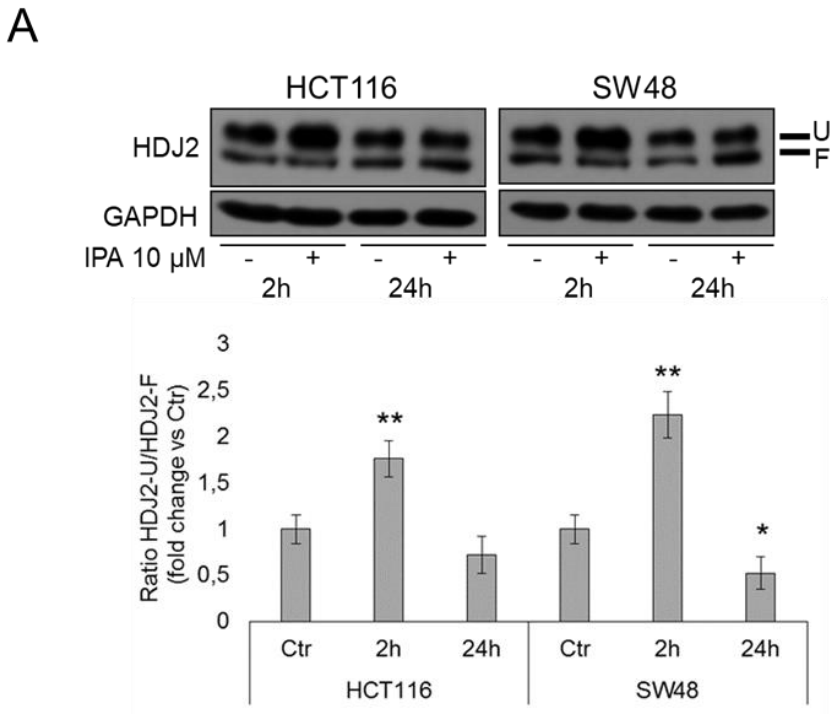

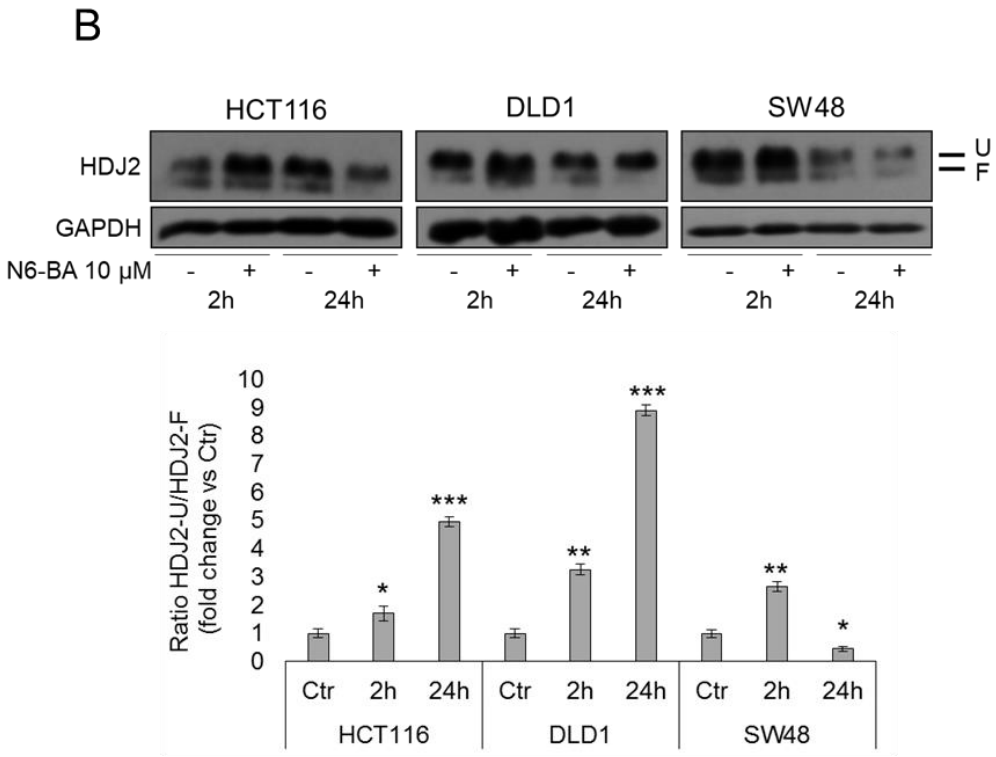

Figure 8. Representative western blot of mobility-shifted Farnesylated (F) and Unfarnesylated (U) HDJ2 on SDS-PAGE gel, in HCT116 and SW48 cells treated with IPA (**A**) or HCT116, DLD1 and SW48 treated with N6-BA (**B**). The histograms represent densitometric analysis of Unfarnesylated HDJ2 expressed as fold change vs. Farnesylated HDJ2 and normalized versus GAPDH. Data are expressed as mean ± SD of three independent experiments * $p < 0.05$, ** $p < 0.01$, *** $p < 0.005$ vs. control.

Involvement of FBXW7 in drug resistance mechanisms and synergistic interaction of IPA and 5-FU

The involvement of FBXW7 in chemoresistance mechanisms is largely accepted. Recent study on human organoids showed that fbxw7ΔG intestinal organoids are less sensitive to 5-fluorouracil (5-FU) treatment [Lorenzi et al, 2016]. One hypothesis explaining resistance to oxaliplatin, 5-FU and tyrosine-kinase inhibitors (TKIs) in CRC and other tumors, involves the failure of another well-known substrate of FBXW7 degradation, the pro-survival Mcl1 protein belonging to the BCL2 family [Tong et al, 2017]. We found that Mcl1 expression in $FBXW7^{wt}$ cells, but not in SW48 $FBXW7^{+/-}$ cells, was strongly reduced by IPA or N6-BA, suggesting that the molecules could potentially control chemoresistance, at least in part, by targeting FBXW7 (Figure 9).

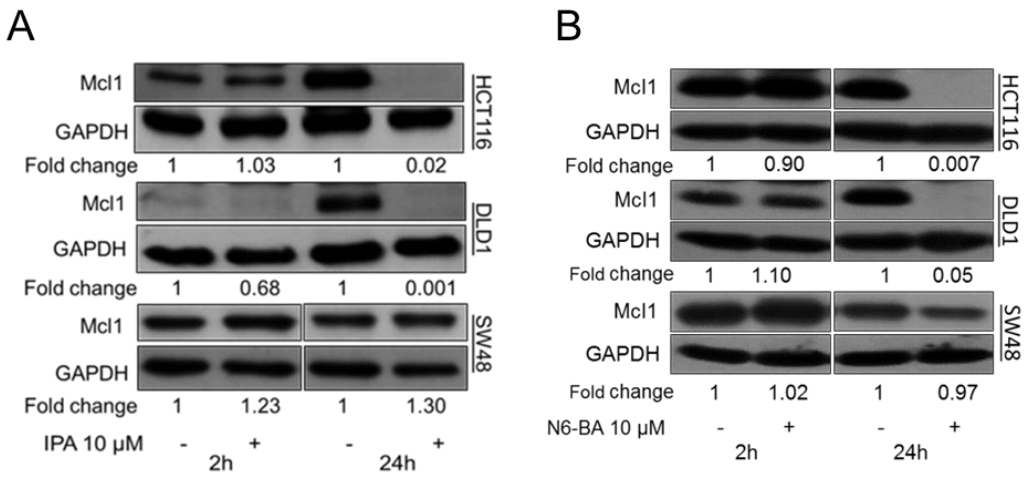

Figure 9. Representative western blot and densitometric analysis (fold change vs. control) of Mcl1 expression in HCT116, DLD1 and SW48 cells treated with IPA (**A**) or N6-BA (**B**). GAPDH was used as loading control.

Therefore, we analysed the pharmacological interaction of IPA and 5-fluorouracil (5-FU) combination using dedicated software CalcuSyn, that allows to calculate Combination Index (CI) and Dose Reduction Index (DRI). As summarized in Table 1, The strongest synergistic interaction (CI 0.11–0.16) has been obtained in HCT116 cells by combined treatment with lowest concentrations of drugs, producing positive DRI. Unexpectedly, despite inhibition of Mcl1, in DLD1 cells IPA and 5-FU combination produced a moderate synergism or nearly additive effect, only for two combinations with intermediate doses, thus antagonizing the effect of 5-FU or IPA used as single agents. Surprisingly, combined treatment of SW48 cells produced a synergistic interaction, with CI slight lower than HCT116, but higher than DLD1 (Table 1). CalcuSyn plots of dose vs. fraction Affected (FA) and FA-CI plots are showed in Figure 10.

Table 1. IPA synergizes with 5FU. Fraction Affected (FA), Combination Index (CI) and Dose Reduction Index (DRI) for IPA and 5FU combination (constant molar ratio 1:2.5) in HCT116, DLD1 and SW48 cells.

HCT116						
Concentration		FA IPA + 5FU	CI and symbols		DRI	
IPA (μM)	5FU (μM)				IPA	5FU
0.08	0.2	0.25	0.11	++++	38.64	11.92
0.16	0.4	0.29	0.16	++++	21.68	8.48
0.31	0.78	0.29	0.31	+++	11.31	4.52
0.63	1.56	0.42	0.33	+++	7.39	5.2
1.25	3.13	0.48	0.5	+++	4.18	3.78
2.5	6.25	0.53	0.79	++	2.35	2.71
5	12.5	0.67	0.95	±	1.56	3.21
10	25	0.79	1.13	-	1.1	4.57

DLD1						
Concentration		FA IPA + 5FU	CI and symbols		DRI	
IPA (μM)	5FU (μM)				IPA	5FU
0.08	0.2	0.19	116.42	-----	23.89	0.01
0.16	0.4	0.35	1.69	---	17.98	0.61
0.31	0.78	0.4	0.99	±	10.3	1.12
0.63	1.56	0.46	0.7	++	5.66	1.91
1.25	3.13	0.45	1.54	---	2.8	0.85
2.5	6.25	0.48	1.78	---	1.49	0.9
5	12.5	0.59	1.23	--	0.93	6.5
10	25	0.83	1.21	--	0.82	3374.52

SW48						
Concentration		FA IPA + 5FU	CI and symbols		DRI	
IPA (μM)	5FU (μM)				IPA	5FU
0.08	0.2	0.21	0.43	+++	6.154	3.701
0.16	0.4	0.21	0.93	±	2.977	1.67
0.31	0.78	0.26	1.02	±	1.991	1.926
0.63	1.56	0.42	0.58	+++	2.091	9.793
1.25	3.13	0.6	0.49	+++	2.12	43.917
2.5	6.25	0.75	0.5	+++	2.03	164.813
5	12.5	0.86	0.48	+++	2.093	779.084
10	25	0.89	0.72	++	1.388	936.115

Fraction Affected (FA), Combination Index (CI) and Dose Reduction Index (DRI) for IPA and 5FU combination (constant molar ratio 1:2.5).
Symbols describe the pharmacological interaction for each combined dose, based on CI obtained from CalcuSyn software (++++ Strong synergism; +++ Synergism; ++ Moderate synergism; ± Nearly additive; - Slight antagonism; -- Moderate antagonism; --- Antagonism; ----- Very strong antagonism).

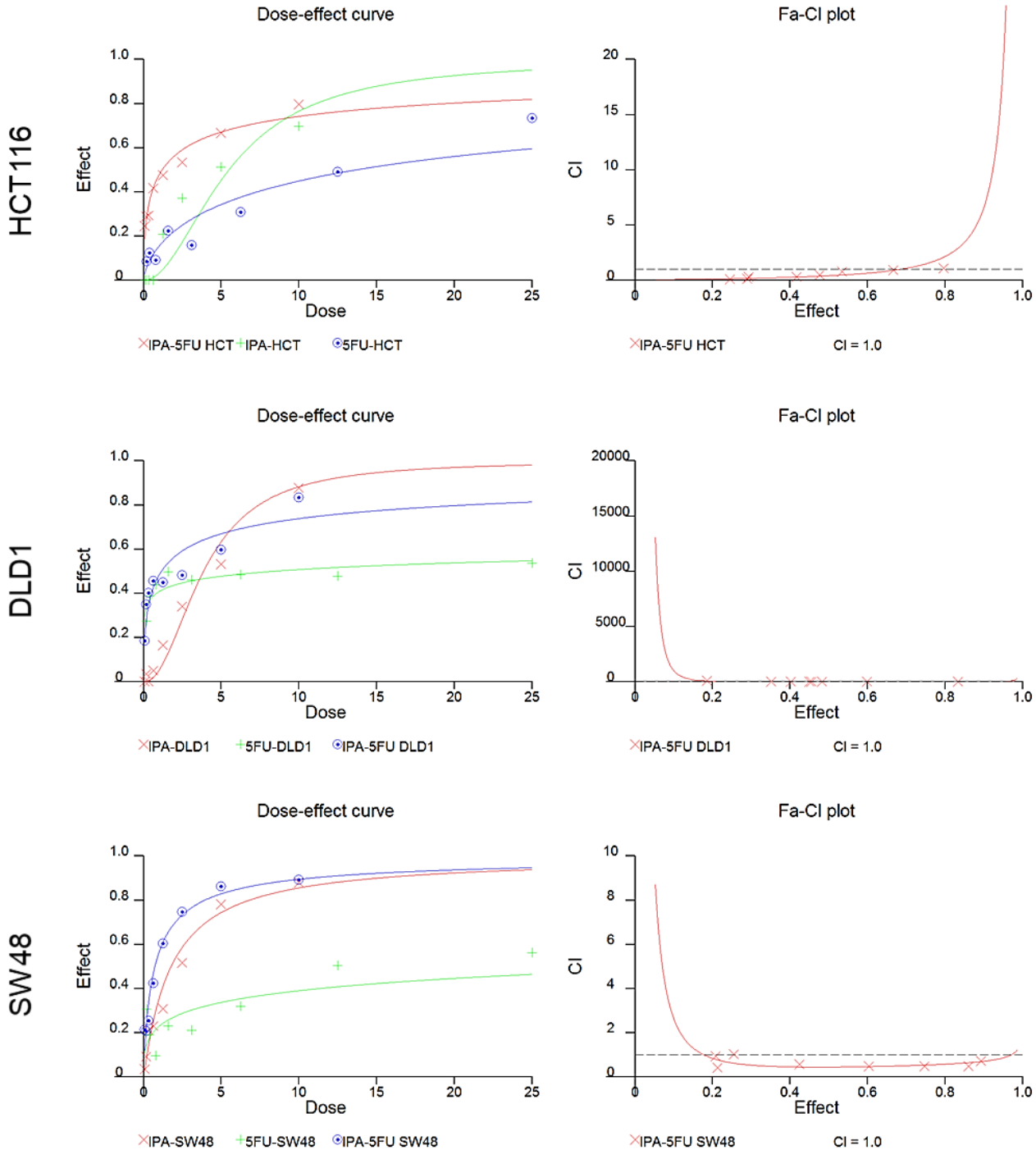

Figure 10. Drug combination analysis. The dose-effect curve was computed using the CalcuSyn software and it showed the dose of the drug vs. the fraction of the cells affected/killed by IPA and 5FU used alone or in combination. Combination Index plot (Fa-CI plot) performed by CalcuSyn software from the affected fraction (Fa) obtained at each dose of the drugs used in combination, at indicated constant molar ratio. A representative experiment of 5 is reported.

GBM results

IPA and N6-BA affect GBM cell proliferation by increasing FBXW7 expression.

It was previously reported that IPA, and even more N6-BA, exerted a marked cytostatic activity against the glioma cell line U87, but did not affect normal human astrocytes viability. The anti-proliferative effect in GBM was mainly associated to the induction of apoptosis, along with blockade of FDPS-dependent protein prenylation, which counteracted oncogenic signaling mediated by EGF receptors [Ciaglia et al, 2017a; Ciaglia et al, 2017b]. Glioma proliferation is found significantly impaired when FBXW7 is overexpressed *in vitro*, suggesting its tumor suppressive role in astroglial cells [Hagedorn et al, 2007]. In turn, FBXW7 downregulation by inactivating mutations or silencing is frequently correlated with G-IV tumors [Sailo et al, 2019]. Aimed to corroborate our results in CRC, as well to investigate if FBXW7 modulation elicited by the modified adenosines is a common mechanism in other cancer systems, we evaluated IPA and N6-BA effects in GBM models (U87, U251 and T98) exhibiting different FBXW7 basal levels. We first assessed cell proliferation and confirmed that, from 5 µM, IPA and N6-BA reduced the proliferation of U87 by over 40%. In U251 cells, a strong dose-dependent inhibitory effect was observed starting from 24h of treatment with both IPA and N6BA at lowest concentration. A significant but fair reduction of proliferation was only detected at the highest dose of IPA or from 5 µM N6-BA after 48h in T98 (Figure 11).

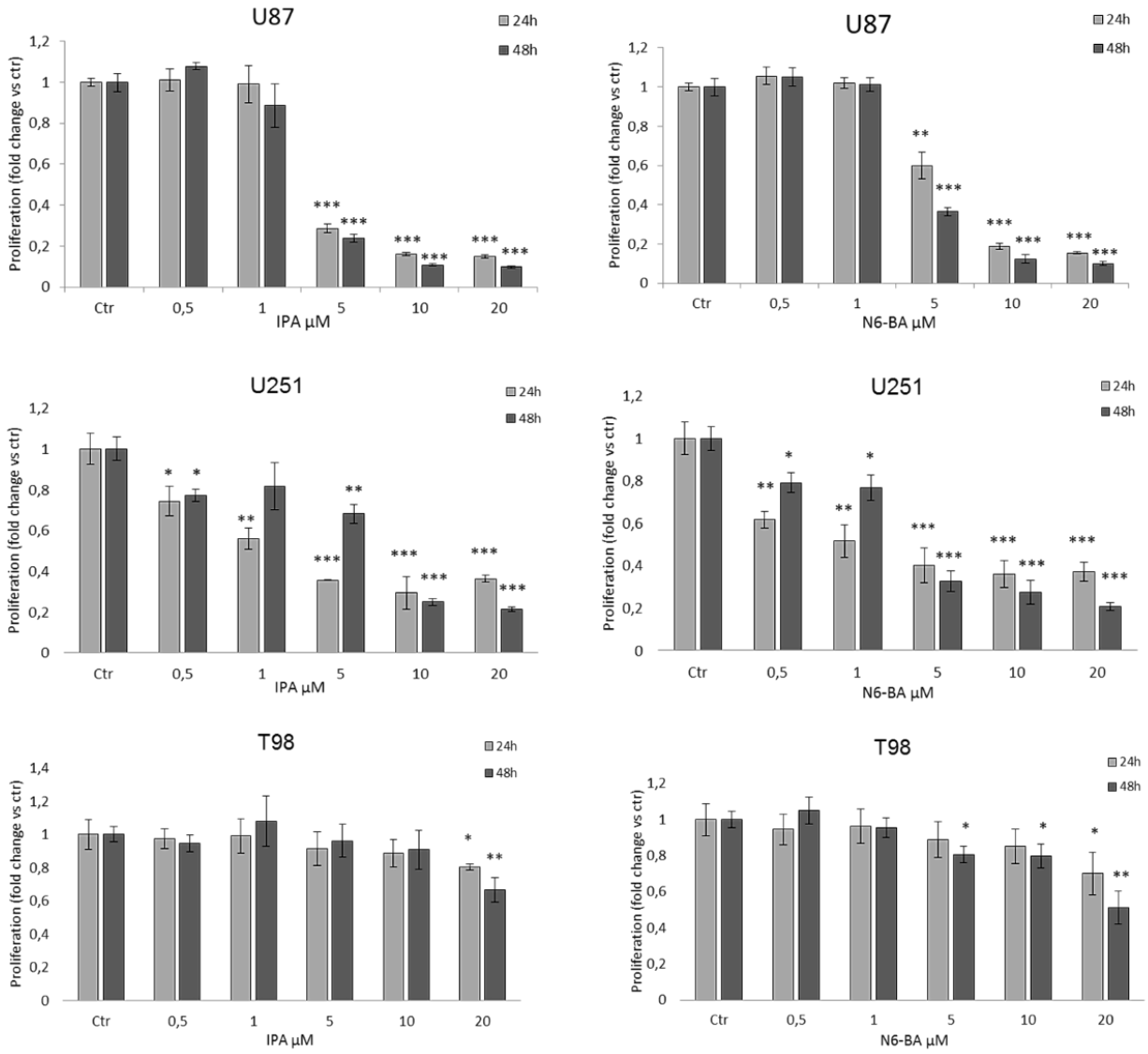

Figure 11. Effect of IPA and N6-BA on GBM cells *in vitro*. BrdU incorporation assay in U87, U251 and T98 cells treated with indicated concentrations of IPA (left column) or N6-BA (right column), for 24 h or 48 h. Data are expressed as mean ± SD of at least three independent experiments. * $p < 0.05$, ** $p < 0.01$, *** $p < 0.005$ vs. control.

Next, we analysed the expression of FBXW7 and its targets in our GBM models. In U87 and U251 cell lines, in which FBXW7 expression is suppressed because of promoter hypermethylation [Gu et al, 2007] and both particularly sensitive to the molecules, 10 µM IPA and N6-BA strongly up-regulated FBXW7 after 24h. As observed in CRC models, the examined downstream targets were coherently modulated with a trend reflecting that of FBXW7. Phosphorylation on c-Myc residue Thr58, tag of FBXW7-dependent degradation, increased at early time was sustained and highly statistically significant after 24h, especially in U251 were the treatments augmented FBXW7

expression over 4-fold. Similarly, also active SREBP1 and Mcl1 levels were reduced (Figure 12A and 12B). Even if, under the same experimental conditions, IPA and N6-BA failed to significantly inhibit T98 cell proliferation and to modulate FBXW7 protein levels, they were able to increase with a less extent Thr58 c-Myc phosphorylation and to efficiently reduce SREBP1 precursor and active form (Figure 12C). These observations enforce our findings in CRC, suggesting that IPA and N6-BA could control cancer cell proliferation and survival by modulating directly or indirectly the tumor suppressor FBXW7.

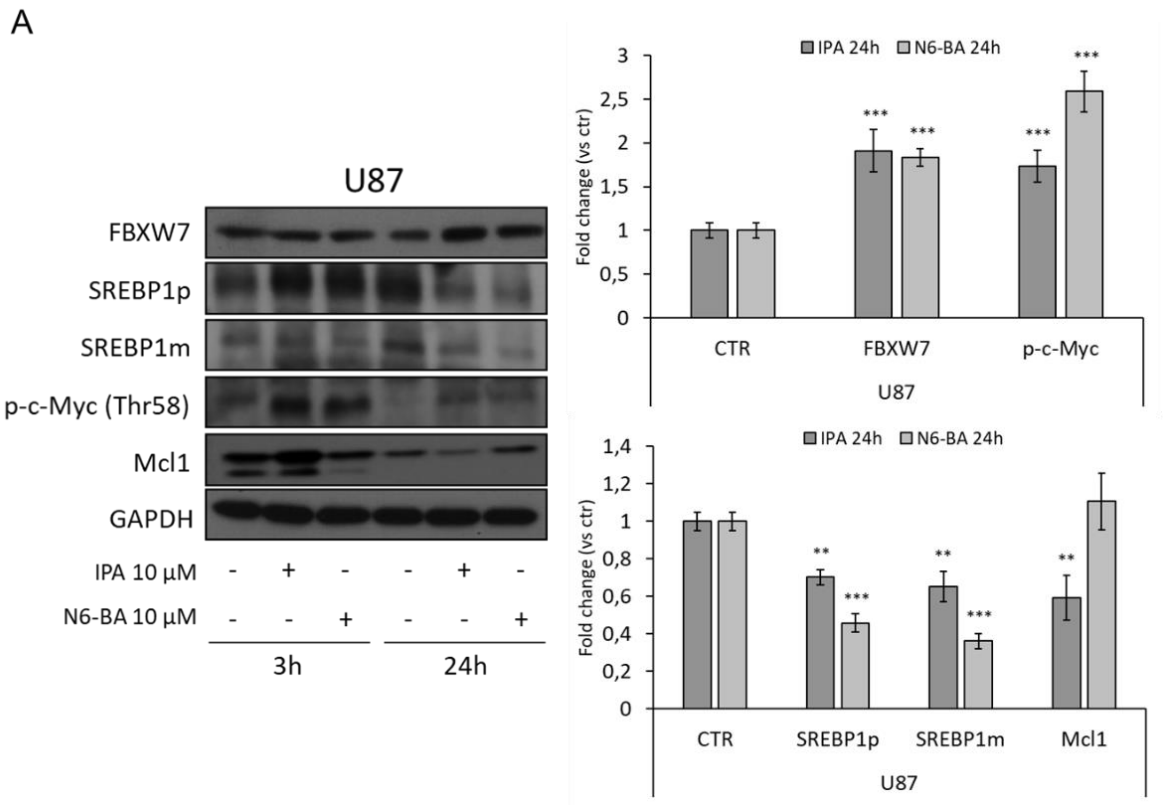

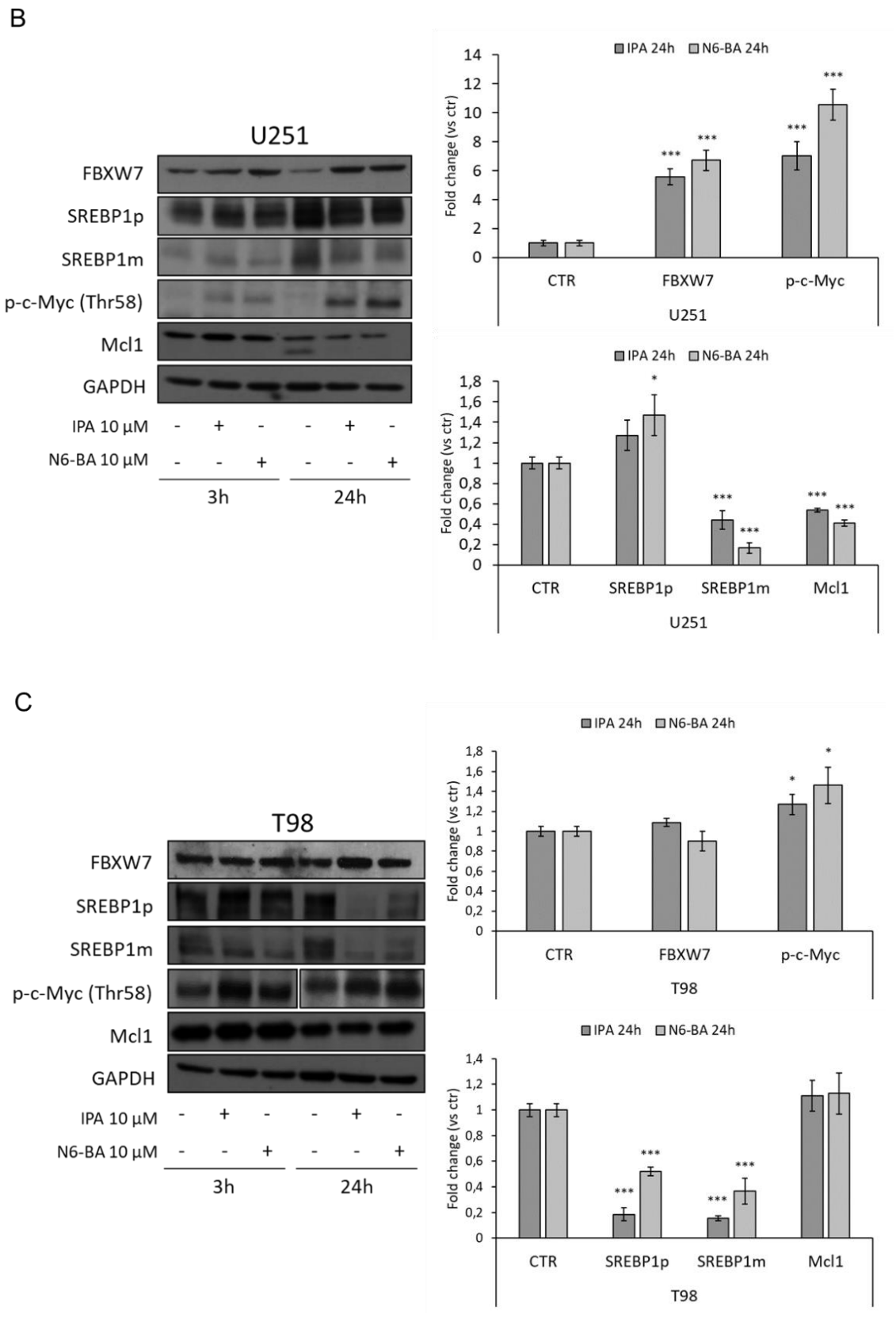

Figure 12. IPA and N6-BA effect on FBXW7 modulation in GBM cells. Representative western blot of FBXW7, SREBP1 precursor (SREBP1p) and mature form (SREBP1m), phosphorylated c-Myc (Thr58) and

Mcl1 protein expression in U87 (**A**), U251 (**B**) and T98 (**C**) treated for 3 and 24h with IPA or N6-BA. The histograms on the right represent the relative densitometric analysis at 24h. GAPDH was used as loading control. Data are expressed as mean ± SD of at least three independent experiments. * $p < 0.05$, ** $p < 0.01$, *** $p < 0.005$ vs. control.

IPA reduces the transcriptional activation of FBXW7 substrates.

IPA and N6-BA impact on c-Myc protein stabilization and reduce SREBP1 levels, especially in U87 and U251 where they strongly re-express FBXW7, but even in the resistant T98. This evidence suggest that the molecules could potentially influence GBM dynamics through transcriptional mechanisms, in a FBXW7-dependent or -independent way, as already debated for CRC. To further corroborate our results, we examined the luciferase activity on the Transcriptional Regulatory Elements (TREs) of c-Myc and additional selected effectors playing crucial role in cancer progression. In IPA-treated U87 cells, the luciferase activity on Myc/Max E-box was significantly reduced, suggesting that the IPA-mediated increase of c-Myc Thr58 phosphorylation effectively represents a tag for its degradation and consequent inactivation. Further, the luciferase assay also revealed a strong downregulation of other oncogenic pathways, including MAPK/ERK, as expected due to the IPA-induced EGFR degradation [Ciaglia et al, 2017a], NFkB and HIF-1, both FBXW7 targets that together cooperate to inflammation and oxidative stress response. Notably, their transcriptional inactivation is aligned with the induction of NRF2 and the reported anti-inflammatory and anti-angiogenic IPA activity [Dassano et al, 2014; Ciaglia et al, 2014; Pisanti et al, 2014]. Coherently, to the suppression of cancer survival pathways corresponded an increase of Rb/E2F and p53 transcriptional activity, matching with the U87 proliferation arrest (Figure 13).

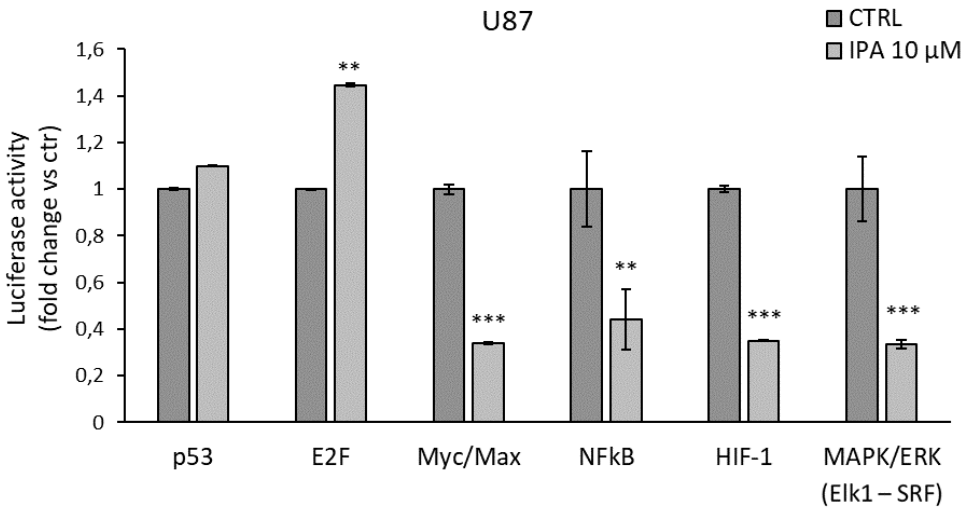

Figure 13. Luciferase activity on selected cancer-related Transcriptional Responsive Elements (TREs). Analysis of luciferase activity of TREs controlled by p53, E2F, Myc, NFkB, HIF-1α or ERK in U87 cell line. The histograms represent luciferase activity measured at 18h from transfection with reporter construct containing the TRE elements and treated with IPA 10 μM or vehicle. Firefly luciferase was normalized to *Renilla* luciferase reading and the data were plotted as fold change (mean ± SD of four independent experiments in triplicate; unpaired two tailed Student's *t*-test ** $p < 0.01$ *** $p < 0.005$) compared to control cells.

IPA could sensitize GBM cells to Temozolomide.

Our research group recently showed that IPA might act as radiosensitizing agent in GBM by attenuating RAD51 foci formation, thus increasing DNA damage before irradiation [Navarra et al, 2020]. Because its involvement in DNA double-strand breaks, FBXW7 was correlated with GBM resistance to ionizing radiation [Fouad et al, 2019]. Moreover, combination of FBXW7 overexpression with Temozolomide (TMZ), drug of choice in GBM therapeutic protocols, was reported to notably sensitize U251 cells to the cytotoxic effect of the drug [Lin et al, 2018]. Based on this evidence and encouraged by our results in CRC and GBM, to further explore the role of the molecules in cancer resistance mechanisms, we evaluated IPA effect in sensitizing GBM to TMZ *in vitro*. To this aim, GBM cells were exposed to 10 μM IPA for 24h. After the incubation, medium was removed, and cells were treated for additional 72h with TMZ (5-50-250-500 μM). In the sensitive U87 and U251 cells, IPA pre-treatment was able to significantly ameliorate the killing effect of TMZ at all the used concentrations and in a dose-dependent manner (Figure 14A and 14B). This result was further confirmed by the analysis of H2Ax phosphorylation levels, mark of DNA damage, induced after 72h by TMZ alone (50 or 250 μM) and incremented with IPA pre-treatment (Figure 14D). In TMZ resistant T98 cells, despite TMZ produced a weak significant reduction of cell viability at the highest concentrations, IPA pre-treatment did not improve its effect at any concentrations tested. However, the different response to the treatments could also be due to other genetic features, such as those affecting DNA repair genes.

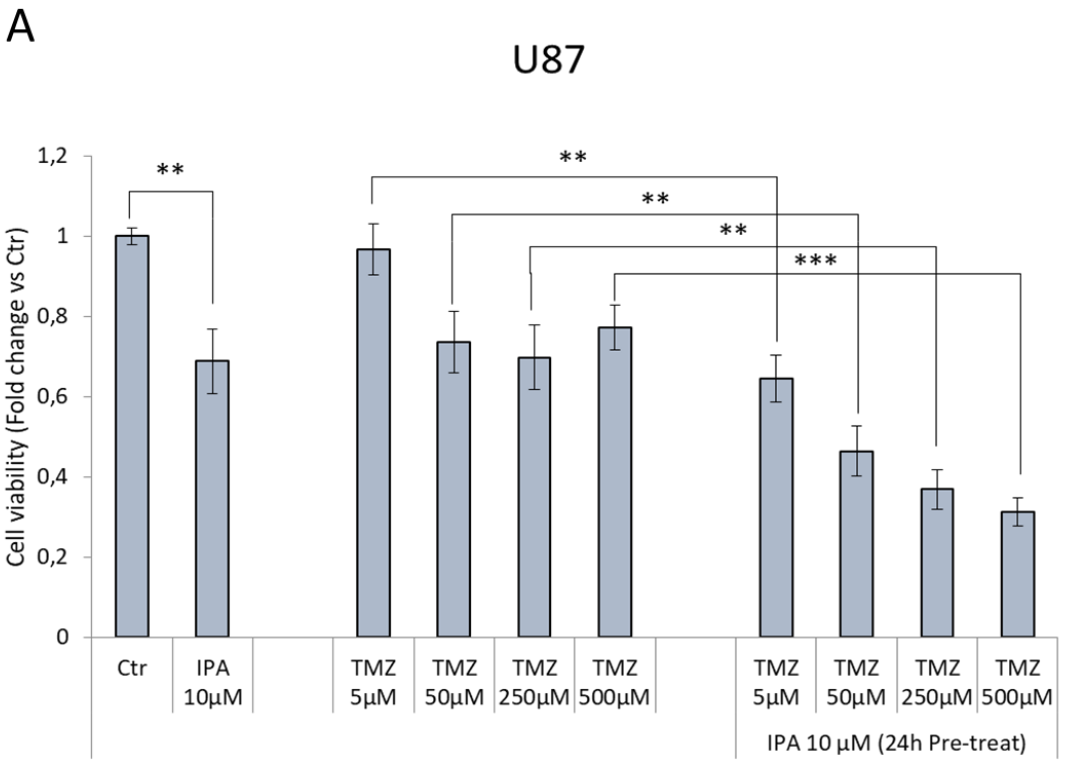
A
U87
Cell viability (Fold change vs Ctr)
1,2
1
0,8
0,6
0,4
0,2
0
**
**
**
**
***
Ctr
IPA 10µM
TMZ 5µM
TMZ 50µM
TMZ 250µM
TMZ 500µM
TMZ 5µM
TMZ 50µM
TMZ 250µM
TMZ 500µM
IPA 10 µM (24h Pre-treat)

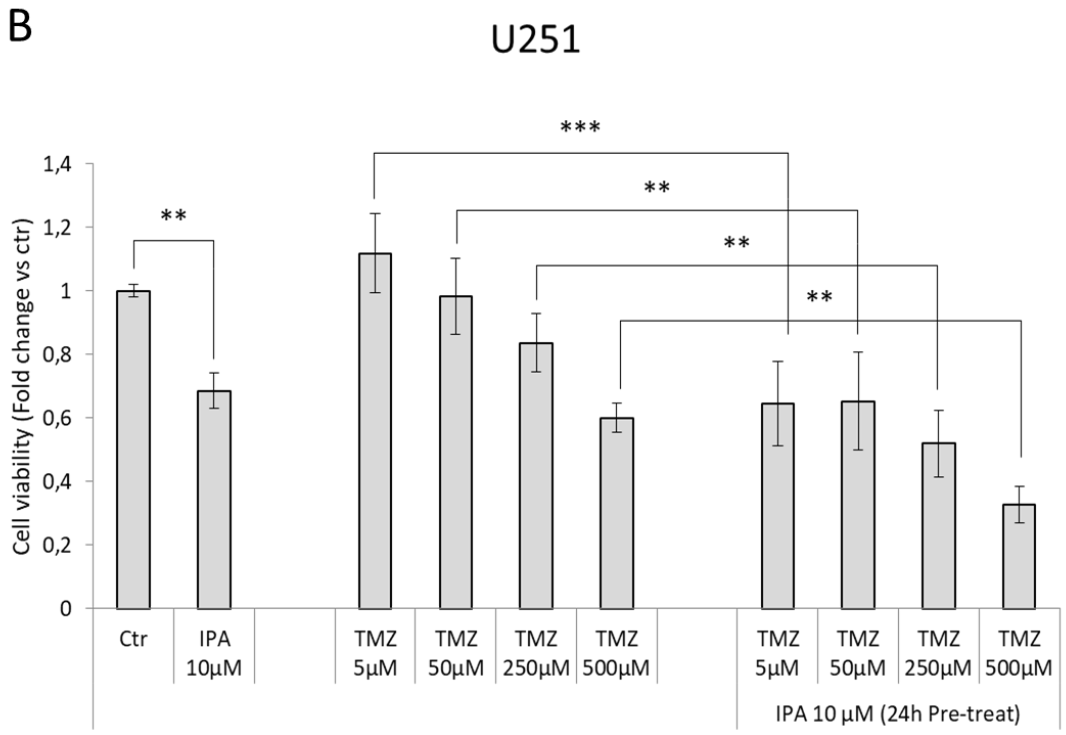
B
U251
Cell viability (Fold change vs ctr)
1,4
1,2
1
0,8
0,6
0,4
0,2
0
***
**
**
**
**
Ctr
IPA 10µM
TMZ 5µM
TMZ 50µM
TMZ 250µM
TMZ 500µM
TMZ 5µM
TMZ 50µM
TMZ 250µM
TMZ 500µM
IPA 10 µM (24h Pre-treat)

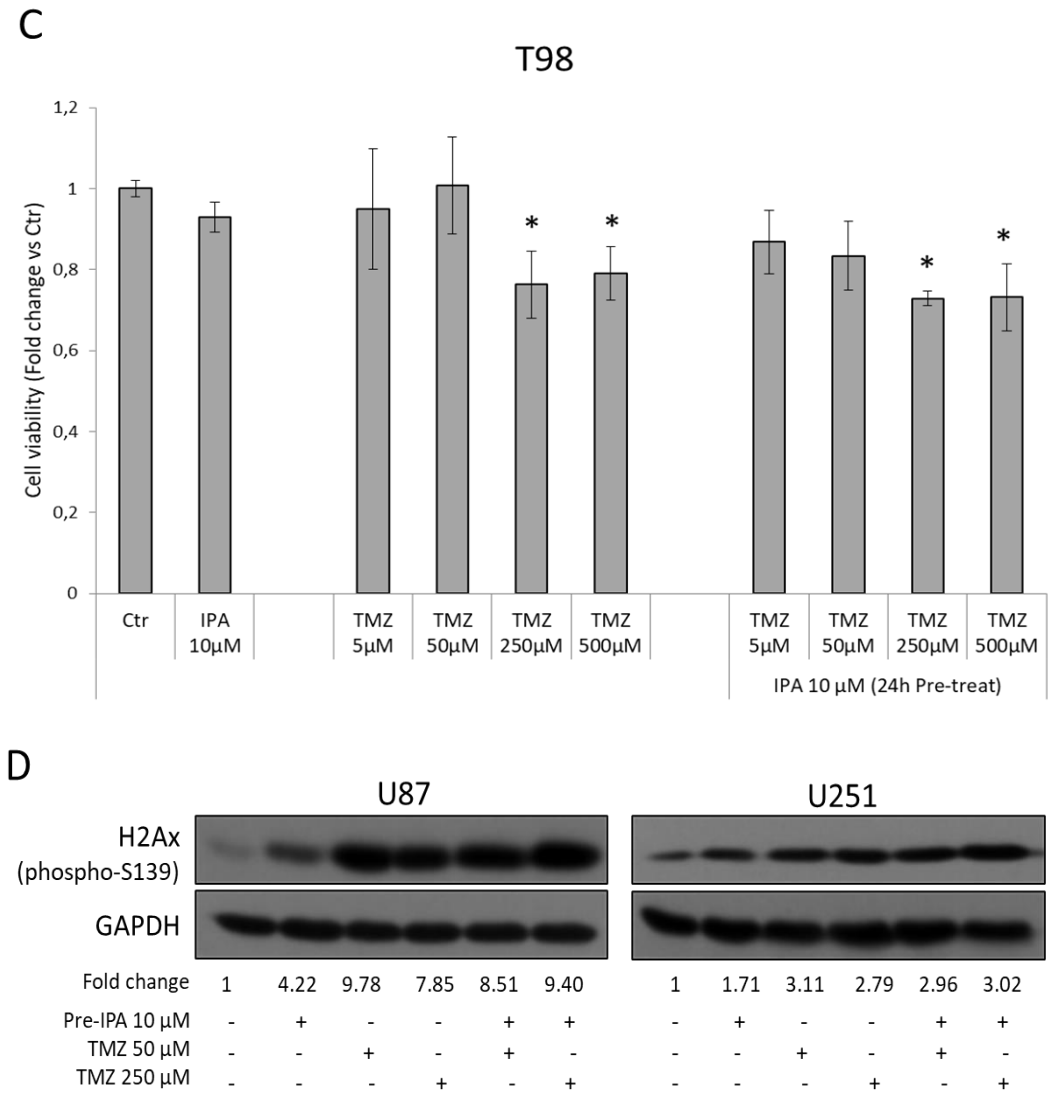

Figure 14. IPA sensitize GBM to TMZ. GBM cells were exposed to 10 μM IPA or vehicle (DMSO) for 24h. After the incubation, medium was removed and replaced with fresh one containing the indicated concentrations of TMZ or the relative vehicle alone. MTT assay was used to assess cell vitality after 72h, expressed as the mean ± SD of three independent experiments. ** $p < 0.01$, *** $p < 0.005$ in U87 (**A**) and U251 (**B**), *$p<0.05$ vs control in T98 (**C**). Representative Western blot and relative densitometric analysis (fold change vs. control) of phosphorylated histone H2Ax (S139), in U87 and U251 cells subjected to the same experimental conditions of the vitality assay (**D**).

In GBM, TMZ resistance is primarily due to the overexpression of the O6-methylguanine DNA methyltransferase (MGMT) which neutralizes the alkylating effect of the drug by removing methyl groups from DNA. Indeed, epigenetic inactivation of MGMT gene is commonly accepted as a favorable prognostic biomarker of TMZ sensitivity [Oldrini et al, 2020]. We then analysed MGMT levels in U251 and T98, respectively characterized by constitutively low and high levels of the

enzyme and different sensitivity to TMZ [Lee, 2016]. In U251, known to have a high percentage of CpG methylation in the MGMT promoter, both IPA and N6-BA were able to further reduce MGMT expression but at different time points. More interestingly, MGMT levels were efficaciously reduced after 24h also in T98, TMZ-resistant cell line that have shown to be less sensitive to the molecules (Figure 15).

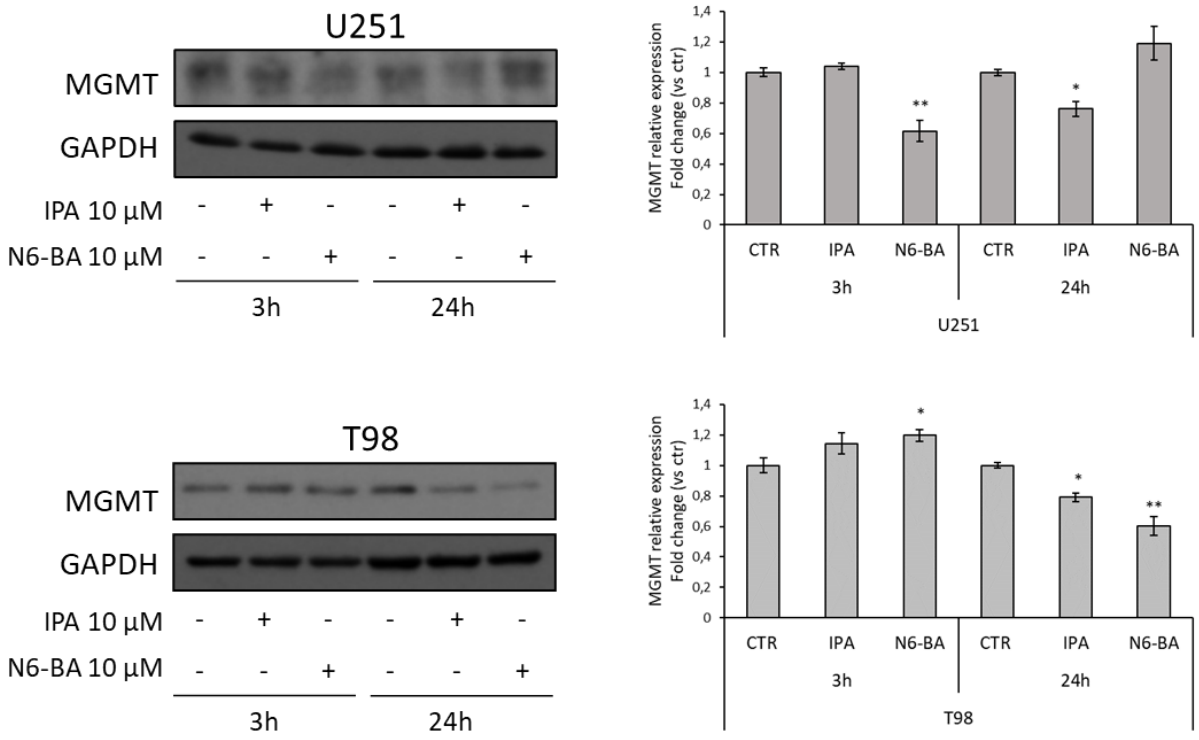

Figure 15. Representative western blot and densitometric analysis (right histograms) of MGMT expression in U251 and T98 cells treated with IPA or N6-BA as indicated. GAPDH was used as loading control. Data are expressed as mean ± SD of at least three independent experiments. * $p < 0.05$, ** $p < 0.01$ vs. control.

IPA and N6-BA could affect DNA methylation.

Several studies in GBM revealed aberrant methylation patterns of specific genes, in addition to MGMT, and suggested that methylation profiles may be used to improve diagnostic accuracy and predict therapeutic response [Wenger et al, 2019]. The evidence that IPA and its analogue N6-BA could influence the expression of methylated genes involved in tumor-related mechanisms, such as FBXW7, MGMT, and potentially others, suggests that they could exert their anti-cancer actions through epigenetic mechanisms. DNA methylation, occurring at C5-position of cytosine, is the major epigenetic modification responsible of chromatin dynamics, triggered and maintained by

DNA methyltransferases (DNMTs) that use S-adenosylmethionine as methyl donor. To prove our hypothesis, we first evaluated the expression of DNMT1 (prevalently involved in methylation maintenance) in whole cell extracts of GBM cell lines treated with IPA or N6-BA. Western blot analysis showed that, at short time, DNMT1 protein amount was effectively reduced by IPA and N6-BA in U87, but only by IPA in T98. After 24h, both the molecules were able to reduce DNMT1 expression in the three GBM cell lines, with an equal extent in U251 and T98 (Figure 16).

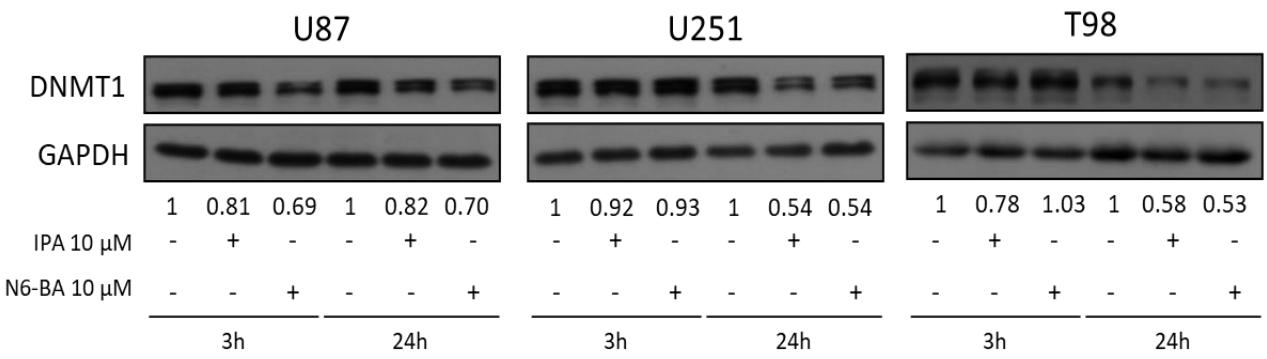

Figure 16. IPA and N6-BA reduce DNMT1 expression. Representative western blot and relative densitometric analysis (fold change vs. control) of DNMT1 expression in U87, U251 and T98 cells treated with IPA or N6-BA. GAPDH was used as loading control.

Subsequently, aimed to evaluate the ability of the two compounds to interfere with epigenetic regulation, we compared their effects with those of a known DNMTs inhibitor, used as demethylating agent. Firstly, we performed a colorimetric assay to quantify DNMTs activity in nuclear extracts of GBM cells treated for 24 h with IPA, N6-BA, 5-Aza-2′-Deoxycytidine (5-AZA-dC or decitabine) or a combination of IPA and 5-Aza-dC. The analysis evidenced that 5-AZA-dC treatment resulted in a significative DNMTs activity inhibition, as expected. IPA was able to robustly reduce the enzymatic activity in U251 and T98 cell lines, while in U87 cells, despite the slight decrease, the effect did not reach statistical significance. Overall, the results suggested that IPA as single agent behaves similarly to the known inhibitor but, interestingly, when it was combined with 5-AZA-dC it slightly restored DNMTs activity in U251 and U87. The aza-cytosine substitutes cytosine during DNA replication and became substrates for DNMTs. The inhibition occurs because the enzymes covalently bond the modified cytosine but fail to transfer the methyl group, consequently undergoing degradation [Stresemann and Lyko, 2008]. We speculated that IPA, as modified adenosine, used together with the aza-cytosine could weakly interfere with it for DNMTs inhibition. Finally, a significant reduction following N6-BA treatment was only detected

in U87 (Figure 17A). DNMT1 expression in nuclear extracts substantially confirmed the trend observed in whole cell lysates, with some discrepancies probably due to the purification methods (Figure 17B).

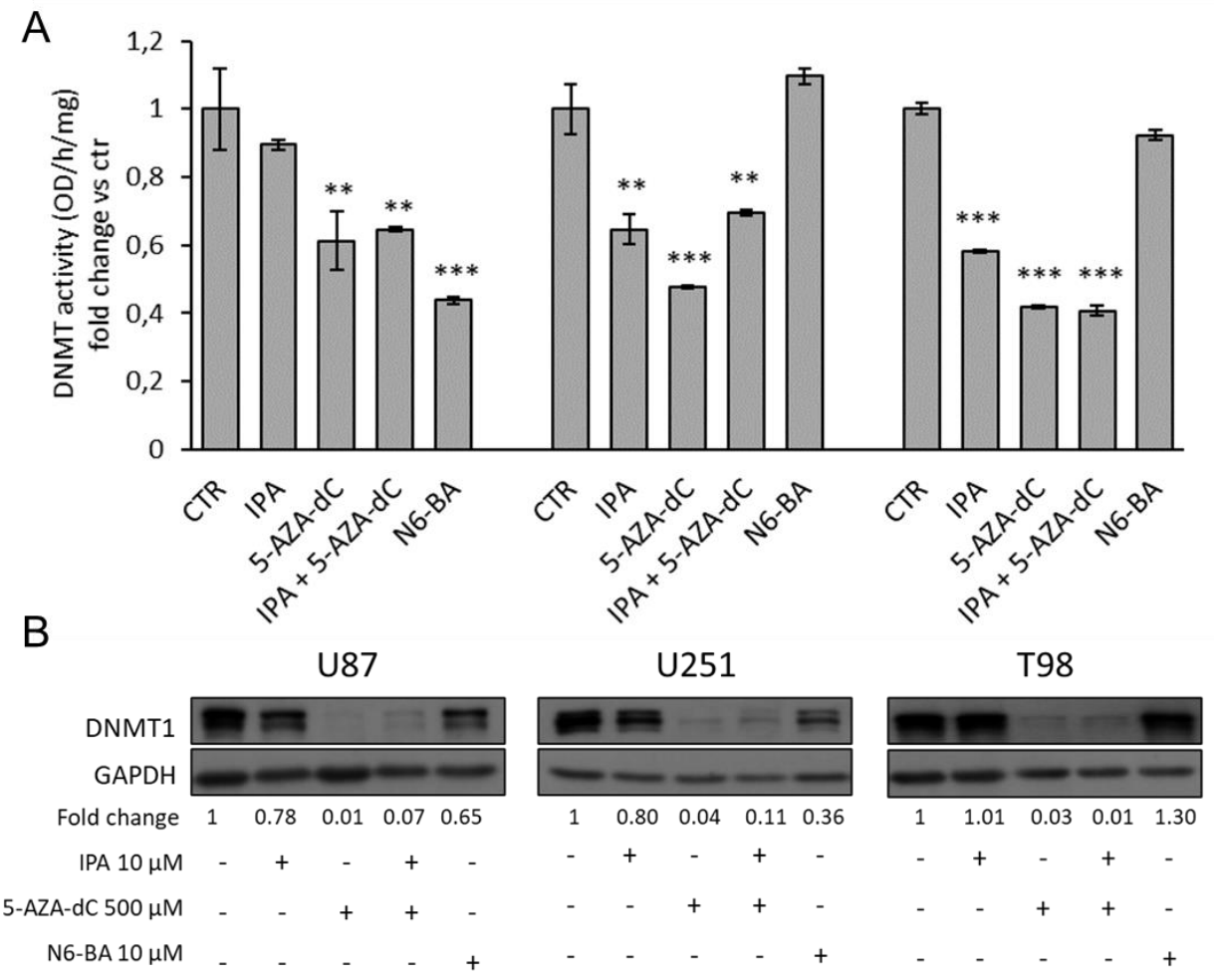

Figure 17. IPA and N6-BA affect DNMTs expression and activity. (**A**) Colorimetric DNMTs activity assay performed using nuclear extracts from GBM cells treated for 24h with IPA (10 µM), 5-AZA-dC (500 µM), IPA+5-AZA-dC combination, N6-BA (10 µM). DNMT activity (OD/h/mg) is expressed as fold change vs. control. Data are expressed as the mean ± SD of six independent experiments. ** $p < 0.01$, *** $p < 0.005$ vs. control. (**B**) Representative western blot and relative densitometric analysis (fold change vs. control) of DNMT1 expression in extracts optimized to preserve enzymatic activity of GBM treated for 24h as indicated. GAPDH was used as loading control.

Therefore, to strengthen these observations, we evaluated quantitative changes in global DNA methylation through an ELISA measuring the percentage of 5-methylcytosine (% 5mC). For this purpose, we isolated genomic DNA from GBM cell lines under the same experimental setting used for the DNMTs enzymatic assay. In U87 and U251, consistent with previous data, 5-AZA-dC as

single agent reduced % 5mC with a commensurate effect to the observed DNMTs inhibition (Figure 18). Coherently with the effect on DNMTs activity, IPA significantly decreased global methylation in U251 and slightly, despite not significantly, in U87 cells, both harbouring methylation of MGMT and FBXW7 promoters. Furthermore, IPA/5-AZA-dC combination reverted the effect of 5-AZA-dC alone in U87, and even produced an increase of methylation reaching statistical significance in U251 (Figure 18). This could be explained with the evidence that high doses of DNA methylation inhibitors, like those used in clinical practice, cause a quick and transient increase of methylation in a small fraction of CpGs might reflecting an adaptation response to the inhibitory stimulus, and hypomethylation occurs after several days [Giri and Aittokallio, 2019]. Surprisingly, despite the inhibition of DNMTs activity, no changes in %5 mC were observed in T98 (Figure 18). However, in this precisely cell line, it was reported that DNMTs suppression did not influence the methylation status in a subset of repressed genes displaying promoter hypermethylation, but it was rather associated with changes in histone modifications [Foltz et al, 2009].

Overall, these results collectively suggested that IPA, and with a less extent N6-BA, could potentially modulate specific cancer-related genes, through a complex mechanism that might involve DNA methyltransferases expression and/or activity and chromatin remodelling.

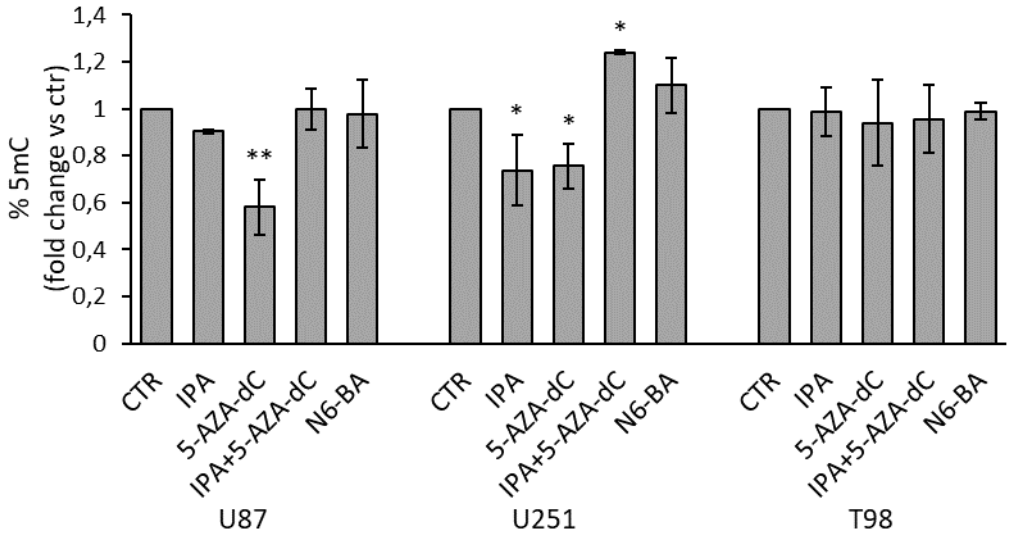

Figure 18. Quantification of global DNA methylation (ELISA) performed using 100 ng of genomic DNA isolated from GBM cells treated for 24h with IPA (10 µM), 5-AZA-dC (500 µM), IPA+5-AZA-dC combination, N6-BA (10 µM). DNA methylation (% 5mC) was expressed as fold change vs. control. Data are expressed as the mean ± SD of three independent experiments. * $p < 0.05$, ** $p < 0.01$ vs. control.

IPA and N6-BA influence histone modifications.

To further investigate the involvement of epigenetic mechanisms in the antitumor effect of the two compounds, we analysed their effect on histone marks commonly related to gene repression or active transcription. In U87 and U251, after 24h both IPA and N6-BA significantly increase the trimethylation on lysine 27 of histone H3 (H3K27me3) and the dimethylation on lysine 9 residue of histone H3 (H3K9me2), suggesting a transcriptional repressive trend (Figure 19). Coherently with the repressive trend, a reduction of global lysine acetylation (H3 pan-acetyl) and lysine 4 dimethylation of H3 (H3K4me2), was observed in all cell lines analysed (Figure 20). In T98 cells, the treatments failed to modulate H3K27me3 but effectively increase H3K9me2 (Figure 19) and simultaneously decrease H3K4me2. In this cell line, pan-lysine acetylation of H3 was only reduced by N6-BA (Figure 20). However, global trend of examined histone marks suggested that IPA and N6-BA induced a transcriptional repressive trend, which is not aligned with enzymatic inhibition of DNMT, but it's compatible with MGMT repression and the observed downregulation of FBXW7-targets playing crucial roles in cell metabolism and survival (c-Myc, SREBP, Mcl1). Of note, we observed that IPA and N6-BA induce the strongest increase of H3K27me3 in U87, where DNMT1 activity was not significantly altered. H3K27me3 is specifically catalyzed by the histone methyltransferase EZH2, recruited together with DNMTs to orchestrate gene silencing. This result is consistent with data here showed and, in particular, with the transcriptional inactivation of oncogenic pathways verified through luciferase assay. Moreover, robust trimethylation of H3K27 is frequently found in the promoter region of epigenetic silenced MGMT, completely repressed in U87 cell line [Chen et al, 2018].

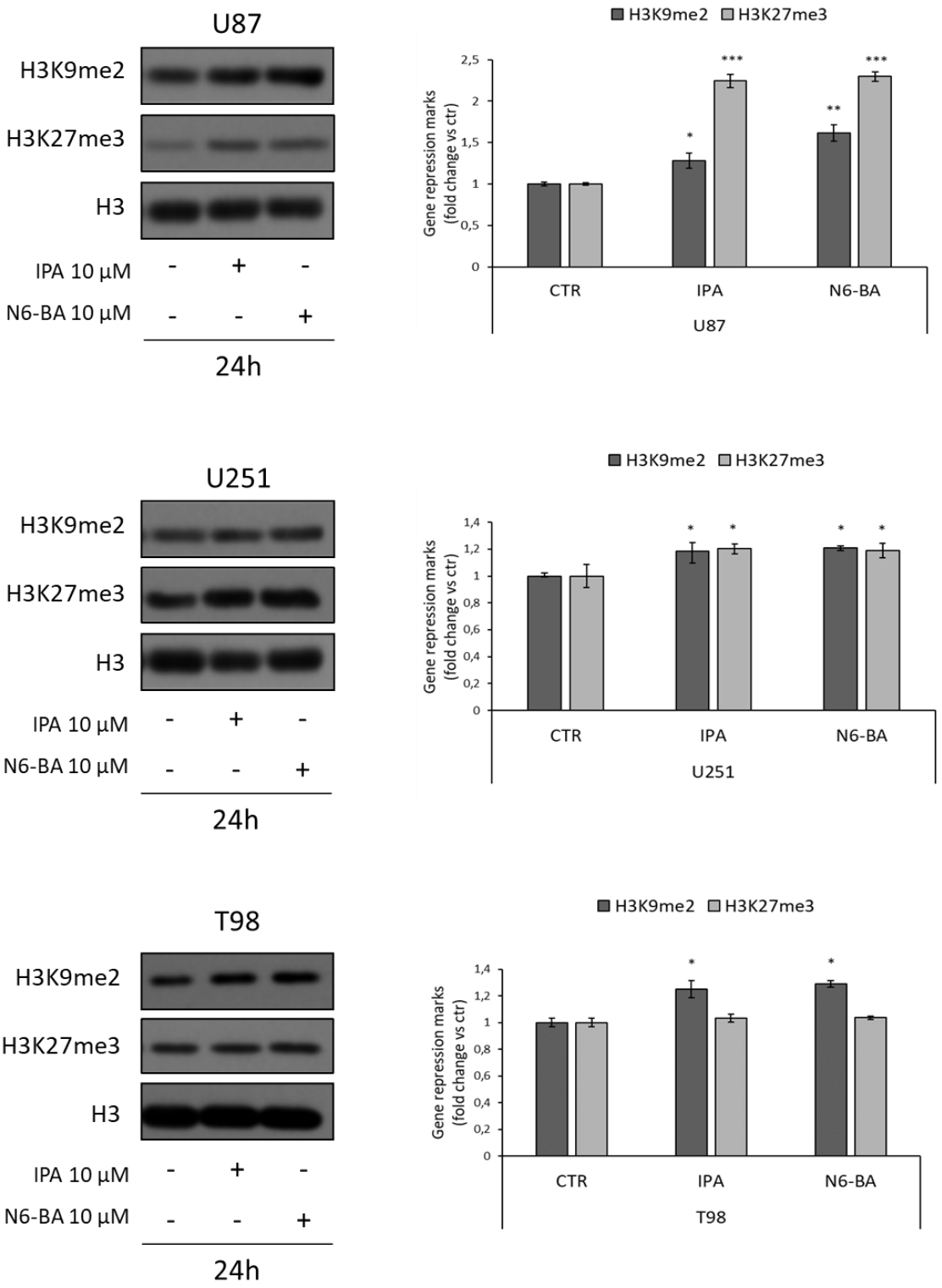

Figure 19. IPA and N6-BA influence histone marks associated with gene repression. Representative western blot and densitometric analysis of H3K9me2 and H3K27me3 in purified histone fractions of GBM cell lines treated with IPA or N6-BA after 24h. H3 was used as loading control. The histograms report the quantification of bands intensity expressed as mean ± SD of three independent experiment. * $p < 0.05$, ** <0.01 *** $p < 0.005$ vs. control.

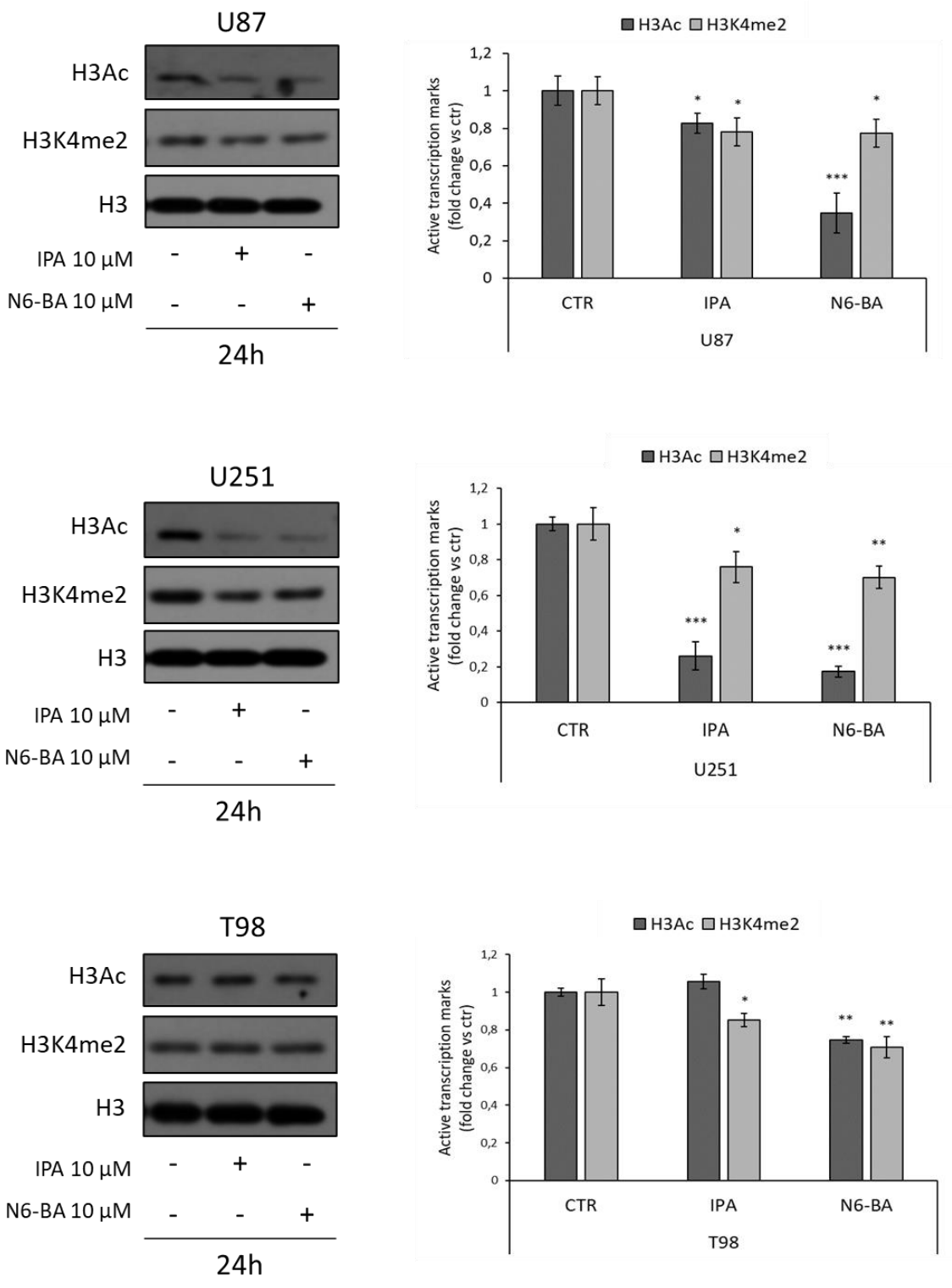

Figure 20. IPA and N6-BA influence histone marks associated with active transcription. Representative western blot and densitometric analysis of H3Ac (acetyl K9 + K14 + K18 + K23 + K27) and H3K4me2 in purified histone fractions of GBM cell lines treated with IPA or N6-BA after 24h. H3 was used as loading control. The histograms report the quantification of bands intensity expressed as mean ± SD of three independent experiment. * $p < 0.05$, ** <0.01 *** $p < 0.005$ vs. control.

IPA and N6-BA exert anti-tumor effects in glioma primary cell lines.

The overall evidence emerging from this dissertation is that IPA or its analogue N6-BA modulate different cancer-related effectors plausibly interfering up-stream with their regulation. This is particularly intriguing in GBM whose intricate epigenetic landscape further complicates its treatment and management. Aimed to further investigate the anti-tumor potential of the adenosine compounds in GBM models endowed with unique genetic features, we established primary cell lines from some fresh glioma patients resected tumors, characterized by high-throughput genotyping methods. We selected GBM55 and GBM58, sharing some single-nucleotide variants associated to drug response, and deletion of X-linked genes involved in chromatin organization and transcription. Through western blot analysis, we evaluated IPA or N6-BA effects on selected targets in primary cell lines verifying that IPA produced a slight but significant upregulation of FBXW7 after 3h in GBM55 and after 24h in GBM58. Moreover, IPA was able to also repress MGMT levels, both at early and prolonged time in GBM58, but only after 3h in GBM55. Finally, IPA mediated an early decrease of DNMT1 levels, followed by a strong reduction or even an abrogation after 24h in both primary cell lines. Very similar to IPA, the benzyl analogue N6-BA substantially decreased DNMT1 and MGMT expression after 24h but failed to significantly modulate FBXW7 (Figure 21A). Expression changes at 24h, were accompanied by a strong reduction of cell density (Figure 21B) compatible with the relevant increase of H2Ax phosphorylation levels (Ser139), mark of DNA damage (Figure 21A). Genetic profiling of patients-resected tumors revealed a great pool of DNA variations, remarking the elevated heterogeneity and complexity of GBM and contributing to expand our knowledge on this malignancy. These preliminary observations in GBM primary cell lines support the hypothesis that IPA and N6-BA could interfere with DNA remodelling and they could represent new valid therapeutic tools in GBM.

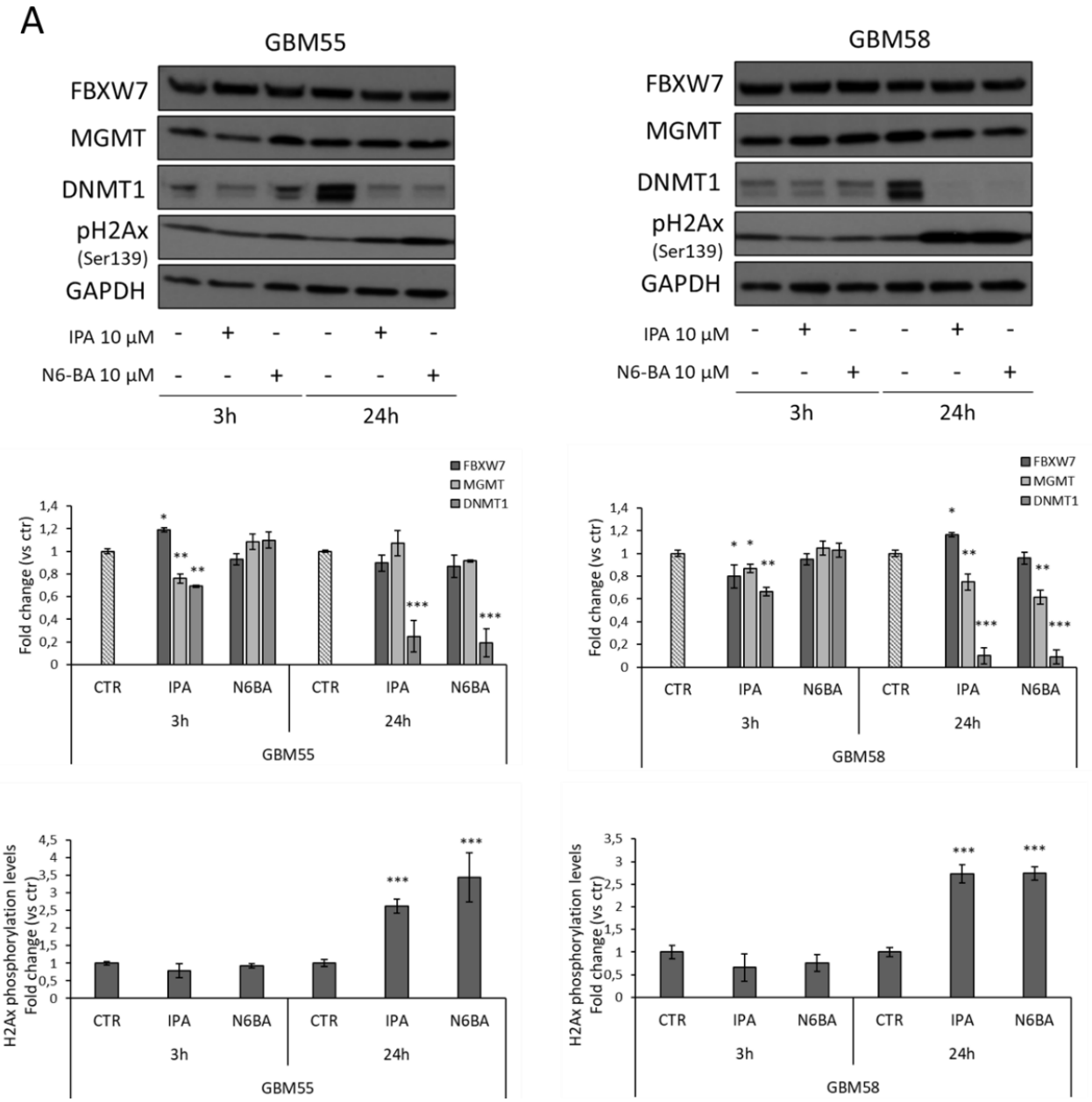
A
GBM55
FBXW7
MGMT
DNMT1
pH2Ax
(Ser139)
GAPDH
IPA 10 µM
N6-BA 10 µM
3h
24h
GBM58
FBXW7
MGMT
DNMT1
Fold change (vs ctr)
CTR
IPA
N6BA
H2Ax phosphorylation levels
Fold change (vs ctr)

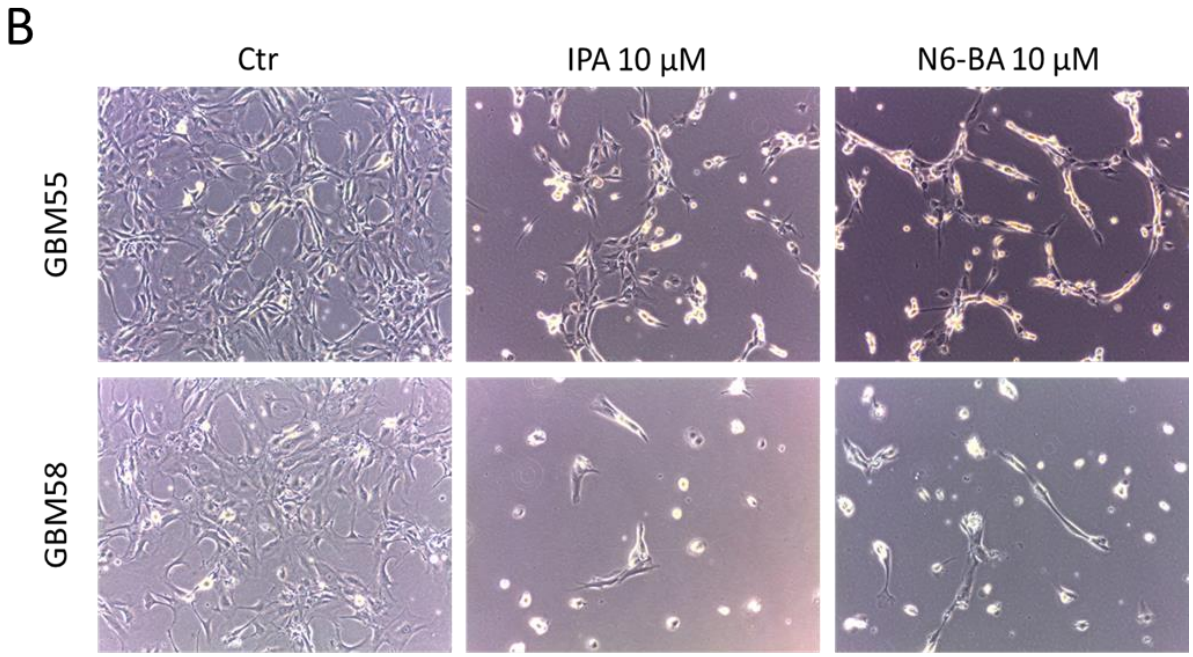

Figure 21. IPA and N6-BA anti-tumor effects in GBM primary cell lines. (**A**) Representative western blot and densitometric analysis of FBXW7, DNMT1, MGMT expression and H2Ax phosphorylation levels in GBM primary cell lines treated for 3 or 24h with the indicated molecules. GAPDH was used as loading control. The histograms report the quantification of bands intensity expressed as mean ± SD of three independent experiment. * $p < 0.05$, ** <0.01 *** $p < 0.005$ vs. control. (**B**) Phase contrast images of GBM55 and GBM58 primary cell lines treated with 10 µM IPA, N6-BA or vehicle alone (Ctr) for 24h. Micrographs were acquired with ZEN imaging software by ZEISS.

DISCUSSION

Antitumor effects of IPA and its analogue N6-BA have been commonly but not exclusively associated with FDPS inhibition, a key enzyme involved in mevalonate pathway, responsible for cholesterol biosynthesis and downstream protein prenylation, often dysregulated in cancer [Bifulco et al, 2008; Laezza et al, 2009; Castiglioni et al, 2013; Ciaglia et al, 2017b]. The modified adenosines act in a similar way negatively regulating tumor growth and, because of their structure, they potentially modulate multiple cell pathways. Despite several mechanisms of actions have been proposed, further investigations are certainly needed to clarify the molecular basis underlying their pleiotropic effects.

FBXW7 is the F-box protein that works as adaptor for SCF E3 ligase [Morreale and Walden, 2016]. FBXW7 role as tumor suppressor is widely accepted since its inactivation have been found in a large spectrum of human cancers, including CRC and GBM, and associated with malignancy [Davis et al, 2014; Iwatsuki et al, 2010; Lin et al, 2018].

The identification of FBXW7 as molecular target of both IPA and N6-BA, enforces our previous reports and provide a believable link between the apparently dissimilar effects observed in different cancer types, suggesting that FDPS inhibition could be achieved either directly [Scrima et al, 2014; Ciaglia et al, 2017b] or indirectly as a consequence of the FBXW7/SREBP1/FDPS axis regulation. Several studies highlighted the interplay between mevalonate pathway and c-Myc regulation. Statins, well-known inhibitors of endogenous cholesterol biosynthesis [Gazzerro et al, 2012], reduce the growth of Brain Tumor Initiating Cells (BTICs), where mevalonate pathway genes - including FDPS - are strongly upregulated, through a feed-forward loop between c-Myc and the mevalonate pathway [Wang et al, 2017]. Recently, novel clues about neoplastic metabolism revealed that c-Myc binds mevalonate genes promoters itself and also induces SREBP1, cooperating synergistically to lipogenesis stimulation, required for the initiation and maintenance of tumorigenic growth *in vitro* and *in vivo* [Gouw et al, 2019]. Furthermore, some reports suggested that cholesterol, one of the end products of mevalonate pathway, or its metabolite 27-hydroxycholesterol (27-HC) control cancer cell proliferation through downregulation of FBXW7. In particular, in breast cancer cells, 27-HC suppresses FBXW7 transcription leading to an increase of c-Myc protein stability [Ma et al, 2016].

We found that, in CRC, IPA is able to transcriptionally inactivate c-Myc and to upregulate FBXW7-c-Myc binding in FBXW7 wild type cells but not, as expected, in SW48 mutant cells

where, despite IPA mediated antiproliferative and pro-apoptotic effects, c-Myc accumulation occurs in a time-dependent manner. Given its central role in cell metabolism and proliferation, c-Myc abundance is strictly regulated at multiple steps. Therefore, especially in cancer cells, c-Myc undergoes a rapid turnover ensuring its availability and adequate protein levels [Farrell and Sears, 2014]. This consideration could explain why - although Thr58 phosphorylation, subsequent ubiquitination and transcriptional c-Myc inhibition - we did not observe the complete abrogation of its protein levels in our CRC models treated with the isopentenyl compound. Further, the different trend of modulation observed in DLD1 and HCT116 cells is not surprising, since the half-life of c-Myc could be a result of genotypes. For instance, Ubiquitin Specific Peptidase 9, X-Linked (USP9x) deubiquitinase positively regulates FBXW7 stability, antagonizing its ubiquitylation and proteasomal degradation. While HCT116 cell line carries wild type USP9x gene, DLD1 cells displays a mutation in its catalytic domain [Khan et al, 2018]. In addition, as previously debated, DLD1 cells are reported to have a high percentage of FBXW7 promoter methylation [Akhoondi et al, 2010]. On the other hand, in DLD1, the upregulation of FBXW7 and the inactivation of Myc responsive elements suggest transcriptional and/or epigenetic IPA-mediated mechanisms.

Recently, we reported the first evidence of IPA anti-glioma ability to induce EGFR ubiquitination through the specific E3 ligase c-Cbl, belonging to the same family of SCF^{FBXW7} [Ciaglia et al, 2017a]. The *in vitro* modulation of FBXW7 expression mediated by IPA and N6-BA in GBM models remarks our observations in CRC and suggests that the molecules could control signalling events, commonly altered in cancer biology, conceivably targeting more than a E3 ligase. Interestingly, the increase of c-Myc phosphorylation on Thr58 in GBM globally reflected the FBXW7 up-regulation, especially in U251 where FBXW7 is strongly repressed because of promoter methylation [Gu et al, 2007], but also arose independently from it. In glioma, c-Myc is particularly important for survival and self-renewal activity of the stem cells compartment, thus its degradation is highly coordinated by the UPS [Wang et al, 2008; Scholz et al, 2020]. In glioma stem cells (GSCs), the deubiquitinase USP13 and the E3 ligase FBXL14 (F-box and leucine-rich repeat protein 14), among others, were found to tightly regulate c-Myc ubiquitination. While USP13 is preferentially expressed in GSCs, stabilizing c-Myc, SCF^{FBXL14} is predominantly expressed in non-GSCs, promoting c-Myc degradation [Fang et al, 2017]. Even though we did not explore other UPS components in GBM, and we did not profile the stem cells behaviour, we could not exclude that the adenosine compounds differentially target UPS players in cancer microenvironment. Besides, FBXW7 has been reported to be essential during brain development and differentiation by

regulating Notch and c-Jun [Hoeck et al, 2010; Matsumoto et al, 2011], as well as in cancer stemness and resistance mechanisms [Yumimoto et al, 2020]. Indeed, in both non–small cell lung cancer and CRC, FBXW7-inactivating mutations leads to Mcl1 accumulation and, in turn, to intrinsic and acquired resistance to oxaliplatin, 5-FU and several TKIs [Bracht et al, 2010; Lorenzi et al, 2016; Tong et al, 2017; Li et al, 2019]. In CRC and GBM, we observe a total or partial abrogation of Mcl1 levels in a FBXW7-dependent way. The find that Mcl1 is downregulated following FDPS silencing [Abate et al, 2017], together with data here showed, corroborates the potential interplay between mevalonate pathway, Mcl1 and E3 ubiquitin ligases, with regard of SCF^{FBXW7}.

Combined treatments reveal an unexpected but plausible evidence. In HCT116 cells, the combined use of IPA and 5-FU produced the strongest synergistic interaction, with a very low CI and a DRI corresponding to the lowest concentrations of the drugs. In SW48 cells, albeit the FBXW7 mutation affects Mcl1 degradation, the combination of IPA and 5-FU was synergistic starting from intermediate concentrations. Unexpected, in DLD1 cells combination of IPA and 5-FU predominantly antagonized, at least for the time point and doses analyzed. Bracht and colleagues, classified 5-FU sensitivity in a panel of CRC cell lines, based on mismatch repair (MMR) status [Bracht et al, 2010]. Although our three in vitro models share MMR deficiency, they found that SW48 cells show an intermediate 5-FU sensitivity, compared to the resistant phenotype of HCT116 and even more of DLD1 cells, that displays the highest GI50. This concurs with our results and FBXW7 wild type in HCT116 cells could dictate the synergism with 5-FU. Beyond the greater basal sensitivity to 5-FU of SW48 cells, the better effect of the combination in these cells could be ascribable to TP53 gene status. Conversely to HCT116 and SW48, displaying wild type TP53, DLD1 cells harbour mutant p53 [Berg et al, 2017]. p53 limits the effects of FBXW7 loss and its mutation is frequently associated with hypermethylation of FBXW7 promoter regions, as occurs in DLD1 cell line. Loss of both p53 and FBXW7 causes chromosomal instability (CIN) of intestinal cancer, accelerating tumorigenesis and conferring advanced phenotypes [Grim et al, 2012]. This probably explains the antagonistic interaction of IPA and 5-FU in DLD1 cells, compared to wild type TP53 cell lines. As well, the response to 5-FU and generally to chemotherapics or their combination can be influenced by several genetic variables, such as stabilizing β-catenin mutations in the case of HCT116 and SW48 [Proto et al, 2017]. This exactly reflects the individual differences between cancer patients, where the high intra- and inter- tumor heterogeneity, dictates the high

variability of response. The ability of IPA to synergize with 5-FU could represents a valuable effect and potentially a good therapeutic option in CRC and other tumors.

In GBM, several E3 ligases, including FBXW7, are involved in DNA damage response [Humphreys et al, 2021]. The WD40 domain of F-box proteins, which is responsible for substrate binding, is also required to bind the poly(ADP-ribose) (PAR) immediately following DNA-double strand breaks (DSBs), and mediates rapid FBXW7 recruitment for X-ray repair cross-complementing protein 4 (XRCC4) ubiquitination and activation of non-homologous endjoining (NHEJ) repair system [Zhang et al, 2019]. In a recent study, FBXW7 was related to TMZ resistance and, in particular, FBXW7 re-expression in a TMZ-resistant U251 clone partially sensitized to the drug, while FBXW7 silencing produced the opposite effect [Lin et al, 2018]. The find that IPA amplifies DNA damage before irradiation, in U251 and GBM primary cell lines, by inhibiting the repair pathway of IR-induced DSBs [Navarra et al, 2020], together with the FBXW7 up-regulation here debated is extremely intriguing since GBM therapeutic protocols include different combination of ionizing radiation and TMZ, and the resistance is modulated by DNA repair systems [Stupp et al, 2005; Oldrini et al, 2020]. We showed the IPA pre-treatment can boost the killing effect of TMZ, starting from a concentration range much lower than EC50, in GBM cell lines already sensitive to the alkylating agent [Lee, 2016], where the modified adenosines strongly impact on proliferation and increase FBXW7 expression. In T98 cells, poorly responsive to the treatments, IPA and N6-BA did not substantially alter FBXW7 protein levels but they both reduced constitutive MGMT, the repair enzyme removing alkyl adducts at specific O6 position of guanine (O^6mG), and whose expression, epigenetically suppressed in U87 and U251, predicts therapeutic susceptibility. Despite this, IPA pre-treatment was not able to significantly improve TMZ efficacy in T98. However, in this resistant model, cell death is induced by higher TMZ concentration and increasing incubation time. Moreover, the acquisition of TMZ resistance *in vitro* is a complex mechanism that involve rapid and not reversible epigenetic rearrangements, thus complicating the individuation of the precise timeframe in which cells are tolerant to the drug [Rabè et al, 2020].

So far, the main evidence emerging from this study is that IPA and its analogue N6-BA could influence the expression of methylated genes involved in tumor-related mechanisms, such as MGMT, FBXW7 and potentially others, suggesting the existence of an epigenetic regulation behind their pleiotropic actions. Our investigations revealed that the modified adenosines overall behave similarly to 5-AZA-dC, known DNA-methyltransferases inhibitor (DNMTi), affecting both the expression of DNMT1, crucial enzyme in the maintenance of DNA methylation patterns, and

DNMT activity in general. Surprisingly, global DNA methylation did not completely reflect DNMTs activity inhibition trend and, in particular, we observed different IPA behaviours. In U87 and U251, IPA reduces global methylation when used as single agent, but in combination with 5-AZA-dC increases the total percentage of 5-methylcytosine. Probably, this unexpected evidence is suggestive of an adaptive response to an excessive inhibitory stimulus, as explained in a recent report analysing DNMTi effects on colon cancer genome methylation [Giri and Aittokallio, 2019]. It is worth mentioning that 5-AZA-dC (decitabine) produces a non-specific reorganization of DNA and the entire process is orchestrated by a multitude of actors, in addition to DNMTs and differently expressed in tumors, including 5-methylcytosine hydroxylases (TETs), histone modification enzymes (HACs, HDACs, HMTs, KDMs), ubiquitin-like proteins that recognize methylated CpG sites or histones, and last but not least non-coding RNA [Cheng et al, 2019]. The *in vitro* assays, used here to examine epigenetic regulation, evaluated a global effect on DNA methylation and did not discriminate between *de novo* or maintenance DNMT activity or gene-specific epigenetic changes, but drew the line for future investigations. Since 2-methylthio-N6-isopentenyladenosine (ms26A) is an evolutionary conserved modification, influencing the functions of the transcription machinery [Yamamoto et al, 2019], we could speculate that exogenous free IPA disturbs RNA modification processes and take into account the comparison with 5-azacytidine too, which integrates in both DNA and RNA. Additionally, it is also plausible that IPA or its metabolites interfere with other methyltransferases that exploit S-adenosylmethionine as methyl donor.

Next generation sequencing of glioma patients resected tumors remarked the huge variability in the individual genetic landscape contributing to pathogenicity. On a series of 11 sequenced tumors, GBM55 and GBM58 share the same p53 SNVs (p.P33R, p.P73R) and, more relevant, X-chromosome deletions of genes with roles in transcription and epigenetic regulation, such as Lysine Demethylase 6A (KDM6A), Lysine Demethylase 5C (KDM5C), Mediator Complex Subunit 12 (MED12) and ATPase/helicase ATRX Chromatin Remodeler (ATRX). In the respective established primary cell lines, IPA or N6-BA abrogation of DNMT1 expression was proportioned to the extreme induction of H2Ax phosphorylation. Together with the modulation of MGMT, this is suggestive of an interplay between DNA modification enzymes and damage response. Besides, DNMT1 was found to co-localize with repair components independently from its role in methylation maintenance [Ha et al, 2001], and this could further explain the observed discrepancies between DNMT activity inhibition and global methylation trend.

FINAL REMARKS

We investigated the effects on cancer-related mechanisms of N6-benzyladenosine by comparing it with the N6-isopentenyladenosine, an endogenous occurring modified nucleoside endowed with pleiotropic anti-tumor actions. The main goal of this work is the identification of FBXW7 as a novel target up-regulated by the modified adenosines in CRC and GBM. FBXW7 is at the crossroad of many cell process and, thus, its suppression correlates with malignancies and chemoresistance. We found that the molecules act in a similar way at multiple steps of cancer progression, in a FBXW7-dependent or -independent fashion, affecting several players involved in cell cycle progression and damage response. The common thread is probably an epigenetic and/or transcriptional regulation.

However, the genotype seems to strongly influence the response to IPA or N6-BA and the combination with chemotherapics, thus a wide correlation is needed to pinpoint their precise mechanism of action. Overall, the obtained results may help to define whether the use of modified adenosines can be a valid tool to optimize for personalized therapy in CRC, GBM and potentially other malignancies.

REFERENCES

Abate, M.; Laezza, C.; Pisanti, S.; Torelli, G.; Seneca, V.; Catapano, G.; Montella, F.; Ranieri, R.; Notarnicola, M.; Gazzerro, P.; Bifulco, M.; Ciaglia, E. Deregulated expression and activity of Farnesyl Diphosphate Synthase (FDPS) in Glioblastoma. *Sci. Rep.* **2017**, *7*, 14123.

Adjei, A.A.; Davis, J.N.; Erlichman, C.; Svingen, P.A.; Kaufmann, S.H. Comparison of potential markers of farnesyltransferase inhibition. *Clin. Cancer Res*. **2000**, *6*, 2318–2325.

Akhoondi, S.; Lindström, L.; Widschwendter, M.; Corcoran, M.; Bergh, J.; Spruck, C.; Grandér, D.; Sangfelt, O. Inactivation of FBXW7/hCDC4-β expression by promoter hypermethylation is associated with favorable prognosis in primary breast cancer. *Breast Cancer Res*. **2010**, *12*, 105.

Akhtar, S.S.; Mekureyaw, M.F.; Pandey, C.; Roitsch, T. Role of Cytokinins for Interactions of Plants With Microbial Pathogens and Pest Insects. *Front. Plant Sci*. **2020**, *10*, 1777.

Berg, K.C.G.; Eide, P.W.; Eilertsen, I.A.; Johannessen, B.; Bruun, J.; Danielsen, S.A.; Bjørnslett, M.; Meza-Zepeda, L.A.; Eknæs, M.; Lind, G.E.; Myklebost, O.; Skotheim, R.I.; Sveen, A.; Lothe, R. A. Multi-omics of 34 colorectal cancer cell lines--A resource for biomedical studies. *Mol. Cancer*. **2017**, *16*, 116.

Bifulco, M.; Malfitano, A.M.; Proto, M.C.; Santoro, A.; Caruso, M.G.; Laezza, C. Biological and pharmacological roles of N6-isopentenyladenosine: An emerging anticancer drug. *Anticancer Agents Med. Chem.* **2008**, *8*, 200–204.

Bracht, K.; Nicholls, A.M.; Liu, Y.; Bodmer, W.F. 5-Fluorouracil response in a large panel of colorectal cancer cell lines is associated with mismatch repair deficiency. *Br. J. Cancer*. **2010**, *103*, 340–346.

Castiglioni, S.; Casati, S.; Ottria, R.; Ciuffreda, P.; Maier, J.A. N6-isopentenyladenosine and its analogue N6-benzyladenosine induce cell cycle arrest and apoptosis in bladder carcinoma T24 cells. *Anticancer Agents Med Chem*. **2013**, *4*, 672-8.

Chen, X.; Zhang, M.; Gan, H.; Wang, H.; Lee, J.H.; Fang, D.; Kitange, G.J.; He, L.; Hu, Z.; Parney, I.F.; Meyer, F.B.; Giannini, C.; Sarkaria, J.N.; Zhang, Z. A novel enhancer regulates

MGMT expression and promotes temozolomide resistance in glioblastoma. *Nat. Commun*. **2018**, *1*, 2949.

Cheng, Y.; He, C.; Wang, M.; Ma, X.; Mo, F.; Yang, S.; Han, J.; Wei, X. Targeting epigenetic regulators for cancer therapy: mechanisms and advances in clinical trials. *Sig. Transduct. Target Ther*. **2019,** *4*, 6.

Chou, T.C. Drug Combination Studies and Their Synergy Quantification Using the Chou-Talalay Method. *Cancer Res*. **2010**, *70*, 440–446.,

Ciaglia, E.; Abate, M.; Laezza, C.; Pisanti, S.; Vitale, M.; Seneca, V.; Torelli, G.; Franceschelli, S.; Catapano, G.; Gazzerro, P.; Bifulco, M. Antiglioma effects of N6-isopentenyladenosine, an endogenous isoprenoid end product, through the downregulation of epidermal growth factor receptor. *Int. J. Cancer*. **2017a**, *140*, 959-972.

Ciaglia, E.; Grimaldi, M.; Abate, M.; Scrima, M.; Rodriquez, M.; Laezza, C.; Ranieri, R.; Pisanti, S.; Ciuffreda, P.; Manera, C.; Gazzerro, P.; D'Ursi, A.M.; Bifulco, M. The isoprenoid derivative N6-benzyladenosine (CM223) exerts antitumor effects in glioma patient-derived primary cells through the mevalonate pathway. *Br. J. Pharmacol*. **2017b**, *174*, 2287-2301.

Ciaglia, E.; Laezza, C.; Abate, M.; Pisanti, S.; Ranieri, R.; D'alessandro, A.; Picardi, P.; Gazzerro, P.; Bifulco, M. Recognition by natural killer cells of N6-isopentenyladenosine-treated human glioma cell lines. *Int. J. Cancer*, **2018**, *142*, 176–190.

Ciaglia, E.; Pisanti, S.; Picardi, P.; Laezza, C.; Sosa, S.; Tubaro, A.; Vitale, M.; Gazzerro, P.; Malfitano, A.M.; Bifulco, M. N6-isopentenyladenosine affects cytotoxic activity and cytokines production by IL-2 activated NK cells and exerts topical anti-inflammatory activity in mice. *Pharmacol. Res*. **2014**, *89*, 1-10.

Colombo, F.; Falvella, F.S.; De Cecco, L.; Tortoreto, M.; Pratesi, G.; Ciuffreda, P.; Ottria, R.; Santaniello, E.; Cicatiello, L.; Weisz, A.; Dragani, T.A. Pharmacogenomics and analogues of the antitumour agent N6-isopentenyladenosine. *Int. J. Cancer*. ***2009***, *124*, 2179-2185.

Davis, R.J.; Welcker, M.; Clurman, B.E. Tumor suppression by the Fbw7 ubiquitin ligase: Mechanisms and opportunities. *Cancer Cell*. **2014**, *26*, 455–464.

De Palma, F.D.E., D'Argenio, V.; Pol, J.; Kroemer, G.; Maiuri, M.C.; Salvatore, F. The Molecular Hallmarks of the Serrated Pathway in Colorectal Cancer. *Cancers (Basel)*. **2019**, *7*, 1017.

Dekker, E.; Tanis, P.J.; Vleugels, J.L.A.; Kasi, P.M.; Wallace, M.B. Colorectal cancer. *Lancet*. **2019**, *10207*, 1467-1480.

Fan H., Gulley M.L. DNA Extraction from Fresh or Frozen Tissues. In the: *Methods in Molecular Medicine*™, Killeen A.A., Eds.; Molecular Pathology Protocols. vol 49, Humana Press, **2001**.

Fang, X.; Zhou, W.; Wu, Q.; Huang, Z., Shi, Y.; Yang, K.; Chen, C.; Xie, Q.; Mack, S.C.; Wang, X.; Carcaboso, A.M.; Sloan, A.E.; Ouyang, G.; McLendon, R.E.; Bian, X.W.; Rich, J.N.; Bao, S. Deubiquitinase USP13 maintains glioblastoma stem cells by antagonizing FBXL14-mediated Myc ubiquitination. *J. Exp. Med*. **2017**, *1*, 245-267.

Farrell, A.S.; Sears, R.C. MYC degradation. *Cold Spring Harb. Perspect. Med*. **2014**, *3*, a014365.

Fearon, E.R. Molecular genetics of colorectal cancer. *Annu. Rev. Pathol*. **2011**, *6*, 479-507.

Fiore, D.; Ramesh, P.; Proto, M.C.; Piscopo, C.; Franceschelli, S.; Anzelmo, S.; Medema, J.P.; Bifulco, M.; Gazzerro, P. Rimonabant Kills Colon Cancer Stem Cells without Inducing Toxicity in Normal Colon Organoids. *Front. Pharmacol*. **2018**, *8*, 949.

Fleming, M.; Ravula, S.: Tatishchev, S.F.; Wang, H.L. Colorectal carcinoma: Pathologic aspects. *J. Gastrointest. Oncol*. **2012**, *3*, 153-73.

Foltz, G.; Yoon, JG.; Lee, H.; Ryken, T.C.; Sibenaller, Z.; Ehrich, M.; Hood, L.; Madan, A. DNA methyltransferase-mediated transcriptional silencing in malignant glioma: a combined whole-genome microarray and promoter array analysis. *Oncogene.* **2009**, *28*, 2667–2677.

Fouad, S.; Wells, O.S.; Hill, M.A.; D'Angiolella, V. Cullin Ring Ubiquitin Ligases (CRLs) in Cancer: Responses to Ionizing Radiation (IR) Treatment. *Front. Physiol.* **2019**, *10*, 1144.

Gallo, R.C.; Whang-Peng, J.; Perry, S. Isopentenyladenosine stimulates and inhibits mitosis of human lymphocytes treated with phytohemagglutinin. *Science*, **1969**, *165*, 400.

Gazzerro, P.; Proto, M.C.; Gangemi, G.; Malfitano, A.M.; Ciaglia, E.; Pisanti, S.; Santoro, A.; Laezza, C.; Bifulco, M. Pharmacological actions of statins: A critical appraisal in the management of cancer. *Pharmacol. Rev*. **2012**, *64*, 102–146.

Giri, A.K.; Aittokallio, T. DNMT Inhibitors Increase Methylation in the Cancer Genome. *Front Pharmacol*. **2019**, *10*, 385.

Gouw, A.M.; Margulis, K.; Liu, N.S.; Raman, S.J.; Mancuso, A.; Toal, G.G.; Tong, L.; Mosley, A.; Hsieh, A.L.; Sullivan, D.K.; Stine, Z.E.; Altman, B.J.; Schulze, A.; Dang, C.V.; Zare, R.N.; Felsher, D.W. The MYC Oncogene Cooperates with Sterol-Regulated Element-Binding Protein to Regulate Lipogenesis Essential for Neoplastic Growth. *Cell Metab*. **2019**, *3*, 556-572.

Grim, J.E.; Knoblaugh, S.E.; Guthrie, K.A.; Hagar, A.; Swanger, J.; Hespelt, J.; Delrow, J.J.; Small, T.; Grady, W.M.; Nakayama, K.I.; Clurman, B.E. Fbw7 and p53 cooperatively suppress advanced and chromosomally unstable intestinal cancer. *Mol. Cell. Biol*. **2012**, *32*, 2160–2167.

Gu, Z.; Inomata, K.; Ishizawa, K.; Horii, A. The FBXW7 beta-form is suppressed in human glioma cells. *Biochem. Biophys. Res. Commun*. **2007**, *4*, 992-998.

Ha, K.; Lee, G.E.; Palii, S.S.; Brown, K.D.; Takeda, Y.; Liu, K.; Bhalla, K.N.; Robertson, K.D. Rapid and transient recruitment of DNMT1 to DNA double-strand breaks is mediated by its interaction with multiple components of the DNA damage response machinery. *Hum. Mol. Genet*. **2011**, *1*, 126-40.

Hagedorn, M.; Delugin, M.; Abraldes, I.; Allain, N.; Belaud-Rotureau, M.A.; Turmo, M.; Prigent, C.; Loiseau, H.; Bikfalvi, A.; Javerzat, S. FBXW7/hCDC4 controls glioma cell proliferation in vitro and is a prognostic marker for survival in glioblastoma patients. *Cell Div*. **2007**, *2*, 9.

Hoeck, J.; Jandke, A.; Blake, S.; Nye, E.; Spencer-Dene, B.; Brandner, S.; Behrens, A. Fbw7 controls neural stem cell differentiation and progenitor apoptosis via Notch and c-Jun. *Nat. Neurosci*. **2010**, *13*, 1365–1372.

Humphreys, L.M.; Smith, P.; Chen, Z.; Fouad, S.; D'Angiolella, V. The role of E3 ubiquitin ligases in the development and progression of glioblastoma. Cell Death Differ. **2021**, *28*, 522-537.

Iwatsuki, M.; Mimori, K.; Ishii, H.; Yokobori, T.; Takatsuno, Y.; Sato, T.; Toh, H.; Onoyama, I.; Nakayama, K.I.; Baba, H.; Mori, M. Loss of FBXW7, a cell cycle regulating gene, in colorectal cancer: Clinical significance. *Int. J. Cancer*, **2010**, *126*, 1828–1837.

Khan, O. M.; Carvalho, J.; Spencer-Dene, B.; Mitter, R.; Frith, D.; Snijders, A. P.; Wood, S. A.; Behrens, A. The deubiquitinase USP9X regulates FBW7 stability and suppresses colorectal cancer. *J. Clin. Invest.* **2018**, *128*, 1326–1337.

Kieber, J.J.; Schaller, G.E. Cytokinin signaling in plant development. *Development*. **2018**, *165*, 149344.

Laezza, C.; Caruso, M.G.; Gentile, T.; Notarnicola, M.; Malfitano, A.M.; Di Matola, T.; Messa, C.; Gazzerro, P.; Bifulco, M. N6-isopentenyladenosine inhibits cell proliferation and induces apoptosis in a human colon cancer cell line DLD1. *Int. J. Cancer*, **2009**, *124*, 1322–1329.

Laezza, C.; Notarnicola, M.; Caruso, M.G.; Messa, C.; Macchia, M.; Bertini, S.; Minutolo, F.; Portella, G.; Fiorentino, L.; Stingo, S.; Bifulco M. N6-isopentenyladenosinen arrests tumor cell proliferation by inhibiting farnesyl diphosphate synthase and protein prenylation. *FASEB J.* **2006**, *20*, 412–418.

Lan, H.; Tan, M.; Zhang, Q.; Yang, F.; Wang, S.; Li, H.; Xiong, X.; Sun, Y. LSD1 destabilizes FBXW7 and abrogates FBXW7 functions independent of its demethylase activity. *Proc. Natl. Acad. Sci. U S A.* **2019**, *116*, 12311-12320.

Lee, S.Y. Temozolomide resistance in glioblastoma multiforme. *Genes Dis*. **2016**, *3*, 198-210.

Li, M.; Qi, Y.; Wei, J.; Lu, L.; Zhao, X.; Zhou, L. N6-Isopentenyladenosine promoted HeLa cell apoptosis through inhibitions of AKT and transforming growth factor β-activated kinase 1 activation. *Tumour Biol*. **2017**, *39*, 1010428317695966.

Li, N.; Babaei-Jadidi, R.; Lorenzi, F.; Spencer-Dene, B.; Clarke, P.; Domingo, E.; Tulchinsky, E.; Vries, R.; Kerr, D.; Pan, Y.; He, Y., Bates, D. O.; Tomlinson, I.; Clevers, H.; Nateri, A. S. An FBXW7-ZEB2 axis links EMT and tumour microenvironment to promote colorectal cancer stem cells and chemoresistance. *Oncogenesis*. **2019**, *8*, 13.

Lin, J.; Ji, A.; Qiu, G.; Feng, H.; Li, J.; Li, S.; Zou, Y.; Cui, Y.; Song, C.; He, H.; Lu, Y. FBW7 is associated with prognosis, inhibits malignancies and enhances temozolomide sensitivity in glioblastoma cells. *Cancer Sci*. **2018**, *109*, 1001-1011.

Lorenzi, F.; Babaei-Jadidi, R.; Sheard, J.; Spencer-Dene, B.; Nateri, A.S. Fbxw7-associated drug resistance is reversed by induction of terminal differentiation in murine intestinal organoid culture. *Mol. Ther. Meth. Clin. Dev*. **2016**, *3*, 16024

Louis, D.N.; Perry, A.; Reifenberger, G.; von Deimling, A.; Figarella-Branger, D.; Cavenee, W.K.; Ohgaki, H.; Wiestler, O.D.; Kleihues, P.; Ellison, D.W. The 2016 World Health Organization Classification of Tumors of the Central Nervous System: A summary. *Acta Neuropathol*. **2016**, *131*, 803.

Ma, L.M.; Liang, Z.R.; Zhou, K.R.; Zhou, H.; Qu, L.H. 27-Hydroxycholesterol increases Myc protein stability via suppressing PP2A, SCP1 and FBW7 transcription in MCF-7 breast cancer cells. *Biochem. Biophys. Res. Commun*. **2016**, *480*, 328–333.

Malta, T.M.; de Souza, C.F.; Sabedot, T.S.; Silva, T.C.; Mosella, M.S.; Kalkanis, S.N.; Snyder, J.; Castro, A.V.B.; Noushmehr, H. Glioma CpG island methylator phenotype (G-CIMP): biological and clinical implications. *Neuro Oncol*. **2018**, *20*, 608-620.

Matsumoto, A.; Onoyama, I.; Sunabori, T.; Kageyama, R.; Okano, H.; Nakayama, KI. Fbxw7-dependent degradation of Notch is required for control of "stemness" and neuronal-glial differentiation in neural stem cells. *J. Biol. Chem*. **2011**, *286*, 13754-13764.

Meisel, H.; Gunther, S.; Martin, D.; Schlimme, E. Apoptosis induced by modified ribonucleosides in human cell culture systems. *FEBS Lett.*, **1998**, *433*, 265.

Morreale, F.E.; Walden, H. Types of Ubiquitin Ligases. *Cell*, **2016**; *165*, 248.

Navarra, G.; Pagano, C.; Pacelli, R.; Crescenzi, E.; Longobardi, E.; Gazzerro, P.; Fiore, D.; Pastorino, O.; Pentimalli, F.; Laezza C.; Bifulco, M. N6-Isopentenyladenosine Enhances the Radiosensitivity of Glioblastoma Cells by Inhibiting the Homologous Recombination Repair Protein RAD51 Expression. *Front. Oncol*. **2020**, *9*, 1498.

Oldrini, B.; Vaquero-Siguero, N.; Mu, Q.; Kroon, P.; Zhang, Y.; Galán-Ganga, M.; Bao, Z.; Wang, Z.; Liu, H.; Sa, J.K.; Zhao, J.; Kim, H.; Rodriguez-Perales, S.; Nam, D.H.; Verhaak, R.G.W.; Rabadan, R.; Jiang, T.; Wang, J.; Squatrito, M. MGMT genomic rearrangements contribute to chemotherapy resistance in gliomas. *Nat. Commun*. **2020**, *11*, 3883.

Ottria, R.; Casati, S.; Baldoli, E.; Maier, J.A.; Ciuffreda, P. N(6)-alkyladenosines: synthesis and evaluation of in vitro anticancer activity. *Bioorg. Med. Chem*. **2010**, *18*, 8396–8402.

Pisanti S, Picardi P, Ciaglia E, Margarucci L, Ronca R, Giacomini A, Malfitano AM, Casapullo A, Laezza C, Gazzerro P, Bifulco M. Antiangiogenic effects of N6-isopentenyladenosine, an endogenous isoprenoid end product, mediated by AMPK activation. *FASEB J*. **2014**, *28*, 1132-44.

Proto, M.C.; Fiore, D.; Piscopo, C.; Franceschelli, S.; Bizzarro, V.; Laezza, C.; Lauro, G.; Feoli, A.; Tosco, A.; Bifulco, G.; Sbardella, G.; Bifulco, M.; Gazzerro, P. Inhibition of Wnt/-Catenin pathway and Histone acetyltransferase activity by Rimonabant: A therapeutic target for colon cancer. *Sci. Rep*. **2017**, 7, 11678.

Proto, M.C.; Gazzerro, P.; Di Croce, L.; Santoro, A.; Malfitano, A.M.; Pisanti, S.; Laezza, C.; Bifulco, M. Interaction of endocannabinoid system and steroid hormones in the control of colon cancer cell growth. *J. Cell. Physiol*. **2012**, *227*, 250–258

Punga, T.; Bengoechea-Alonso, M.T.; Ericsson, J. Phosphorylation and ubiquitination of the transcription factor sterol regulatory element-binding protein-1 in response to DNA binding. J. *Biol. Chem*. **2006**, *281*, 25278–25286.

Rabé, M.; Dumont, S.; Álvarez-Arenas, A.; Janati, H.; Belmonte-Beitia, J.; Calvo, G.F.; Thibault-Carpentier, C.; Séry, Q.; Chauvin, C.; Joalland, N.; Briand, F.; Blandin, S.; Scotet, E.; Pecqueur, C.; Clairambault, J.; Oliver, L.; Perez-Garcia, V.; Nadaradjane, A.; Cartron, P.F.; Gratas, C.; Vallette, F.M. Identification of a transient state during the acquisition of temozolomide resistance in glioblastoma. *Cell Death Dis*. **2020**, *11*, 19.

Rajabi, M.; Mehrzad, J.; Gorincioi, E.; Santaniello, E. Antiproliferative activity of N (6)-isopentenyladenosine on HCT-15 colon carcinoma cell line. *Nucleic Acid Ther*. **2011**, *21*, 355–358.

Ranieri, R.; Ciaglia, E.; Amodio, G.; Picardi, P.; Proto, M.C.; Gazzerro, P.; Laezza, C.; Remondelli, P.; Bifulco, M.; Pisanti, S. N6-isopentenyladenosine dual targeting of AMPK and Rab7 prenylation inhibits melanoma growth through the impairment of autophagic flux. *Cell Death Differ*. **2018**, *25*, 353–367.

Safa, A.R.; Saadatzadeh, M.R.; Cohen-Gadol, A.A.; Pollok, K.E.; Bijangi-Vishehsaraei, K. Glioblastoma stem cells (GSCs) epigenetic plasticity and interconversion between differentiated non-GSCs and GSCs. *Genes Dis*. **2015**, *2*, 152-163.

Sailo, B.L.; Banik, K.; Girisa, S.; Bordoloi, D.; Fan, L.; Halim, C.E.; Wang, H.; Kumar, A.P.; Zheng, D.; Mao, X.; Sethi, G.; Kunnumakkara, A.B. FBXW7 in Cancer: What Has Been Unraveled Thus Far? *Cancers*. **2019**, *11*, 246.

Sakakibara, H. Cytokinins: activity, biosynthesis, and translocation. *Annu. Rev. Plant Biol*. **2006**, *57*, 431-49.

Scholz, N.; Kurian, K.M.; Siebzehnrubl, F.A.; Licchesi, J.D.F. Targeting the Ubiquitin System in Glioblastoma. *Front Oncol*. **2020**, *10*, 574011.

Schweizer, U.; Bohleber, S.; Fradejas-Villar, N. The modified base isopentenyladenosine and its derivatives in tRNA. *RNA Biol*. **2017**, *14*, 1197-1208.

Scrima, M.; Lauro, G.; Grimaldi, M.; Di Marino, S.; Tosco, A.; Picardi, P.; Gazzerro, P.; Riccio, R.; Novellino, E.; Bifulco, M.; Bifulco, G.; D'Ursi, A.M. Structural evidence of N6-isopentenyladenosine as a new ligand of farnesyl pyrophosphate synthase. *J. Med. Chem*. **2014**, *25*, 7798-803.

Sinicrope, F.A.; Sargent, D.J. Molecular pathways: microsatellite instability in colorectal cancer: prognostic, predictive, and therapeutic implications. *Clin. Cancer Res*. **2012**, *18*, 1506-1512.

Skaar, J.R.; Pagan, J.K.; Pagano, M. SCF ubiquitin ligase-targeted therapies. *Nat. Rev. Drug Discov*. **2014**, *13*, 889-903.

Skoog, F.; Strong, F.M.; Miller, C.O. Cytokinins. *Science*. **1965**, *148*, 532-533.

Spallek, T.; Melnyk, C. W.; Wakatake, T.; Zhang, J.; Sakamoto, Y.; Kiba, T.; Yoshida, S.; Matsunaga, S.; Sakakibara, H.; Shirasu, K. Interspecies hormonal control of host root morphology by parasitic plants. *Proc. Nat. Acad. Sci*. **2017**, *114*, 5283–5288.

Stresemann, C.; Lyko, F. Modes of action of the DNA methyltransferase inhibitors azacytidine and decitabine. *Int. J. Cancer*. **2008**, *123*, 8-13.

Strnad, M. The aromatic cytokinins. *Physiol. Plant*. **1997**, *101*, 674–688.

Stupp, R.; van den Bent, M. J.; Hegi, M. E. Optimal role of temozolomide in the treatment of malignant gliomas. *Curr. Neurol. Neurosci*. **2005**, *5*, 198–206.

Takeishi, S.; Nakayama, K.I. Role of Fbxw7 in the maintenance of normal stem cells and cancer-initiating cells. *Br. J. Cancer*, **2014**, *111*, 1054–1059.

Tong, J.; Tan, S.; Zou, F.; Yu, J.; Zhang, L. FBW7 mutations mediate resistance of colorectal cancer to targeted therapies by blocking Mcl-1 degradation. *Oncogene*. **2017**, *36*, 787–796.

Wang, J.; Wang, H.; Li, Z.; Wu, Q.; Lathia, J.D.; McLendon, R.E.; Hjelmeland, A.B.; Rich, J.N. c-Myc is required for maintenance of glioma cancer stem cells. *PLoS One*. **2008**, *3*, e3769.

Wang, X.; Huang, Z.; Wu, Q.; Prager, B.C.; Mack, S.C.; Yang, K.; Kim, L.J.Y.; Gimple, R.C.; Shi, Y.; Lai, S.; Xie, Q.; Miller, T.E.; Hubert, C.G.; Song, A.; Dong, Z.; Zhou, W.; Fang, X.; Zhu, Z.; Mahadev, V.; Bao, S.; Rich, J.N. MYC-Regulated Mevalonate Metabolism Maintains Brain Tumor-Initiating Cells. *Cancer Res*. **2017**, *77*, 4947–4960.

Welcker, M.; Orian, A.; Jin, J.; Grim, J.E.; Harper, J.W.; Eisenman, R.N.; Clurman, B.E. The Fbw7 tumor suppressor regulates glycogen synthase kinase 3 phosphorylation-dependent c-Myc protein degradation. *Proc. Natl. Acad. Sci. U S A.* **2004**, *101*, 9085–9090.

Wenger, A.; Ferreyra Vega, S.; Kling, T.; Bontell, T.O; Jakola, A.S.; Carén, H. Intratumor DNA methylation heterogeneity in glioblastoma: implications for DNA methylation-based classification. *Neuro Oncol*. **2019**, *21*, 616-627.

Yamamoto, T.; Fujimura, A.; Wei, F.Y.; Shinojima, N.; Kuroda, J.I., Mukasa, A., Tomizawa, K. 2-Methylthio Conversion of N6-Isopentenyladenosine in Mitochondrial tRNAs by CDK5RAP1 Promotes the Maintenance of Glioma-Initiating Cells. *iScience*. **2019**, *21*, 42-56.

Yang, Y.; Gao, X.; Zhang, M.; Yan, S.; Sun, C.; Xiao, F.; Huang, N.; Yang, X.; Zhao, K.; Zhou, H.; Huang, S.; Xie, B.; Zhang, N. Novel Role of FBXW7 Circular RNA in Repressing Glioma Tumorigenesis. *J. Natl. Cancer Inst*. **2018**, *110*, 304-315.

Yumimoto, K.; Nakayama, K.I. Recent insight into the role of FBXW7 as a tumor suppressor. *Semin Cancer Biol*. **2020**, *67*, 1-15.

Zhang, Q.; Mady, A.S.A.; Ma, Y.; Ryan, C.; Lawrence, T.S.; Nikolovska-Coleska, Z.; Sun, Y.; Morgan, M.A. The WD40 domain of FBXW7 is a poly(ADP-ribose)-binding domain that mediates the early DNA damage response. *Nucleic Acids Res*. **2019**, *47*, 4039-4053.

Zwack, P.J.; Rashotte. A.M. Cytokinin inhibition of leaf senescence. *Plant Signal Behav*. **2013**, *8*, e24737.

LIST OF ABBREVIATIONS

5-AZA-dC, 5-Aza-2'-deoxycytidine or Decitabine;

5-FU, 5-fluorouracil;

BrdU, bromodeoxyuridine;

CK, cytokinin;

CRC, Colorectal cancer;

DNMT, DNA methyltransferase;

FBXW7, F-box WD repeat domain-containing;

FDPS, Farnesyl Disphosphate Synthase;

GBM, Glioblastoma multiforme;

GSK3β, Glycogen Synthase Kinase 3β;

IPA or i6A, N6-isopentenyadenosine;

MGMT, O6-methylguanine DNA methyltransferase;

N6-BA, N6-benzyladenosine;

SCF complex, SKP, Cullin, F-box containing complex;

SD, Standard Deviation;

SREBP, Sterol Responsive Element Binding Protein;

TMZ, Temozolomide;

UPS, Ubiquitin-Proteasome System.